2008

Probing And Tuning The Size, Morphology, Chemistry And Structure Of Nanoscale Cerium Oxide

Satyanarayana Kuchibhatla
University of Central Florida

Showcase of Text, Archives, Research & Scholarship

PROBING AND TUNING THE SIZE, MORPHOLOGY, CHEMISTRY AND
STRUCTURE OF NANOSCALE CERIUM OXIDE

A dissertation submitted in partial fulfillment of the requirements for the degree of
Doctor of Philosophy in the Department of Mechanical, Materials and
Aerospace Engineering in the College of Engineering and Computer Science
at the University of Central Florida, Orlando, Florida, USA

by

Satyanarayana VNT Kuchibhatla
Master of Technology (M.Tech.), IITBombay, INDIA

Spring Term
2008

Major Professor: Sudipta Seal

ABSTRACT

Cerium oxide (ceria)-based materials in the nanoscale regime are of significant fundamental and technological interest. Nanoceria in pure and doped forms has current and potential use in solid oxide fuel cells, catalysis, UV- screening, chemical mechanical planarization, oxygen sensors, and bio-medical applications. The characteristic feature of Ce to switch between the +3 and + 4 oxidation states renders oxygen buffering capability to ceria. The ease of this transformation was expected to be enhanced in the nanoceria. In most the practical scenarios, it is necessary to have a stable suspension of ceria nanoparticles (CNPs) over longer periods of time. However, the existing literature is confined to short term studies pertaining to synthesis and property evaluation.

Having understood the need for a comprehensive understanding of the CNP suspensions, this dissertation is primarily aimed at understanding the <u>behavior of CNPs in various chemical and physical environments</u>. We have synthesized CNPs in the <u>absence</u> of any surfactants at room temperature and studied the aging characteristics. After gaining some understanding about the behavior of this functional oxide, the synthesis environment and aging temperature were varied, and their affects were carefully analyzed using various materials analysis techniques such as high resolution transmission electron microscopy (HRTEM), UV-Visible spectroscopy (UV-Vis), and X-ray photoelectron spectroscopy (XPS).

When the CNPs were aged at room temperature in as-synthesized condition, they were observed to spontaneously assemble and evolve as fractal superoctahedral structures. The reasons for this unique polycrystalline morphology were attributed to the symmetry driven assembly of the individual truncated octahedral and octahedral seed of the ceria. HRTEM and Fast Fourier Transform (FFT) analyses were used to explain the agglomeration behavior and evolution of the octahedral morphology. Some of the observations were supported by molecular dynamic simulations. Poly (ethylene glycol) (PEG) and ethylene glycol (EG) were used to control the kinetics of this morphology evolution. The ability to control the agglomeration of CNPs in these media stems from the lower dielectric constant and an increased viscosity of the EG and PEG based solvents. CNPs when synthesized and aged in frozen conditions, i.e. in ice, were found to form one dimensional, high aspect ratio structures. A careful analysis has provided some evidence that the CNPs use the porous channels in ice as a template and undergo oriented attachment to form nanorods. When the aging treatment was done near freezing temperature in solution, the nanorods were not observed, confirming the role of channels in ice.

When synthesized in aqueous media such as DI water, PEG and EG; CNPs were observed to exhibit a reversible oxidation state switching between +3 and +4. Band gap values were computed from the optical absorption data. The changes in the band gap values observed were attributed to the changes in the oxidation state of CNPs as opposed to the quantum confinement effects, as expected in other nanoparticle systems. The work

presented in this dissertation demonstrates, with evidence, that in order to obtain a comprehensive understanding of the properties of nanoscale materials it is of paramount importance to monitor their behavior over relatively longer periods of time under various ambient environments.

While the solution based techniques offer a versatility and low cost route to study the fundamental properties of nanomaterials, they suffer some inherent problems such as precursor contamination and uncontrolled chemical reactions. Especially when analyzing the behavior of ceria-based materials for applications like solid oxide fuel cells, a great control in the density and crystalline quality are desired. In order to achieve this, as a first step pure ceria thin films were synthesized using oxygen plasma assisted molecular beam epitaxy (OPA-MBE). The ceria films were analyzed using various *in situ* and *ex situ* techniques to study the crystal structure, growth mode and epitaxial quality of the films. It was observed that the epitaxial orientation of the ceria films could be tuned by varying the deposition rate. When the films were grown at low deposition rate (< 8 Å/min) ceria films with epitaxial (200) orientation were observed where as the films grown at high deposition rates (up to 30 Å/min) showed (111) orientation. Theoretical simulations were used to confirm some of the experimental facts observed in both nanoparticles and thin films.

ACKNOWLEDGEMENTS

I take this opportunity to express my sincere gratitude to all the teachers who bestowed the knowledge upon me at various levels. I am grateful to Prof. Sudipta Seal, my major advisor for this doctoral dissertation work. From the very first day I joined his group in 2004, Dr. Seal has provided me the opportunities to improve my core competency, aptitude, oral and written communication skills. I am fortunate to have received an opportunity to work with two more excellent mentors Drs. Donald R Baer and Theva Thevuthsan. I strongly believe that the interaction with this trio and the training I have received under their mentorship will definitely give me an edge over others with similar credentials as mine. I could knock their door without much hesitation at any time and get the information or clarifications I needed. I think it is appropriate to thank Ajay along with my mentors as I believe the significant amount of time Ajay and I have spent in discussing and arguing (?) with each other on the scientific aspects is the key behind the progress we have made in understanding the unique properties of CNPs. I am thankful to my seniors Drs. Debasis Bera, Swanand Patil, Vishwanathan Venkatachalapathy and Sameer Deshpande, from whom I have received my preliminary hands on training on various instruments and learnt the basics of doctoral research. I should also thank the scientists in the Interfacial and Nanoscale Science Facility at the Environmental Molecular Sciences Laboratory (EMSL). Specially, Drs. Shuttha Shutthanandan, Nachimuthu Ponnusamy, Mark Engelhard, Chongmin Wang and Scott Lea have been really helpful for me throughout my stay in EMSL. I sincerely thank my dissertation committee members (Drs. D.R. Baer, S. Thevuthasan, R. Kumar, H. Heinrich, H.J. Cho

Materials Society and the American Ceramic Society for providing opportunities to present my research in their annual technical meetings. I appreciate the financial support from the UCF-SGA, graduate studies for participating in these events.

I would like to thank Waheeda, Karen, Cindy, Kari, Judy and Arlene at UCF and Barbara, Heather and Shannon at EMSL for their administrative support during the course of my Ph.D. They have been really helpful to me with various administrative aspects. I should also thank the engineers in the materials characterization facility (MCF) at UCF and the crafts support in EMSL. I also thank the UCF-editor Nathalia for her help in making this dissertation more readable by providing proper formatting suggestions.

While most of the above people have helped me in technical aspects, there is another set of people who have been with me during the time of my doctoral studies. I would like to thank my friends and room mates in Orlando and Richland. Especially, I would like to thank Mahadevan, Vikas, Satyajeet, Mohanthy, Prakash, Vaidy, Naveen, Rajesh, and Sita. Although not with me physically the moral support from my friends Veerababu, Anjan, Ramesh and Krutika was very important.

I would also like to take this opportunity to thank my mentor, teacher Prof. Mohan and his wife Mrs. Lakshmi Mohan for their continuous support from my IIT days and I owe them a lot for being with me and for their blessings. I would like to acknowledge the encouragement given by Prof. Bhargav (Andhra University, INDIA) for pursuing

materials research during my undergraduate program. I would like to express my sincere gratitude to Prof. Y. Hanumantha Rao (YHR) my chemistry teacher and others from intermediate days (high school). I should thank Mr. J. Kumaraswamy and other family friends for their support throughout my career. I thank the "Syndicate Bank, India" for providing me with an education loan to start the doctoral studies in United States of America.

I am not sure how to thank or what are the appropriate words to express my gratitude to my mother, father, siblings and other family members. My mother, father and brother have made a lot of sacrifices to see me achieve this milestone. I strongly trust, what ever I have achieved today is because of their prayers and blessings for me.

While working on this acknowledgement document, I have realized a great fact. Although my name will be appended with a Ph.D. and a doctoral degree is conferred upon me, I think my part in reaching this stage is very minute and it is only possible because of the incredible and invaluable contributions of all the people I mentioned here and many others who did not get acknowledgements. Hence, I bow my head at the lotus-feet of the supreme master and the almighty for taking the form of all these people and being with me forever.

TABLE OF CONTENTS

LIST OF TABLES

CHAPTER 1: INTRODUCTION

The quest for improving the performance of materials in various functional applications and the enthusiasm to mimic Nature to produce ultra-strong, highly versatile and low cost materials has been the major driving force in the past decade of materials research. Various groups across the globe have obtained a significant control over the size, shape, self-assembly composition and physico-chemical properties of "metallic materials". However, the same is still in its infancy when it comes to the functional oxides. Use of fluorite structured oxides (e.g. ceria and zirconia) for fast ion conduction in solid oxide fuel cells (SOFCs), as catalyst supports and, lately, in bio-medical applications makes the understanding of their size, shape and structural evolution of paramount importance. It is already established that energetically and topologically favored structures are needed to properly utilize various properties of these materials. Despite the significant attention and numerous publications devoted to nano-sized materials, the physics and chemistry which influence their properties are sometimes not fully explored. Understanding and controlling the properties of nanoscale materials remains a significant challenge to the scientific community across the globe [1, 2].

1.1 Organization of the Dissertation

The main focus of this dissertation is the room temperature, wet chemical synthesis of CNPs (NPs) and their aging and environment dependent variations in their size, shape, self-assembly and chemistry. Emphasis in the latter part is devoted to studies on molecular beam epitaxy (MBE) based growth of pure and doped ceria thin films, tuning

of their orientation, and vacancy engineering through dopants to understand the mechanism of oxygen ion conductivity.

Different chapters in this dissertation are reproductions (partial or complete) of various publications resulting from the author's research work during the course of his doctoral studies at the Surface Engineering and Nanotechnology Facility in the Advanced Materials Processing and Analysis Center at the University of Central Florida, Orlando, FL-USA and the Environmental Molecular Sciences Laboratory at the Pacific Northwest National Laboratory, Richland, WA-USA [Proper citations are included as appendix at the end of the document]. Sometimes, the publications are edited to suit the format of the dissertation and to provide context-based emphasis on various topics.

The main focus of this dissertation is to "probe and tune the size, shape (morphology), self-assembly, structure, and chemistry of nano-materials as a function of time (aging time), and environment (solvent, additives and synthesis conditions). Before going to the heart of the topic, a general overview on some of the fundamental aspects of nano-scale materials and a summary of features of interest in nanoceria will be provided in the following sections.

1.2 Fundamentals of Nanostructured Materials
 "There is plenty of room at the bottom", the 1959 visionary statement [3] of the legendary Richard Feynman is being realized in less than half a century by consistent efforts and significant contributions from the scientific community across the globe.

Progress made in past few decades has resulted in a myriad of newer classes of materials proving the ability to tune matter as a whole for achieving exciting technological advancement for the benefit of mankind. From the invention of carbon fullerene structures, carbon nanotubes by Ijima [4] and the equally important discovery of inorganic fullerene structures by Tenne [5], there have been numerous reports that discussed the fundamental and technological importance of novel nanostructured materials.

1.2.1 Significance of Nanostructured Materials

The word "nano" was just a metrics that indicates one billionth of a unit quantity until recently; however, it is now a publicly known term that is redefining the understanding of matter at an extraordinary pace every day. Nobel Prize-winning inventions of bucky balls and carbon fullerene structures, the first electron microscope image of carbon microtubules, later called as carbon nanotubes (CNTs), followed by the invention of inorganic fullerenes and anisotropic nanostructures, can be termed as major breakthroughs in the field of nanoscience and technology. Synthesis of size and shape-controlled nanostructures (triangles, cubes, tubes, wires, rods, and fibers), their self-assembly, properties, and possible applications are under rigorous research. Realizing the potential importance of nanotechnology, state–of-the-art research and development centers with excellent processing, characterization, and device fabrication facilities are being developed by national and state governments, private institutions and corporations.

A number of reviews and text books have been published on nanoscience and nanotechnology, endorsing the status of the 21st century's leading science and technology

based on fundamental and applied research during the last few decades [6-20]. The significantly different physical properties of these novel materials have been ascribed to their characteristic structural features between isolated atoms and bulk macroscopic materials [12]. "Quantum confinement", the most popular term in the nano world, is essentially due to the changes in atomic structure as a result of the direct influence of the ultra small length scale on energy band structure. The exceptional electronic, mechanical, optical, and magnetic properties of the nanoscale materials can all be attributed to the changes in the total energy and structure of the system. In the free electron model, the energies of the electronic states and the spacing between energy levels both vary as a function of $1/L^2$, with L being the dimension in a given direction [21]. At nanoscale dimensions the normally collective electronic properties of the solid become severely distorted, and the electrons at this length scale tend to follow the "particle in a box" model, which might often require higher order calculations to account for band structure [21]. The electronic states are more like those found in the localized molecular bonds than the macroscopic solids. The main implication of such confinement is the change in the system total energy; and hence the overall thermodynamic stability. For example, Cr with a body centered cubic (BCC) structure was reported to be stable in the A15 structure at nanoscale and high purity conditions and in a bcc structure in presence of oxygen impurity [13]. The chemical reactivity, being a function of the system structure and the occupation of the outermost energy levels, will be significantly affected at such a length scale, causing a corresponding change in the physical properties. Recently, size dependant variation in the oxidation state and the lattice parameter has been reported by

4

our group in cerium oxide nanoparticles [22]. Combination of both "bottom up" and "top down" approaches has been efficiently used in producing the functionally important nanoscale materials and the devices [23, 24].

1.2.2 Structural Aspects

When the dimensions of a system are reduced to the nanoscale domain, the number of atoms at the surface significantly increases along with the increase in surface area per unit volume.

Specific Surface Area = $\dfrac{4\Pi r^2}{\dfrac{4}{3}\Pi r^3 \rho} = \dfrac{3}{\rho r}$; hence when the dimensions decrease from micron-level to nano-level, the specific surface area increases by 3 orders in magnitude. In such a case, large proportions of the atoms will either be at or near the grain boundaries [12]. While the increase in surface area and the surface free energy lead to a reduction in the inter-atomic distance for metals, the opposite was reported for semiconductors and metal oxides. Various morphologies obtained in the nanostructures can be explained through multiple twinned crystalline particles and the relative surface energies of various crystallographic planes. The dislocations in nanostructures might not be the thermodynamically stable defects; higher internal compressive strains and reduced vacancy concentration are the characteristics of nanostructures. These factors were reported to contribute towards deviations in the mechanical properties of the nanomaterials and an inverse Hall–Petch relation is under rigorous investigation [25]. Another aspect of controversy is the phase stability in systems like tetragonal zirconia. While a clear understanding exists in case of the bulk system, the same has stimulated a

noteworthy debate in the case of undoped nanocrystalline zirconia [26]. It was concluded that among various parameters such as nano size, strain induced grain-growth confinement, simultaneous presence of monoclinic phase [27], the oxygen ion vacancies stabilize the tetragonal phase at room temperature in the nanocrystalline system.

1.2.3 Electronic Transport Properties

The characteristic electronic properties of the nanostructures are a result of tunneling currents, purely ballistic transport, and coulomb blockade effects. As the dimensions of the system become comparable to the de Broglie wavelength of the electrons, energy bands may cease to overlap. However, owing to their wave-like nature, electrons can tunnel quantum mechanically between two closely adjacent nanostructures. If a voltage is applied between two nanostructures, which aligns the discrete energy levels, resonant tunneling occurs abruptly, increasing the tunneling current. When all the scattering centers are eliminated due to the extremely small size of the material and purely specular boundary reflections resulting from smooth sample boundaries, the electron transport becomes purely ballistic. This particular behavior can be used in wave guide applications. Conduction in highly confined structures is very sensitive to the presence of other charge carriers and their charge state. These coulomb blockade effects result in conduction processes involving a single electron. The requirement of a very small amount of energy for such conduction can be utilized in operating switches, transistors, or memory elements.

1.2.4 Medicine and Biosciences

Significant numbers of nanophase materials and nanoscale systems for biological applications and the use of biological precursors for the synthesis and property enhancement of the nanoscale materials are under extensive investigation. One major example is the bio-mineralization of nanocrystallites in a protein matrix, which is highly important for the formation of bone and teeth. Chemical storage and transport mechanisms within the organs are also fields of major interest. Biomimicry is the process of using biological systems as a guide to synthesize nanoscale materials. Using such systems was found to impart precision and selectivity to the nanostructures synthesized. In addition to the aforementioned aspects, biocompatibility of textured implants, cellular engineering, medical sensors, and drug delivery are among the various important fields of interest in the "nano–bio" regime [28]. In most of these applications, it is mandatory to have a stable dispersion of the particles with controlled size and physico chemical properties [29].

1.2.5 Characterization

From the aforementioned arguments and the experience from the dealing with bulk materials, it is evident that an appropriate characterization will play a crucial role in determining various properties. Three broadly approved aspects of characterization are

    A. Morphology

    B. Chemistry

    C. Crystal structure

Various techniques that can be used to identify the above mentioned features and the corresponding resolutions are illustrated in Figures 1.-3 [30].

7
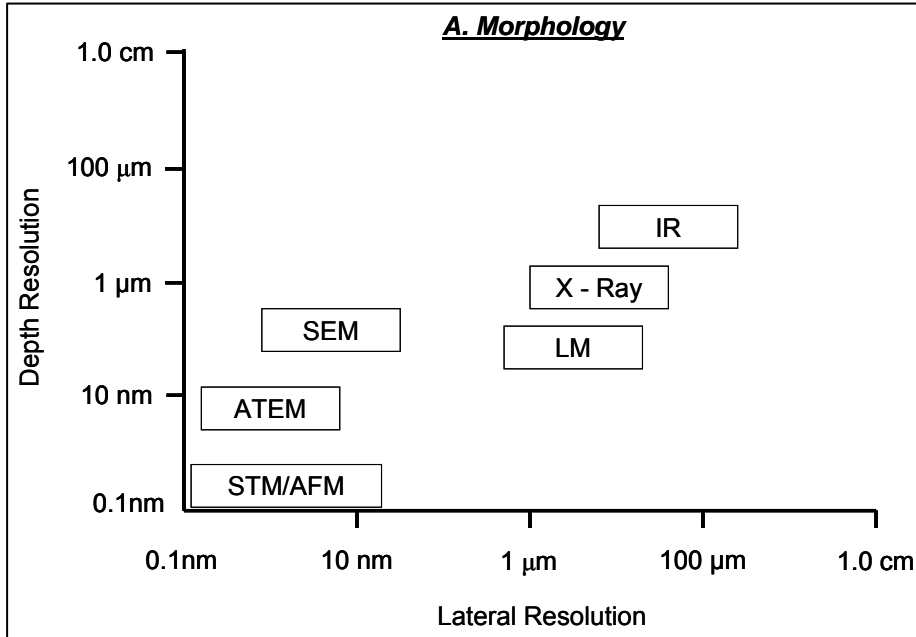
Figure 1. Various techniques used to characterize the morphology of materials and their corresponding depth and lateral resolution.
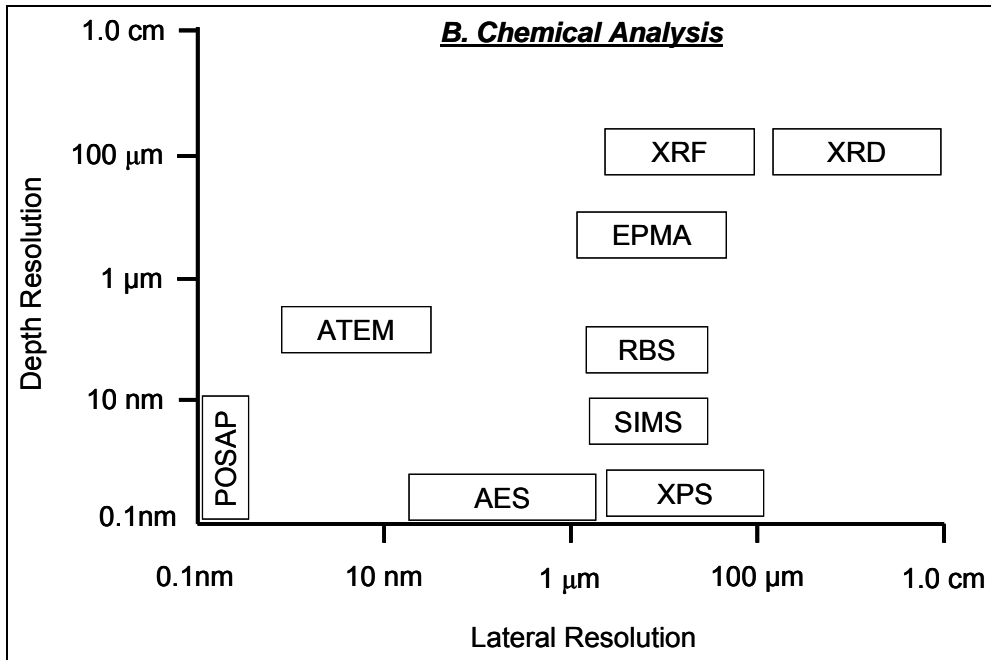
Figure 2: Various techniques used to characterize the chemistry of materials and their corresponding depth and lateral resolution
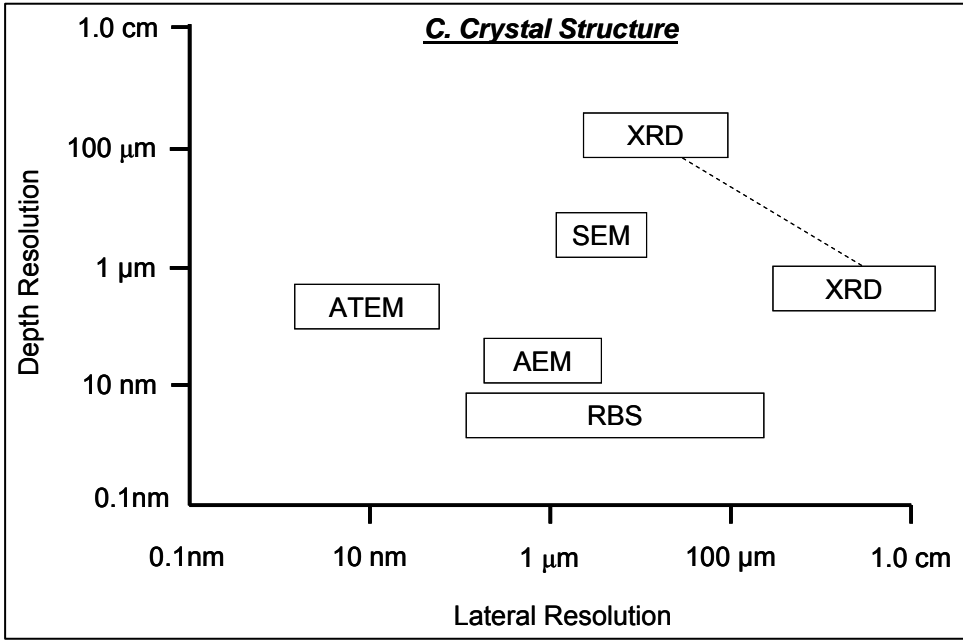
Figure 3: Various techniques used to characterize the crystal structure of materials and their corresponding depth and lateral resolution.

<u>1.2.5 Applications</u>

Field emission devices for x-ray instruments, flat panel displays and other vacuum nanoelectronic applications are some examples where nanotechnology has already been introduced. Nanotechnology has become indispensable for applications such as probes for biological and chemical separation, sensors and their purification, catalysis, energy storage, and composites for structural materials, filling materials, and coatings. During the last two decades, tremendous research efforts have been dedicated to understand the properties of nanomaterials, which are of utmost importance for advanced applications. The properties of nanomaterials can be tailored to numerous engineering applications via atomic-level structural control of materials. However, the real challenge lies in the integration of nanostructured materials into the devices and retaining nanostructures in bulk components.

1.3 Synthesis of Nanostructures

It is well appreciated across the disciplines, both fundamental sciences and engineering technologies, that the ultimate performance of any device or material is purely based on its structure, composition, electronic configuration, and valence states of the cations or anions (in case of compounds). These aspects direct the fundamental structural building blocks which in turn are scaled-up according to the need. While both bottom-up [building larger objects with smaller building blocks, i.e. using atomistic synthesis methods] and top-down [using the bulk materials to produce nanoscale objects, i.e. using methods such as sever plastic deformation] have been widely used for nanoscale materials synthesis; a significant emphasis is dedicated to the bottom-up approach. The versatility offered by

the bottom-up approach stems from the ability of the synthesis techniques to offer a blend of atomic scale control and ease of formation at various scales as desired.

Among the various techniques explored, soft-chemistry or wet chemical methods have been established to engineer the materials with specific characteristics based on the basic structural units. The soft-chemical methods offer economic, high yield, easy to adopt, and environmentally benign methodologies to synthesize nanoparticles that can be scaled-up if necessary. However, they suffer from incorporation of chemical impurities from precursors, insufficient control on the reaction kinetics. In some cases, the purity of the final products may have to be compromised. However, some of these aspects can be overcome when the synthesis is undertaken carefully. The soft-chemistry techniques, initially introduced by the French solid-state chemists Rouxel and Livage in 1970s, are no more confined to a well-defined area of science but are accepted widely as novel methodologies to tailor materials with desired chemistry, morphology and dimensions of interest.

In a quite contrasting note, often deemed as a very expensive technique, molecular beam epitaxy (MBE) is known to provide very high quality materials (nano-scale thin films and clusters) with atomic scale precision in structure, chemistry and morphology. Initially, the technique has been widely used for the synthesis of semiconductor materials for various fundamental studies. Of late, oxygen plasma-assisted molecular beam epitaxy (OPA-MBE) has evolved as an ideal technique for developing high quality epitaxial oxide

materials [31]. The high quality epitaxial, highly oriented films provide an ideal material platform to understand the fundamental characteristics of the materials in various state-of-the-art technological applications such as SOFCs, spintronics, and high-T_c -superconductors. For example, epitaxial ceria and zirconia-based oxide thin films, solid electrolytes for SOFCs, are seen as ideal materials for mechanistic understanding of oxygen ion conductivity. Although the technique may not be ideal for bulk production of electrolyte materials for SOFCS, a clear understanding of the mechanisms from these high purity single crystal materials and the use of materials produced from economic bulk techniques (soft-chemistry) can be viewed as an ideal marriage of various bottom-up approaches for the nano-scale materials synthesis. Hence, this dissertation focuses on both soft-chemistry and OPAMBE techniques to synthesize nanoceria and understand its characteristic features.

1.4 Cerium Oxide (ceria, CeO₂) Nanoparticles

Nano-ceria (nCeria) is among the frequently studied oxides because of current and potential uses as a catalyst [32], as an electrolyte in SOFC technology [33, 34], and for UV-blocking applications [35]. Chemical-mechanical planarization and solar cells [36] are among the newer applications where the nanoceria particles may have an impact. Our group has recently shown the ability of CNPs to protect retinal cells (*in vivo*) from reactive oxygen species (ROS) and to protect human breast-line cells from radiation damage during cancer treatment by mimicking superoxide dismutase (SOD) activity [37, 38]. Among various applications, our group at UCF demonstrated that nanoscale oxide

materials have better performance, ranging from traditional applications like oxidation resistance coatings [39, 40] to mind-probing and the most sensitive biological applications. Various collaborative research projects are investigating the effect of nCeria particles in different applications, such as cell longevity [41], radiation protection [38], neuroprotection in retinal cells [42], and free radical scavengers [43].

1.5 Doped Ceria as SOFC Electrolyte Material
High efficiency, minimal pollution, and wide choice of fuels have made SOFCs a promising alternative energy converter (or transducer). There has been a quest for viable replacements to yttria-stabilized zirconia (YSZ) as electrolyte to reduce the current operating temperature of fuel cells (from approximately $\leq 1000^{o}C$) thereby improving the overall economics of the SOFCs. Among the various possibilities, the fuel cell community has appreciated the potential of doped ceria as a low and intermediate temperature fuel cell electrolyte. Both theoretical and experimental works have established the higher oxygen ionic conductivity in the intermediate temperature range with the aliovalent-doped ceria. Since nanomaterials have demonstrated altered and in many cases enhanced properties compared to bulk materials in general, doped ceria nanostructures have the potential to enhance ionic conductivity in comparison to the bulk material. In these conductors, migration barriers to bulk diffusion and vacancy-dopant interaction are the key parameters that control the activation energy for oxygen ion diffusion. The vacancy-dopant interaction is represented by the association energy of vacancy dopant clusters, which is a result of the electronically delicate balance between elastic and electrostatic interactions. In addition to reducing the activation energy for

14

oxygen ion diffusion, dopants should also ensure negligible electronic conductivity, and chemical and structural integrity of the base material. Samarium (Sm) was proven as the best dopant for ceria [44].

In contrast to the traditional powder-processed electrolytes, high quality single crystal films and hetero junctions are excellent SOFC electrolytes to understand fundamental behavior. In general, thin film electrolytes demonstrate higher ionic conductance due to thickness reduction [45, 46]. In the nanoscale thin film regime, higher ionic conductivities could be realized by using multilayered films and multilayered hetero structures [47, 48]. Also, previous and ongoing research in the Interfacial and Nanoscale Science facility of the W.R. Wiley Environmental Molecular Sciences Laboratory has proven that the use of multilayered doped ceria/zirconia electrolytes can enhance the overall conductivity of the electrolyte [47]. This was attributed to the asymmetric interfacial segregation of the dopant, domain boundaries, misfit dislocations and the strain associated with the hetero junctions. Another major factor that controls the conductivity is the individual layer thickness in a multilayered system. It is thought that there is an optimum individual layer thickness above or below which the conductivity will be lower. The highest conductivity values in these multilayered nanostructures are likely to be governed by nanoscale effects. While the higher thicknesses might avoid semi-infinite space charge effects, ultra low thicknesses may lead to significant effects stemming from the lack of uniformity and associated problems. In addition to these aspects, a major parameter that controls the properties of oxygen-plasma assisted MBE

grown films is the substrate temperature during growth. The growth temperature not only decides the crystallinity of the film, but also the overall quality. In general well-oriented single crystal films show enhanced ionic conductivities in comparison to their polycrystalline counterparts.

The key property of nano-Ceria in either the traditional applications or in the nano-bio regime is their ability to effectively switch between the +3 and +4 oxidation states. While the UHV techniques like MBE help in understanding the behavior of highly pure materials, solution based techniques help large scale production and low cost processing for various applications. Hence, it is quite interesting to simultaneously study the material properties under different conditions. For successful application and integration of these materials in industrial products, it is imperative to study the size, shape, structure and chemistry under different storage conditions, such as various temperatures, presence and absence of polymers, and stabilizing agents.

REFERENCES

1. Billinge, S.J.L. and I. Levin, The problem with determining atomic structure at the nanoscale. Science, 2007. **316**(5824): p. 561-565.

2. Campbell, C.T., S.C. Parker, and D.E. Starr, The effect of size-dependent nanoparticle energetics on catalyst sintering. Science, 2002. **298**(5594): p. 811-814.

3. Feynman, R., There is plenty of room at the bottom. Eng. Sci, 1960. **23**(22).

4. Iijima, S., Helical microtubules of graphitic carbon. Nature, 1991. 354(6348): p. 56., Iijima, S. and T. Ichihashi, Single shell carbon nanotubes of 1-nm diameter. Nature, 1993. 363: p. 603.

5. Tenne, R., Fullerene-like structures and nanotubes from inorganic compounds. Endeavour, 1996. 20(3): p. 97.

6. Wang, Z.L. and C. Hui, eds. Electron Microscopy of Nanotubes. 2003, Kluwer Academic Publishers.

7. Baraton, M.-I., ed. Synthesis, Functionalization and Surface Treatments of Nanoparticles. 2003, American Scientific Publishers.

8. Yang, P., ed. The Chemistry of Nanostructured Materials. 2003, World Scientific Publishing Co. Pvt. Ltd.

9. Koch, C.C., Nanostructured Materials - Processing, Properties, and Applications. Materials Science and Processing Technology Series, ed. G.E. Macguire and S.M. Rossnagel. 2002.

10. Rao, C.N.R., et al., Inorganic nanowires. Progress in Solid State Chemistry, 2003. **31**(1-2): p. 5.

11. Xia, Y.N., et al., One-dimensional nanostructures: synthesis, characterization, and applications. Adv. Mater., 2003. **15**: p. 353.

12. Suryanarayana, C., The structure and properties of nanocrystalline materials: Issues and concerns. JOM-Journal Of The Minerals Metals & Materials Society, 2002. **54**(9): p. 24-27.; Suryanarayana, C., Nanocrystalline Materials. International Materials Reviews, 1995. **40**(2): p. 41-64.; Suryanarayana, C., Recent Developments in Nanostructured Materials. Advanced Engineering Materials, 2005. **7**(11): p. 983-992.

13. Suryanarayana, C. and C.C. Koch, Nanocrystalline materials - Current research and future directions. Hyperfine Interactions, 2000. **130**(1-4): p. 5-44.

14. Gleiter, H. and P. Marquardt, Nanocrystalline Structures - An Approach To New Materials. Zeitschrift Fur Metallkunde, 1984. **75**(4): p. 263-267.

15. Gleiter, H., Nanostructured materials: State of the art and perspectives. Nanostructured Materials, 1995. **6**(1-4): p. 3-14.

16. Gleiter, H., Nanostructured materials: Basic concepts and microstructure. Acta Materialia, 2000. **48**(1): p. 1-29.

17. Gleiter, H., Nanocrystalline materials. Progress in Materials Science, 1989. **33**(4): p. 223.

18. Vishwanathan, V., et al., Challenges and Advances in Nanocomposite Processing Techniques. Mater. Sci. Eng. R, 2006, **54**(5-6), p: 121-285

19. Drake, C., et al., Fundamental Insights of Sensing Mechanism in Metallic Nanostructure based Sensors. International Materials Reviews, 2007, **52,** p. 289-317.

20. Cavaleiro, A. and J.T.M. De Hosson, Nanostructured Coatings. 2006, New York: Springer - Science.

21. Law, M., J. Goldberger, and P. Yang, Semiconductor nanowires and nanotubes. Annual Review of Materials Research, 2004. **34**(1): p. 83-122.

22. Deshpande, S., et al., Size dependency variation in lattice parameter and valency states in nanocrystalline cerium oxide. Applied Physics Letters, 2005. **87**(13).

23. Barth, J.V., G. Costantini, and K. Kern, Engineering atomic and molecular nanostructures at surfaces. Nature, 2005. **437**(7059): p. 671.

24. Yin, Y. and A.P. Alivisatos, Colloidal nanocrystal synthesis and the organic-inorganic interface. Nature, 2005. **437**(7059): p. 664.

25. Song, H.W., S.R. Guo, and Z.Q. Hu, A coherent polycrystal model for the inverse Hall-Petch relation in nanocrystalline materials. Nanostructured Materials, 1999. **11**(2): p. 203.

26. Shukla, S. and S. Seal, Mechanisms of room temperature metastable tetragonal phase stabilization in zirconia. International Materials Reviews, 2005. **50**(1): p. 45-64.

27. Oleshko, V.R., et al., High-resolution and analytical TEM investigation of metastable-tetragonal phase stabilization in undoped nanocrystalline zirconia. Journal Of Nanoscience And Nanotechnology, 2004. **4**(7): p. 867-875.

28. Coombs, R.R.H. and D.W. Robinsons, eds. Nanotechnology in Medicine and Biosciences. 1996, Gordon and Breach: New York.

29. Kuchibhatla, S., A.S. Karakoti, and S. Seal, Colloidal stability by surface modification. Journal of Materials, 2005. **57**(12): p. 52-56.

30.Kelsall, R., I. Hamley, and M. Geoghegan, eds. Nanoscale Science and Technology. 2005, John Wiley & Sons Ltd.

31. Chambers, S.A., Epitaxial growth and properties of thin film oxides. Surface Science Reports, 2000. **39**(5-6): p. 105-180.

32.Fu, Q., H. Saltsburg, and M. Flytzani-Stephanopoulos, Active Nonmetallic Au and Pt Species on Ceria-Based Water-Gas Shift Catalysts. Science, 2003. **301**(5635): p. 935-938.; Campbell, C.T. and C.H.F. Peden, Chemistry - Oxygen vacancies and catalysis on ceria surfaces. Science, 2005. **309**(5735): p. 713-714.

33.Stambouli, A.B. and E. Traversa, Solid oxide fuel cells (SOFCs): a review of an environmentally clean and efficient source of energy. Renewable & Sustainable Energy Reviews, 2002. **6**(5): p. 433-455.

34.Shao, Z.P. and S.M. Haile, A high-performance cathode for the next generation of solid-oxide fuel cells. Nature, 2004. **431**(7005): p. 170-173.

35.Tsunekawa, S., T. Fukuda, and A. Kasuya, Blue shift in ultraviolet absorption spectra of monodisperse CeO_{2-x} nanoparticles. Journal of Applied Physics, 2000. **87**(3): p. 1318-1321.

36.Corma, A., et al., Hierarchically mesostructured doped CeO_2 with potential for solar-cell use. Nature Materials, 2004. **3**(6): p. 394-397.

37.Chen, J., et al., Rare earth nanoparticles prevent retinal degeneration induced by intracellular peroxides. Nature Nanotechnology, 2006. **1**(2): p. 142-150.

38.Tarnuzzer, R.W., et al., Vacancy engineered ceria nanostructures for protection from radiation-induced cellular damage. Nano Letters, 2005. **5**(12): p. 2573-2577.

39. Patil, S., S.C. Kuiry, and S. Seal, Nanocrystalline ceria imparts better high-temperature protection. Proceedings of the Royal Society Of London Series A-Mathematical Physical and Engineering Sciences, 2004. **460**(2052): p. 3569-3587.

40. Patil, S., et al., Synthesis of nanocrystalline ceria particles for high temperature oxidation resistant coating. Journal Of Nanoparticle Research, 2002. **4**(5): p. 433-438.

41. Strawn, E.T., C.A. Cohen, and B.A. Rzigalinski, Cerium oxide nanoparticles increase lifespan and protect against free radical-mediated toxicity. Faseb Journal, 2006. **20**(5): p. A1356-A1356.

42. Chen, J., et al., Nanoceria particles confer neuroprotection in retinal cells in vitro. Investigative Ophthalmology & Visual Science, 2005. **46**.

43. Callahan, P., et al., Deleterious effects of microglia activated by in vitro trauma are blocked by engineered oxide nanoparticles. Journal of Neurotrauma, 2003. **20**(10): p. 1057-1057.

44. Andersson, D.A., et al., Optimization of ionic conductivity in doped ceria. Proceedings of the National Academy of Sciences of the United States of America, 2006. **103**(10): p. 3518-3521.

45. Saraf, L., et al., Oxygen transport studies in nanocrystalline ceria films. Journal of Materials Research, 2005. **20**(5): p. 1295-1299.

46. Maier, J., Space-Charge Regions in Solid 2-Phase Systems and Their Conduction Contribution .3. Defect Chemistry and Ionic-Conductivity in Thin-Films. Solid State Ionics, 1987. **23**(1-2): p. 59-67.

47. Azad, S., et al., Nanoscale effects on ion conductance of layer-by-layer structures of gadolinia-doped ceria and zirconia. Applied Physics Letters, 2005. **86**(13).

48. Wang, C.M., et al., Distribution of oxygen vacancies and gadolinium dopants in ZrO_2-CeO_2 multi-layer films grown on alpha-Al_2O_3. Solid State Ionics, 2006. **177**(15-16): p. 1299-1306.

CHAPTER 2:
SIZE, SHAPE AND SELF-ASSEMBLY OF CNPS

Self–assembly is recognized as one of the major experimental strategies for the development of nanostructure ensembles [1]. A wide spectrum of morphologies such as rods [2, 3], tubes [4], spheres [5], cubes [6], and stars [7], have been reported. The existing reports on self-assembly have relied upon preformed patterns, soft or hard templates for attaining desired morphology and dimensions [8]. Growth of a set of crystallographic planes can be achieved using preferentially attached surfactant molecules. Time dependent size, shape and stability of oxide nanostructures are of fundamental and technological interest. Cerium oxide is one of the widely studied oxide materials for chemical mechanical planarization [9], solid oxide fuel cells [10], environmental catalysts [11], oxidation resistance coatings [12], and recently in bio-medical applications [13-17]. Unsurprisingly such vast applications of cerium oxide have been aptly supported by wide research and literature along with synthesis characterization and application of nano cerium oxide particles (CNPs). Variation in the lattice parameter of cerium oxide as a function of size, dopant concentration and the formation of nanorods of ceria through supramolecular assembly of micelles were reported recently [2, 18, 19]. The existing literature lacks understanding as well as reports of template free self-assembly of CNPs in simple solvent systems such as water and glycols.

As part of this dissertation work, CNPs were synthesized (see 2.1.2) using environmentally friendly (green), room temperature, wet-chemical methods. The size, shape and self-assembly of CNPs were monitored as a function of time at different

23

temperatures and local environments. While sections 2.1 and 2.2; deal with the room temperature aging of the CNPs, section 2.3 deals with the effects of aging under frozen conditions. Significance of various aging conditions and the role played by various environments has been discussed in detail. A detailed HRTEM analysis of the structures obtained at different aging periods have been analyzed using both online and offline analysis techniques. An effort has been made to explain the underlying mechanisms that drive the final configuration. MD simulations have been used to validate the experimental observations.

2.1 Hierarchical Assembly of Inorganic Nanostructure Building Blocks to Octahedral Superstructures– A True Template Free Self-assembly

A systematic study of the morphological evolution of cerium oxide nanostructures as a function of time is presented in this chapter. CNPs were synthesized in poly(ethylene glycol) (PEG) based solvents (S1). It was realized that the nanoparticles agglomerate through a hierarchical assembly to form octahedral superstructures with time. The system was studied for two years, and after a number of iterations, we imputed the morphology formation to the inherent structural features of cerium oxide and the ease of attaining low energy configuration. HRTEM studies revealed the formation of octahedral superstructures from a non-specific initial morphology, after 1-3 weeks of aging, Figure 4. The agglomeration behavior of CNPs in the absence of the polymer additives was simultaneously analyzed as a reference system.

It is evident from Figure 4(a) that the 15-20 nm agglomerate in freshly prepared solution has no specific morphology. Selected area diffraction pattern in the inset (Figure 4(b))

confirms the fluorite structure of ceria (fm3m, JCPDS -34-0394). The 20 %PEG solution

was found to contain agglomerates of 50 – 70 nm with polyhedral morphology when

aged at room temperature for one week. However, no specific morphology was found in

the nanoparticles synthesized in the absence of PEG. The samples were aged at room

temperature for 8 weeks and analyzed using HRTEM. The presence of individual 3 – 5

nm CNPs constituting the agglomerates up to tens of nanometers was observed. While

the water-based system precipitated after 3-4 weeks and exhibited irregularly faceted

polyhedral agglomerates (S2), the 20 %PEG suspension was found stable with polyhedral

structures of well defined edges, corners and faces, Figures 4 c, e, f, g). The polyhedral

structures were aligned in specific patterns on the TEM grids (S3).
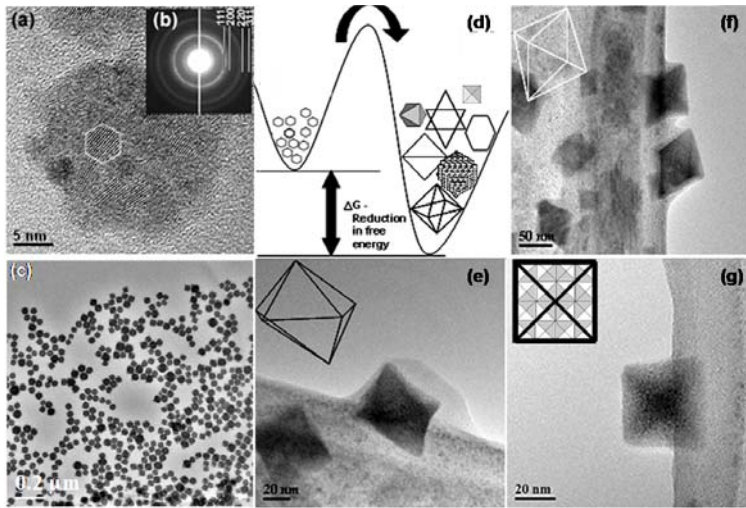
Figure 4: HRTEM image of a) a representative high magnification image showing the
individual particle of ~5 nm constituting the bigger agglomerate; b) SAED pattern
confirming the fluorite structure of ceria; c) well-dispersed polyhedral structures after 2
weeks of aging d) block diagram showing the reduction of energy through agglomeration
of individual octahedral crystals; HRTEM images of polyhedral ceria agglomerates at
different angles to the beam; e, f) agglomerates clearly showing the faces, edges and
corners of the polyhedral structure, and g) top view image of the polyhedral structure
showing 4 triangular faces converging at an apex. Insets in e, f, g show the schematics of
the octahedral shape at different angles.

After a detailed analysis of images collected at various tilt angles, Figure 5, the polyhedral structures were confirmed as octahedral superstructures formed through a hierarchical assembly of individual octahedral building blocks (3 − 5 nm) (S4). Initially, the ability of PEG to impart controlled conformation to the agglomerates was thought to be the driving force behind these polycrystalline octahedral assemblies. Uekawa et al [20] have reported the synthesis of monodispersed spherical CNPs in presence of PEG without any long term stability studies. The single crystal polyhedral ceria particles with octahedral morphology are reported in the literature. [21, 22] The {111} planes were proven to be the most stable through MD simulations. Irrespective of the starting seed, the final 3 − 10 nm particles were reported to be {111} octahedra or [23] truncated {111} octahedra [21]. However, the existing literature lacks any long term stability studies in this system. We use the analogy from the previous experimental results and geometric models proposed to explain the mesostructured assemblies to investigate the octahedral superstructures [8, 24]. We hypothesize the formation of hierarchically assembled octahedral superstructures to be a multistage process. First, the individual octahedral (3 − 5 nm) nuclei agglomerate to form 15 − 20 nm agglomerates through dynamic self-assembly. The agglomerates in the freshly prepared samples (Figure 4a) lead to a specific polyhedral shape by the realignment of the individual building blocks in the agglomerate with due course of time (Figure 4c) [1]. The equilibrium between the agglomerated and the non-agglomerated parts of the system drives the second stage through an oriented hierarchical assembly, leading to larger octahedral super-structures. We envision the process to follow the models proposed by Liu et al [8, 24] for mesostructured silicates.

26

Patterned and non-patterned slides were utilized to heterogeneously grow various morphologies through self similar growth of silicates. The morphologies of superstructures were reported to vary with the composition of the precursors. The nanoceria octahedra in our study fall under the quartet octahedron model proposed by Liu et al [24]. The primary ceria building blocks are the octahedra of $3 - 5$ nm and they further grow to secondary and tertiary octahedra through oriented assembly, Figure 5. When two building blocks with adsorbed PEG or water come together, the capillary forces between them facilitate the solvent removal and strengthen the agglomerate through van der Walls forces [25]. The role of Ostwald ripening in the later stages of the superstructure formation cannot be ignored. The inset 4(g) is a top view model of the hierarchical assembly corresponding to the HRTEM image shown in Figure 4(g). A precise model depicting the possible route of hierarchical assembly is shown in Figure 5 [8, 24]. In an attempt to find the role of PEG, the precipitates from the water-based ceria have been analyzed after 4 and 8 weeks of ageing after re-dispersing them in the solution. Sharp edged octahedra were found in the HRTEM analysis, scaling up to 200 nm along with a few nonuniform polyhedra. This clearly indicates that the morphology can be attained without PEG. Hence, the initial proposition that "the PEG is driving the morphology is revised", and it only plays a role in enhancing the kinetics and stabilizing the sol. This can be ascribed to the reduced interfacial energy and the ability of PEG to assist the intra-agglomerate alignment. Also, the nonpolar PEG coating quickly facilitates the inter – agglomerate interaction, whereas the same is not true for particles suspended

in water [26]. The enhanced stability of the CNPs in a PEG-based system is a result of higher viscosity and lower dielectric constant of the solvent (S5).
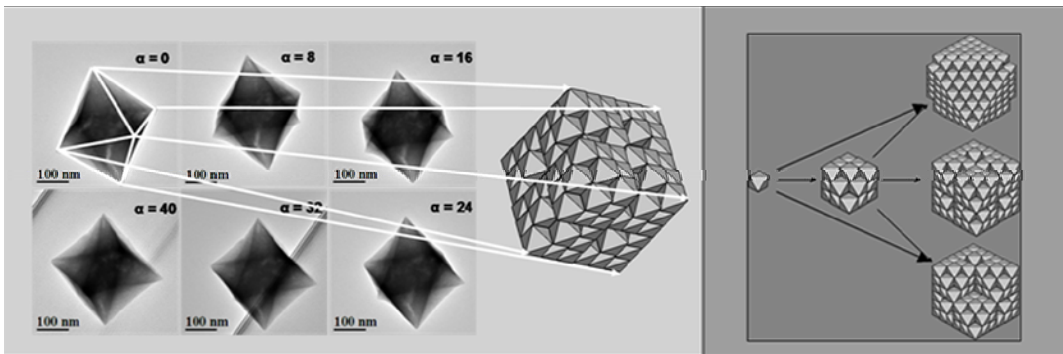
Figure 5: (left) HRTEM Images at various tilt angles, the edges and corners of the 2-D image are mapped to the edges and corners of the octahedral superstructure. The agglomerate upon tilting at various angles elucidates the octahedral geometry (right) proposed mechanism of superstructure formation

Hence, we propose that the octahedral hierarchical assembly of the CNP is inherent to the ceria system. Our preliminary experiments using other synthesis media also support the same. Further, the variation in the oxidation states of the Ce as a function of aging, and synthesis medium is studied using UV-Vis. The Ce 4+ oxidation state was found to reduce and almost disappear as a function of time. The variation in oxidation state is useful in biomedical applications to impart protection from reactive oxygen species [13-17]. Both the PEG and water based ceria systems have shown ~ 0% transmission in the UV – B and UV – C (310 – 210) regions, making our solutions ideal for the UV blocker applications (S6). In this chapter we presented a simple, economic, room temperature method for the preparation of hierarchically assembled octahedral superstructures from nanoscale building blocks without any template or external driving forces. Proposed

dynamic self-assembly also emphasizes the importance of long-term ageing on the nanoparticles.

REFERENCES

1. Whitesides, G.M. and B. Grzybowski, Self-assembly at all scales. Science, 2002. 295(5564): p. 2418-2421.

2. Kuiry, S.C., et al., Spontaneous Self-Assembly of Cerium Oxide Nanoparticles to Nanorods through Supraaggregate Formation. J. Phys. Chem. B, 2005. 109(15): p. 6936-6939.

3. Vantomme, A., et al., Surfactant-Assisted Large-Scale Preparation of Crystalline CeO_2 Nanorods. Langmuir, 2005. 21(3): p. 1132-1135.

4. Ye, C., et al., Zinc Oxide Nanostructures: Morphology Derivation and Evolution. J. Phys. Chem. B, 2005. 109(42): p. 19758-19765.

5. Ewers, T.D., et al., Spontaneous Hierarchical Assembly of Rhodium Nanoparticles into Spherical Aggregates and Superlattices. Chem. Mater., 2005. 17(3): p. 514-520.

6. Lee, C.H., et al., Ambient Pressure Syntheses of Size-Controlled Corundum-type In_2O_3 Nanocubes. J. Am. Chem. Soc., 2006. 128(29): p. 9326-9327.

7. Yamamoto, M., et al., Synthesis and Morphology of Star-Shaped Gold Nanoplates Protected by Poly(vinyl-2-pyrrolidone). Chem. Mater., 2005. 17(22): p. 5391-5393.

8. Tian, Z.R., et al., Shape-Selective Growth, Patterning, and Alignment of Cubic Nanostructured Crystals via Self-Assembly. Nano Lett., 2003. 3(2): p. 179-182.

9. Feng, X., et al., Converting Ceria Polyhedral Nanoparticles into Single-Crystal Nanospheres. Science, 2006. 312(5779): p. 1504-1508.

10. Andersson, D.A., et al., From the Cover: Optimization of ionic conductivity in doped ceria. PNAS, 2006. 103(10): p. 3518-3521.

11.Fu, Q., H. Saltsburg, and M. Flytzani-Stephanopoulos, Active Nonmetallic Au and Pt Species on Ceria-Based Water-Gas Shift Catalysts. Science, 2003. 301(5635): p. 935-938.

12.Patil, S., S.C. Kuiry, and S. Seal, Nanocrystalline ceria imparts better high-temperature protection. Proceedings of The Royal Society Of London Series A-Mathematical Physical And Engineering Sciences, 2004. 460(2052): p. 3569-3587.

13.Callahan, P., et al., Deleterious effects of microglia activated by in vitro trauma are blocked by engineered oxide nanoparticles. Journal of Neurotrauma, 2003. 20(10): p. 1057-1057.

14.Chen, J., S. Seal, and J.F. McGinnis, Inorganic Nanoparticles Prevents Light-Induced Blindness in Rats. Invest. Ophthalmol. Vis. Sci., 2006. 47(5): p. 4848-.

15.Chen, J., et al., Nanoceria Particles Confer Neuroprotection in Retinal Cells in vitro. Invest. Ophthalmol. Vis. Sci., 2005. 46(5): p. 186-.

16.Ellison, A., et al., Engineered oxide nanoparticles protect against cell damage associated with in vitro trauma. Journal of Neurotrauma, 2003. 20(10): p. 1105-1105.

17.Tarnuzzer, R.W., et al., Vacancy engineered ceria nanostructures for protection from radiation-induced cellular damage. Nano Letters, 2005. 5(12): p. 2573-2577.

18.Deshpande, S., et al., Size dependency variation in lattice parameter and valency states in nanocrystalline cerium oxide. Applied Physics Letters, 2005. 87(13).

19.Patil, S., et al., Role of trivalent La and Nd dopants in lattice distortion and oxygen vacancy generation in cerium oxide nanoparticles. Applied Physics Letters, 2006. 88(24).

20.Uekawa, N., et al., Synthesis of CeO_2 spherical fine particles by homogeneous precipitation method with polyethylene glycol. Chemistry Letters, 2002(8): p. 854-855.

21.Sayle, T.X.T., S.C. Parker, and D.C. Sayle, Shape of CeO_2 nanoparticles using simulated amorphization and recrystallization. Chemical Communications, 2004(21): p. 2438-2439.

22.Wang, Z.L. and X.D. Feng, Polyhedral shapes of CeO_2 nanoparticles. Journal Of Physical Chemistry B, 2003. 107(49): p. 13563-13566.

23.Adelung, R., et al., Charge density waves affected by Rb nanowire network formation on 1T-TaS2. Applied Surface Science, 2000. 162-163: p. 666.

24.Zhengrong R. Tian, J.L.J.A.V.B.M.H.X., Hierarchical and Self-Similar Growth of Self-Assembled Crystals. Angewandte Chemie International Edition, 2003. 42(4): p. 413-417.

25.Manoharan, V.N. and D.J. Pine, Building materials by packing spheres. MRS Bulletin, 2004. 29(2): p. 91-95.

26.Zaslavsky, B.Y., et al., Dielectric Properties of Water in the Coexisting Phases of Aqueous Polymeric Two-phase Systems. J Chem Soc Faraday Trans I, 1989. 85(9): p. 2857 - 2865.

2.1.2 Supporting Information
S1: Experimental Work

Cerium(III)nitrate hexahydrate (99%); Poly(ethylene glycol) (Molecular weight ~600); 30% hydrogen peroxide, and 27% ammonium hydroxide were procured from SIGMA-ALDRICH Inc. Ce(III) precursor was dissolved in PEG and DI water mixed solvents. A required quantity of 30% hydrogen peroxide was added drop wise as an oxidizer. Typical quantities of the reagents were chosen to yield 30mM ceria suspensions. 20, 50 and 100% PEG solvents were used for synthesis and the major emphasis was on the 20PEG solvent. The transparent colorless solution slowly turns pale to dark yellow indicating the formation of the cerium oxide. The ceria dispersed sol was aged at room temperature in closed glass bottles. Representative samples were taken at different time intervals: 15 min, 1 day, 1, 2, 3 and 6 weeks, etc, by dipping the carbon coated grids in ceria sol. HRTEM was used to characterize the size and shape of CNPs, (FEI TECNAI F-30). Selected area electron diffraction (SAED) patterns were collected to confirm the structure.
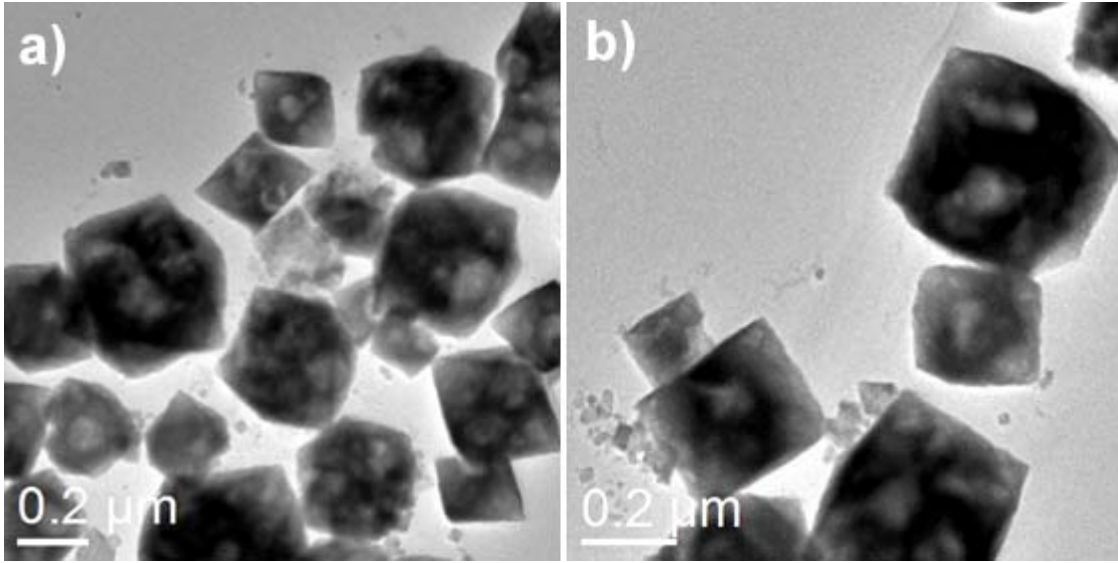
Figure S2: Precipitate from the a) water-based and b) PEG-based colloids with irregular polyhedral shapes. Significant precipitation was observed after 3-4 weeks of aging in water based system and 7-8 weeks in 20%PEG system.
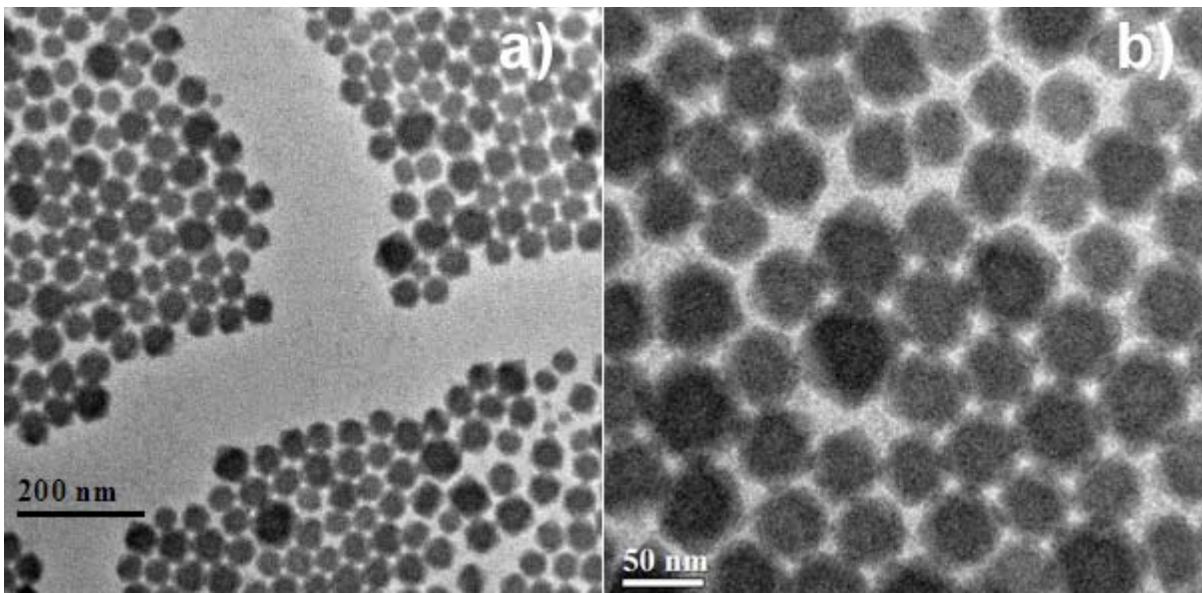
Figure S3: HRTEM images indicating the alignment of the octahedral superstructures over significant areas on the TEM grid into specific patterns. Samples were collected from the CNP suspensions aged for 2 weeks at room temperature.
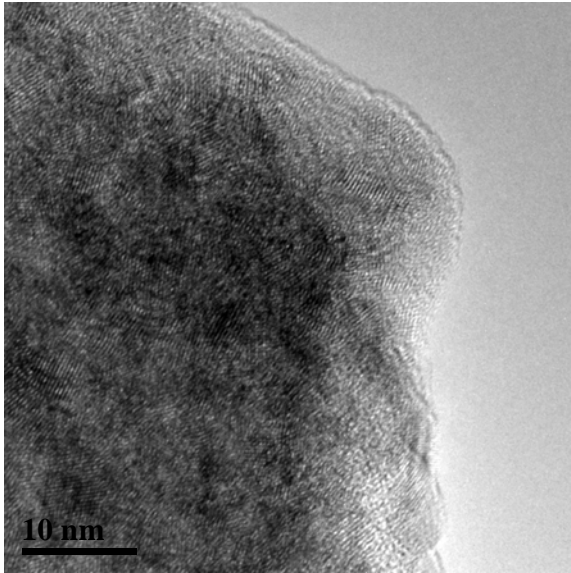
Figure S4: HRTEM image of one of the corners of an octahedral superstructure depicting that individual 3-5 nm particle size is retained in the agglomerate.

Table 1 (S5): Dielectric constant and viscosity of different solvents (room temperature)

Solvent	Dielectric constant	Viscosity, cps
DI Water	79	0.8872
PEG600	13.0	36.45
20 PEG600 + 80 DI Water	65.80	8.00
50 PEG600 + 50 DI Water	46	18.665
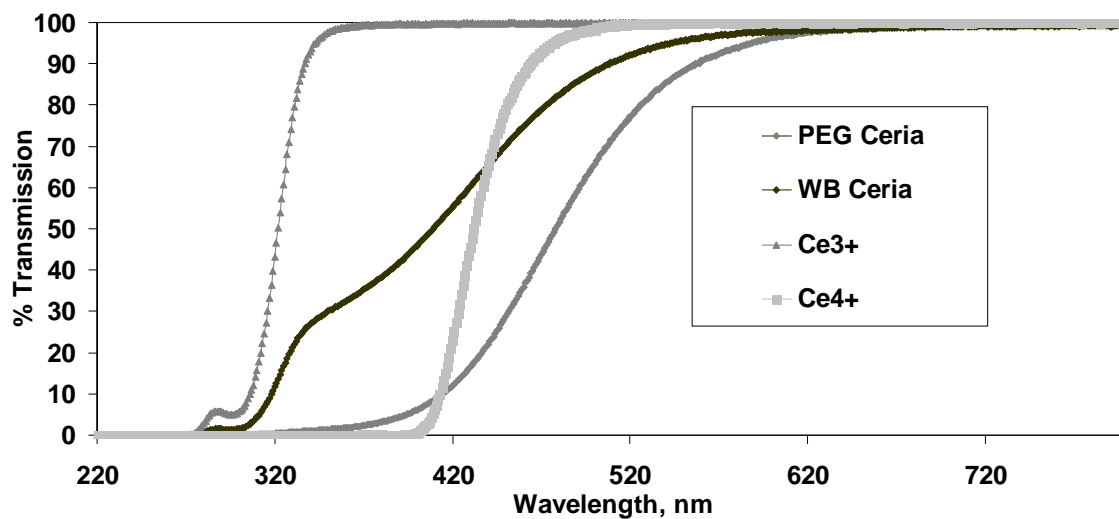
Figure S6: Comparative UV-Vis transmission plots of the 20PEG and water based ceria along with the pure Ce(III), Ce(IV) spectra. The Ce(III) spectrum has no absorption in the visible region where as the Ce(IV) has a significant absorption in both visible and UV regions.

2.2 Symmetry-Driven Spontaneous Self-Assembly of Nanoscale Ceria Building Blocks to Fractal Super-octahedra

2.2.1 Introduction

The quest for improving the performance of materials in various functional applications and the enthusiasm to mimic the nature to produce ultra-strong, highly versatile and low cost materials has been the major driving force in the past decade of materials research. Albeit a significant amount of knowledge and understanding has been gained, a wide range of aspects in the materials world are still elusive to scientists. For example, researchers are able to control the size, shape, self-assembly and properties of "metallic materials" [1]. However, the same control is still in its infancy, when it comes to the functional oxides. Use of fluorite structured oxides (ceria, zirconia etc.) for fast ion conduction in solid oxide fuel cells (SOFCs), as catalyst support and, lately, in solar cells and bio-medical applications makes the understanding of their size, shape, and structural evolution of paramount importance [2-5]. It is well established that energetically and topologically favored structures are needed to properly utilize various properties of these materials [6].

CNPs, have gained a significant attention from chemists, physicists and materials scientists due to its fundamentally and technologically interesting redox chemistry [5]. CNPs can efficiently switch between +3 and +4 oxidation states depending on the ambient conditions. It was shown that the increased defect concentration at the surface of ultra-small particles (smaller than 10 nm), can improve its performance in catalysis, solar cells and in disease treatment/prevention. Soft chemistry routes have been widely used to

39

synthesize CNPs. Several research groups, including our group, showed that the individual CNPs have octahedral and truncated octahedral morphology surrounded by {111} and {200} planes. While Sayle and co-workers have used MD simulation to examine this fact, Gunter's group used electron tomography to confirm the octahedral morphology of the CNPs [7-9]. However, most of the experimental and theoretical studies have been confined to "single crystal" ceria particles synthesized through relatively high-energy conditions. In contrast, we have synthesized the CNPs at room temperature and aged for relatively longer periods (several days to weeks), and we have observed their spontaneous self-assembly [10]. After a systematic analysis, we have proposed an appropriate model for the template free, hierarchical assembly of CNPs at room temperature: The truncated octahedral seeds of ceria preferentially assemble into secondary and tertiary structures, while retaining the octahedral symmetry through close packing similar to the growth of fractal structures. Earlier, Alvarez [11] has systematically explained the significance of various polyhedral morphologies in inorganic chemistry. It was quoted "despite the small recognition, the "superoctahedron" [an octahedron made of a number of octahedra] does exist in chemistry". However, most of these reported instances were with metallic clusters or at the atomic bonding level. For the first time we report "superoctahedra" in oxide nanostructures.

Here, we analyze the appropriateness of the proposed model through HRTEM analysis and support the findings with MD simulations. Details about the synthesis of CNPs and their time dependent hierarchical assembly can be found in the previous chapter [10]. The

HRTEM images were collected using an FEI-TECNAI F-30 system at 300 kV with a point to point resolution of 0.2 nm. Image analysis was done using the GATAN digital micrograph software. TEM images of the CNPs were collected in as-synthesized condition and at different aging times. The TEM samples were prepared by dipping a holey-carbon coated copper grid in the nanoparticles suspension. These grids were dried at room temperature in anaerobic conditions and used for imaging. Detailed methodologies of the MD simulations used in this manuscript are published previously. The simulations have successfully predicted the formation of single crystal octahedral particles of ceria, in collusion with the experimental findings [7, 12].

2.2.2 Purpose and Significance of FFT HRTEM Analysis

High-resolution electron microscopy is an indispensable technique for understanding the internal structural and morphological aspects of nanoscale materials [13]. Bright-field imaging coupled with diffraction analysis is often used to achieve this. A specimen, for BF imaging, is illuminated with a near-parallel or parallel beam of electrons, which pass through the specimen and form a magnified image below the objective lens and other imaging lenses. The amplitude and phase variations of the electron beam depend on the properties of the specimen and on the aberrations of the microscope and are recorded on a CCD camera. Even in a perfectly aligned microscope, the images acquired often suffer from a significant amount of unwanted noise either from crystalline or amorphous supports used to hold the samples [14, 15]. In case of nanoparticles prepared in solutions, the particles are collected on an amorphous holey carbon grid. This noise may create problems while analyzing the structures of nanoparticles. Furthermore, it may be very

41

tedious to work with ultra small particles to attain their individual diffraction pattern. Even with a smallest possible aperture, the area under selection may have a number of particles contributing to the diffraction pattern and may result in features not true for an individual particle. Hence, use of image processing techniques to analyze the individual nanoparticles and smaller agglomerates is an effective alternative. Image processing in the Fourier space and the inverse Fourier transforms eliminate the unwanted noise from the images. Fourier transforms of micrographs of a carbon film, when obtained live, can also be used for correcting the astigmatism of the objective lens.

Earlier, Fourier transforms of the image are similar to diffraction patterns for the imaging done under weak phase object approximation (WPOA) [1]. The intensity of the transform was calculated by Tomita et al. given by,

$$L(u,v) = \delta(u,v) + 4\sigma^2\phi^2(u,v)\sin^2\gamma * (\frac{Sin(a\pi u)}{\pi u}\frac{Sin(b\pi v)}{\pi v})^2$$

Where a, b present the dimensions of the area in which the transform is collected. δ is the delta function in two dimensions, ϕ is the Fourier transform of $\phi(x,y)$ -the phase change, u, v are the co-ordinates of the diffraction plane and σ is the interaction constant. The WPOA may not be valid in case of the small particles that result in inelastic scattering and even in some cases refraction effects. However, *Jose-Yacaman* et al [1] have later shown that the Fast-Fourier Transform (FFT) can be used for crystallographic analysis under dynamical scattering conditions also. Although, the intensities of the diffraction spots may not be equal to those obtained in the FFT, the distance between the spots in FFT is still equal to *g*. Most significant advantage offered by the FFT analysis results

42

from the ability to choose the area of interest. Even very small sizes can be chosen within an image and processed to obtain the crystallographic information in the nanoparticles, as we show later in this paper.

In as synthesized condition, CNPs were found to form 15 – 20 nm agglomerates constituted with 3-5 nm individual particles, Figure 6a, 6b. The selected area electron diffraction pattern (SAEDP) could be indexed with the ceria fluorite structure (PDF# - 034 – 0394) Figure-6a, inset. The high-magnification micrograph clearly shows that most of the lattice fringes correspond to the {111} lattice planes with a majority of the surface planes in Bragg condition. The FFT presented as inset clearly shows the preferred orientation in these primary agglomerates, as discussed later. It should be noted that the agglomerates do not have any specific morphology in as synthesized condition. When the solutions are continued to age for a week or more [10], the polyhedral structures were observed in the size range of 50-70 nm, Figure 7a. The dimension of these polyhedral structures increased up to 150 nm with further aging. Despite the larger agglomerate size, the individual building blocks remained 3 – 5 nm in size, Figure 7b. The crystallinity and preferred orientation of the polyhedra are confirmed by SAEDP (inset Figure 7a) and FFT (inset Figure 7b), respectively. Having observed the consistent evolution of the polyhedral superstructures, we have compared this morphology with existing platonic solids and it was clear from the images taken at different tilt angles that the morphology matches with the "octahedral". Following is an effort to explain why and how this "superoctahedra" form from the individual octahedral building blocks. In order to

understand the topotactic nature of the "superoctahedra", a systematic approach is adopted. First, we explain why an octahedron is a preferred morphology and what drives the formation of octahedral building blocks, then analyze the characteristics of the individual particles followed by primary agglomerates and then the agglomeration of the individual agglomerates to final structure. These analyses are further confirmed by the results from MD simulations.
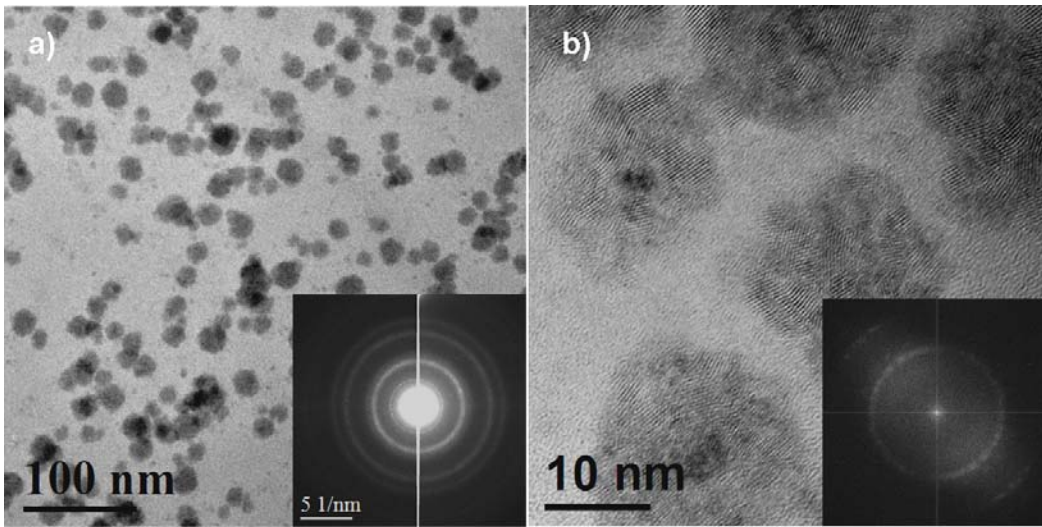
Figure 6: a) TEM images of as synthesized CNPs showing 15-20 nm agglomerates (inset) SAED pattern confirms the ceria fluorite structure (b) high resolution images with lattice fringes with 3-5 nm individual particles (inset) FFT pattern

44
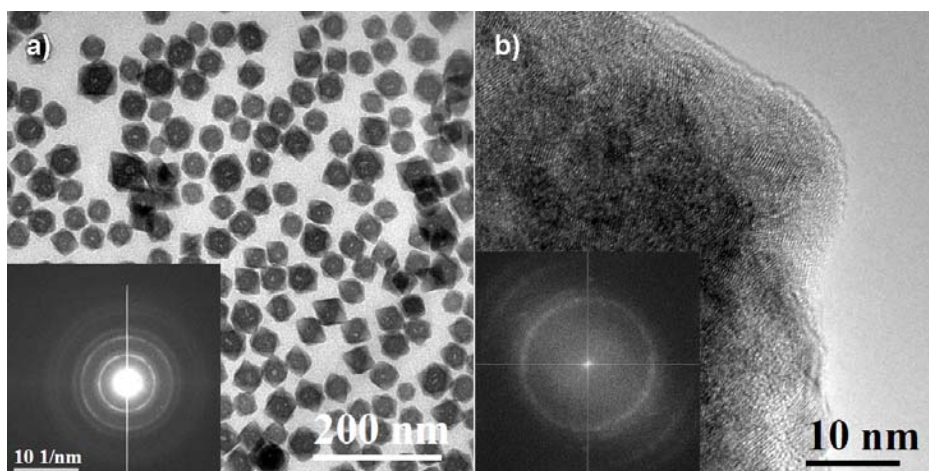
Figure 7: a) TEM images of CNPs aged for a week or longer showing ~50 nm polyhedral agglomerates (inset) SAED pattern confirms the ceria fluorite structure (b) high resolution image of a portion of the super-octahedra (inset) FFT pattern

2.2.3 Why Octahedra?

The octahedron is among the 5 platonic solids that have the maximum symmetry. The cube and the octahedron being the duals of each other and also the possibility of attaining a packing similar to cubic from octahedral packing, can be attributed to the formation of the octahedral assemblies. Whitesides et al., proposed ground rules of assembly [16] like maximal packing density, surface to volume ratio and the structural stability are implicit in such morphology evolution. In another study, Vinothan and Pine [17] have shown with the help of microspheres that the octahedral packing is one of the densest ways to assemble the structures. Octahedra are among the most energetically stable shapes and among the minimum-moment clusters. For a given volume, the surface area of the octahedron is only 18% more than that of a sphere. Given the faceted nature of the individual building blocks it is not unnatural that the final morphology is also faceted. One significant example of such a phenomenon is the fractal structure evolution.

2.2.4 How Did The Morphology Evolve?

The formation of a particular shape is purely because of the arrangement of different planes and their conformation in different energetically favorable orientations. The reason for time dependence of these shapes can be readily understood by the fact that the planes that are growing are the close packed {111} constituting the facets of the individual building blocks following the Wulff criterion. When the growth process is not complete, then the octahedron will end up as a truncated octahedron with both {100} and {111} facets constituting the surface. The individual nanoparticle with {111} and {100} facets and the schematic models of the octahedral and truncated octahedral facets are shown in Figure 8.

During the course of agglomeration, the particles try to have planes with similar inter-planar spacing at the interface to attain coherency, hence is the tendency for the {111} planes at the interface as shown in Figure 9. When two particles come together with similar planes at an angle (no specific alignment), they result in incoherent interfaces and interfacial defects. However, they will spontaneously try to align the planes to have a low-energy interface. This can be achieved by intra agglomerate rotation as presented in Figure 8(1c). The nature of the interface when two particles with aligned and mis-aligned {111} planes is also shown in Figure 8. The dotted lines help the readers visualize as a top view image of an octahedron, with the basal plane normal to the electron beam. The visualization of different planes in an individual particle constituting the agglomerates and their relative orientation could be achieved through FFT analysis. The analysis presented in Figure 10 helps avoid the redundant noise from the image and helps resolve

46

the {111} fringes in an individual particle. The inter-fringe distance could be measured by using the profile tool of the digital micrograph software, which in turn corresponds to the inter-planar spacing. The $d_{\{111\}}$ for fluorite structured ceria is ~ 0.31 nm and the Figure 10(e) confirms the same.
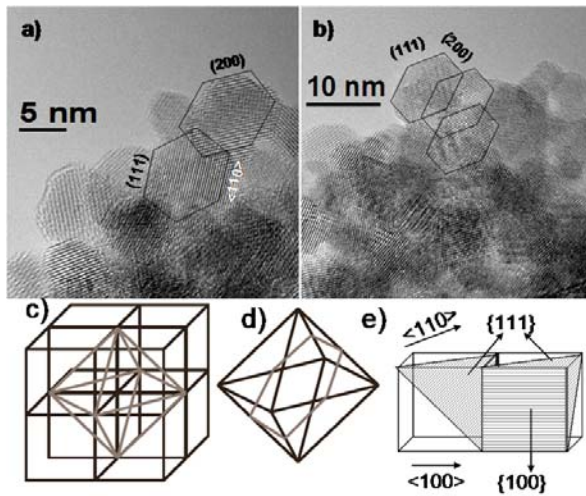
Figure 8: Different regions identified in a) and b) indicate the individual nanoparticles building blocks with octahedral symmetry enclosed by the low energy {111} {200} planes c) shows the schematic of a octahedron in a cubic cell d) shows a possible truncation plane in the octahedron that appears as a hexagon in top view e) various planes and directions of interest are identified in a cube
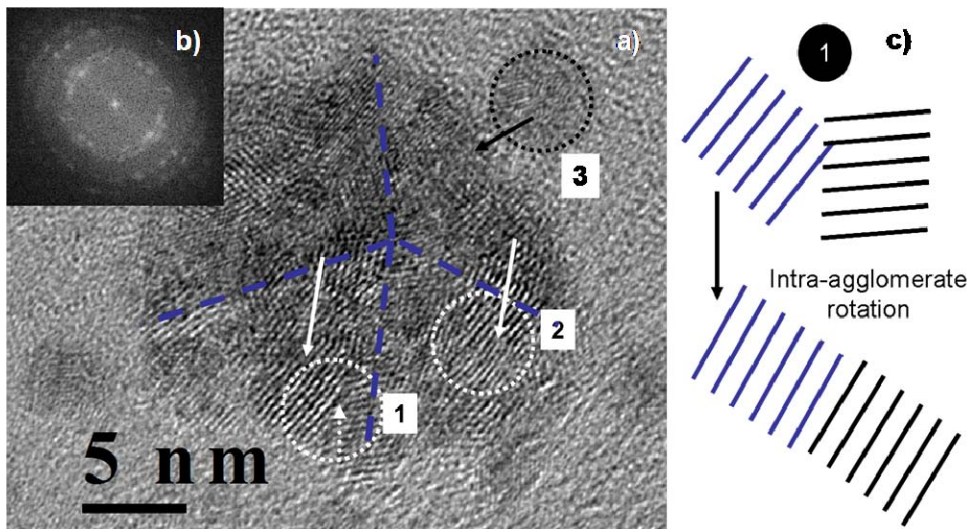
Figure 9: (a) an agglomerate of ~20 nm consisting of various smaller particles. The inset (b) is a FFT pattern of the image indicating the polycrystalline nature of the agglomerate. The (1) white dotted circle indicates two different particles coming together at an angle. This kind of interaction between two particles will result in a high-energy interface and interfacial defects (shown with a dotted white arrow in the picture). As shown in the Figure (c) the particles may undergo intra-agglomerate rotation and eventually align the planes to attain a low-energy interface (3). The black dotted circle indicates the ~3 nm size of individual constituents in the agglomerate (2), the white dotted circle shows the joining of two particles with similar planes with coherent interface, the arrow indicates an interfacial dislocation.
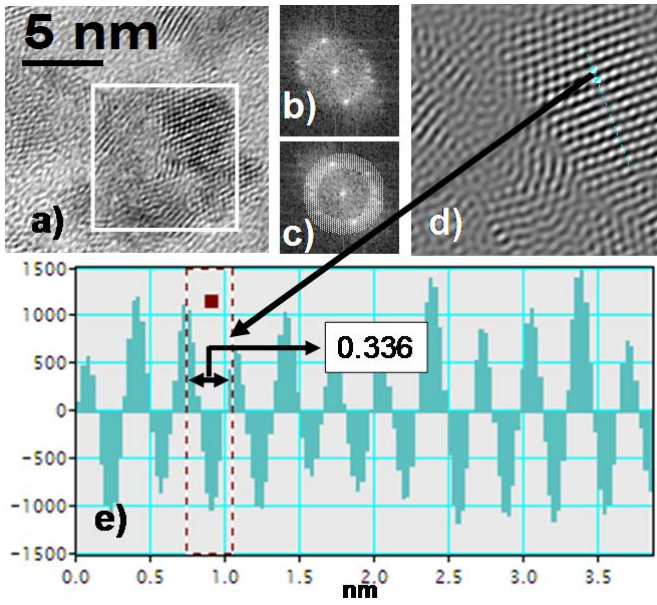
Figure 10: a) HRTEM image of the as-synthesized ceria indicating the presence of ~15 nm agglomerates constituting at least three different particles as shown in the boxed area. b) FFT of the boxed region in a) c) the masking of the diffraction circle to avoid unnecessary noise from the image and d) is the inverse FFT of the masked region. This process helps obtaining distinct lattice fringes corresponding to the planes that are properly aligned with respect to the zone axis, providing a better possibility of estimating the inter-planar spacing (d-spacing) and thereby identifying the planes. Here, the fringes correspond to the {111} planes of ceria with fluorite structure.

One important aspect that needs caution while analyzing the lattice fringes is presented in Figure 11Three different regions of a single agglomerate of CNPs with the corresponding FFT patterns are presented in Figure 11a. The region (1) shows 6 different spots (identified with dotted circles) corresponding to {111} and {220} planes. Whereas the regions (2) and (3) have two spots and no spots, respectively. This is indicative that the region (3) is completely out of alignment with respect to the <110> zone axis. When the planes are perfectly aligned with the electron beam to fall in <110> zone axis, the FFT pattern will be similar to the schematic shown in Figure 11(b).

49
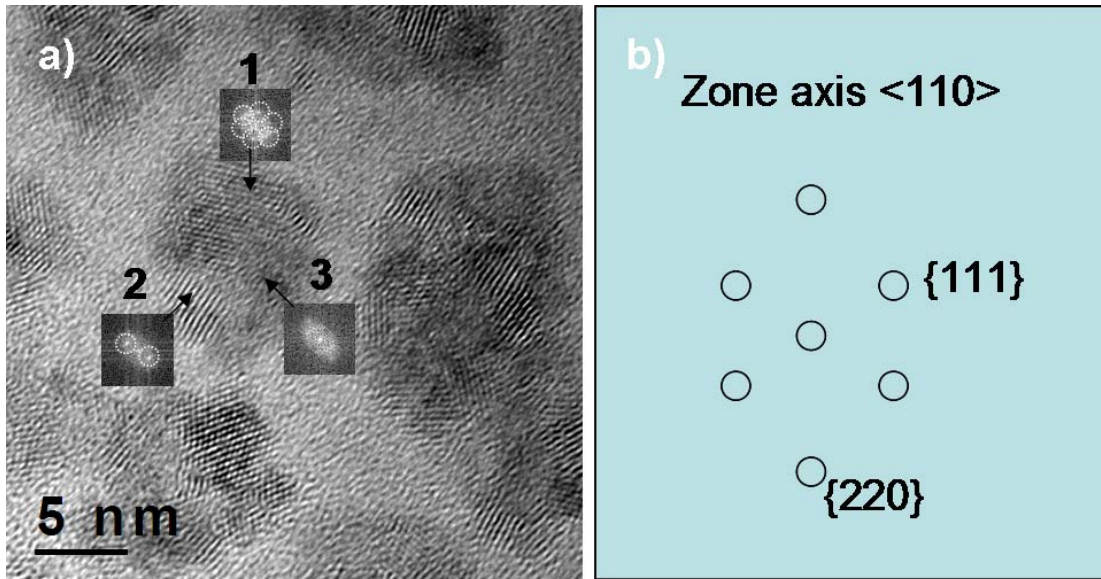
Figure 11: 1,2 and 3 are FFTs collected at three different regions of the agglomerate shown in the Figure. It is clear from the FFT and the way the lattice fringes appear that the individual particles are at different angles to the incident beam. Ideally, for a <110> zone axis in fluorite structure, the FFT should be similar to the schematic on the right side. The variation in the orientation of the grains or individual truncated octahedral building blocks is evident, which with time may re-orient to attain low interfacial energy through intra-agglomerate rotation as explained in Figure (9).

When two smaller agglomerates come together and agglomerate further forming a secondary structure, while evolving as an octahedron, some more defects may form. The strain at the interface is often relieved through formation of interfacial defects as shown in the Figure 12. It is very difficult to visualize any features or defects from the as-obtained image. However, when planes corresponding to {111} are selectively masked and a filtered image is acquired the features become evident as shown in Figure 12(b).

50

Within the agglomerate, nanoparticles are found to form twin and twist boundaries to accommodate interfacial strain.
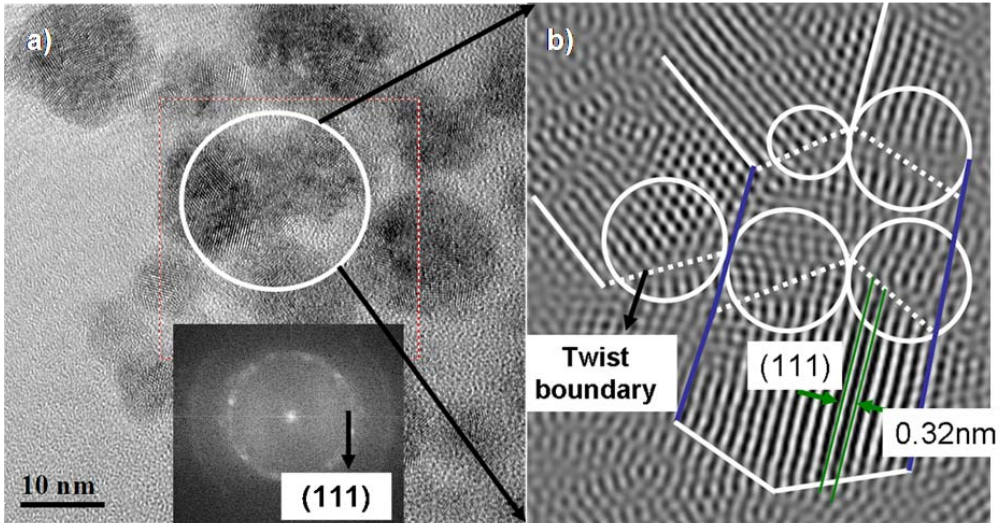
Figure 12: a) HRTEM image of the CNP agglomerates, the white circle shows at least 3 different smaller agglomerates forming a larger agglomerate and the inset is a FFT of the region marked with red-dots (b) is a Fourier filtered image formed by selectively masking the {111} planes, applying inverse Fourier transform. Various interfacial defects and inter-particle boundaries could be identified.

So far, we have seen the characteristics of the individual particles and the agglomerates. The next and most important aspect of interest is the nature of the final super-octahedron. While the low magnification micrograph (colors inverted to enhance the features) shows the 8 faces (similar to the {111} facets in single crystal octahedron), 6 corners and 12 edges, the high resolution images confirm the presence of 3-5 nm individual particles in the 50-70 nm agglomerates (Figure 13). It is also interesting to note, the FFT patterns obtained from the superoctahedra show preferred orientation.
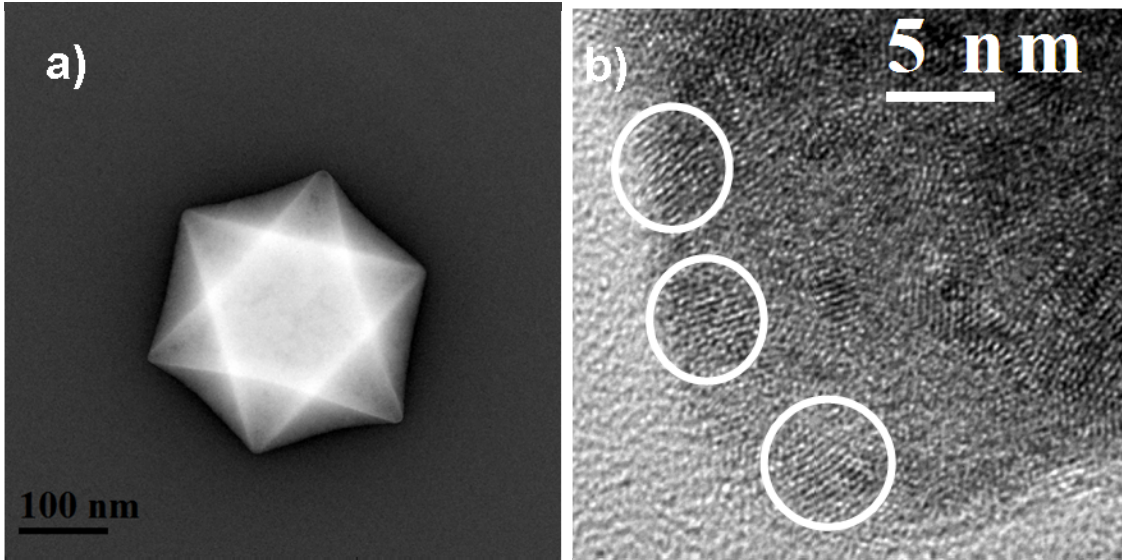
Figure 13: a) Image showing corners, faces and edges of the octahedron (colors in a BF TEM image were reversed to enhance the clarity) b) HRTEM image of a corner of the octahedron with individual building blocks of ~5nm identified with circles.

Randomly oriented, polycrystalline ceria will have a diffraction pattern as shown in Figure 14a). However, the FFT patterns of Figure 14 (c) and (e) show partial diffraction rings for the {220}, {311} planes as indentified by rectangular boxes in Figure 14 (c) and (e). Earlier Penn et al [18] have shown the preferred orientation of nanoparticles through epitaxial attachment. However, most of the observations were confined to either two or three individual particles combining together or the recrystallization of the agglomerates into a single-crystal structure. Here, we report a slightly different but significant observation, where the nanoparticles agglomerate with preferred orientation as a function of time and the super-structures continue to grow in size with the individual building blocks remaining at the same size.

52
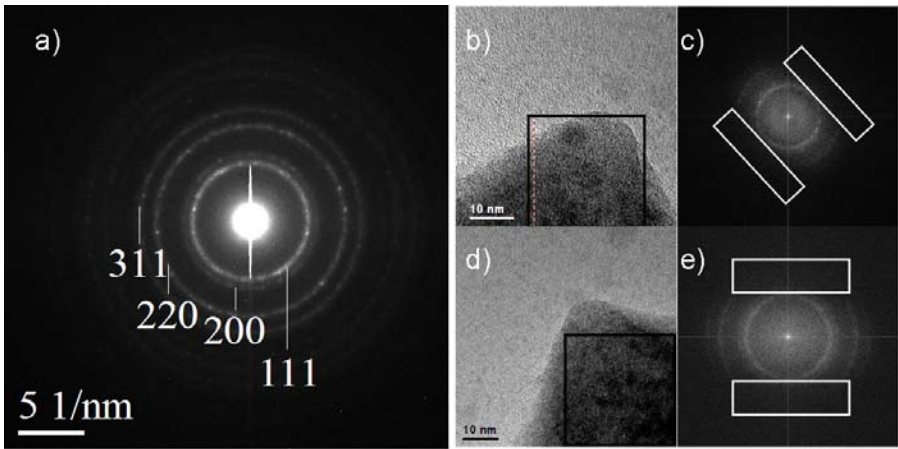
Figure 14: a) SAED pattern of an ideal polycrystalline, randomly oriented, fluorite structured CNPs, complete circles corresponding to different planes are identified in the diffraction pattern. (b) and (d) show corners of two super-octahedral structures and The FFTs of regions marked in the Figures are shown in (c) and (e).

The FFTs exhibit partial diffraction circles for the higher-order {220}, {311} planes indicating that they have some preferred orientation or the images are plagued by astigmatism. The regions identified with white rectangles show the discontinuity in the diffraction circles. However, the "super-octahedra" (middle) being polycrystalline, it is not possible to precisely determine what is that preferred orientation.

Many researchers have synthesized CNPs in the past. Most of the studies were confined to very short time periods. We, for the first time, studied the aging characteristics of the CNPs in as-synthesized condition for almost 300 days at room temperature. The realization of these fractal structures in ceria and the unique morphology was only possible because of the long-term aging studies undertaken by our group. With the increasing use of the nanoparticles in multiple applications, where they are often supplied in suspension, our findings are significant as they predict the time-dependent

agglomeration tendency of nanoparticles at room temperature in the absence of any surfactants.
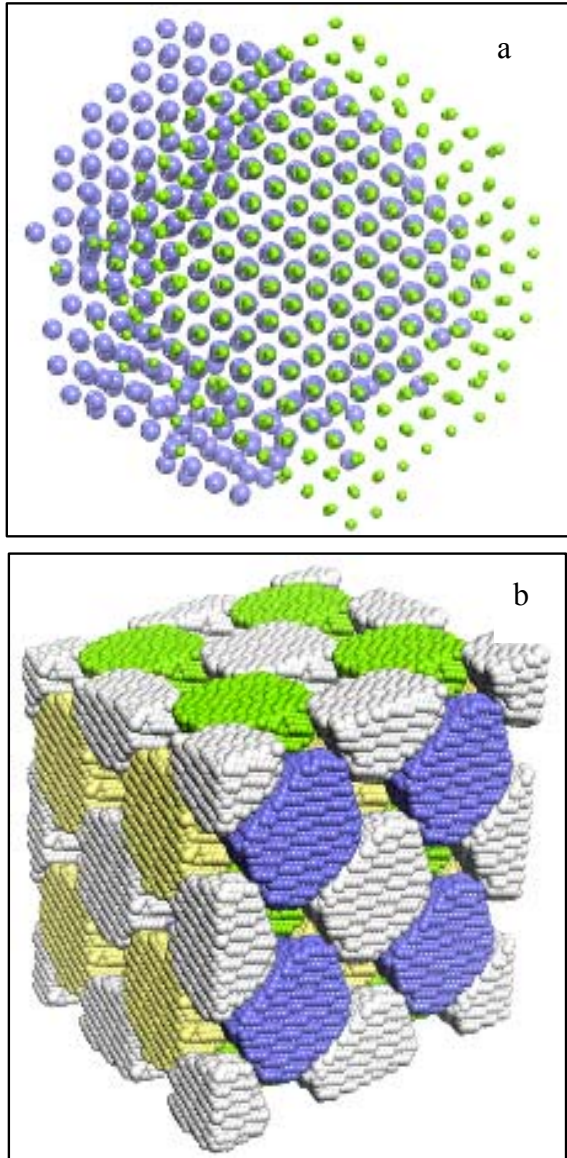
Figure 15: (a) View showing the epitaxy between the nanoparticles attached at {111} surfaces; (b) Close packed structure comprising CeO$_2$ nanocrystals (which corresponds to Figure 13a). Cerium is colored to help visualize the individual CeO$_2$ nanocrystal secondary building units.

In order to understand the agglomeration behavior of single crystalline octahedral CNPs, we have used MD simulations along with the experiments. The results of the MD simulations were found to match the experimental observations. When two nanoparticles come together they form dislocations at the interface and also try to rotate and align with time, Figure 15. When the nanoparticle building blocks were allowed to attain a low-energy configuration, they spontaneously resulted in the octahedral assembly agreeing with the experimental results.

2.2.5 Conclusions
With HRTEM and FFT analysis, we have shown that the individual building blocks of CNPs spontaneously assemble to form super-octahedral structures. The superoctahedra are shown to be a result of the fractal agglomeration of nanoscale octahedral building blocks of ceria. With the help of FFT the orientation of the nanoparticles within the agglomerates and their interfacial defects were analyzed. The nanoparticles undergo an intra-agglomerate rotation to align in a preferred direction while forming the final morphology. MD simulations have been used to confirm the experimental observations.

REFERENCES

1. Jose-Yacaman, M., M. Marin-Almazo, and J.A. Ascencio, High resolution TEM studies on palladium nanoparticles. Journal of Molecular Catalysis A: Chemical, 2001. **173**(1-2): p. 61-74.

2. Murray, E.P., T. Tsai, and S.A. Barnett, A direct-methane fuel cell with a ceria-based anode. Nature, 1999. **400**(6745): p. 649-651.

3. Chen, J., et al., Rare earth nanoparticles prevent retinal degeneration induced by intracellular peroxides. Nat Nano, 2006. **1**(2): p. 142-150.

4. Corma, A., et al., Hierarchically mesostructured doped CeO_2 with potential for solar-cell use. Nature Materials, 2004. **3**(6): p. 394-397.

5. Campbell, C.T. and C.H.F. Peden, Chemistry - Oxygen vacancies and catalysis on ceria surfaces. Science, 2005. **309**(5735): p. 713-714.

6. Feng, X.D., et al., Converting ceria polyhedral nanoparticles into single-crystal nanospheres. Science, 2006. **312**(5779): p. 1504-1508.

7. Sayle, D.C., S.A. Maicaneanu, and G.W. Watson, Atomistic models for CeO_2(111), (110), and (100) nanoparticles, supported on yttrium-stabilized zirconia. Journal of the American Chemical Society, 2002. **124**(38): p. 11429-11439.

8. Xu, X.J., et al., Reconstruction of 3D morphology of polyhedral nanoparticles. Nanotechnology, 2007. **18**(22).

9. Wang, Z.L. and X.D. Feng, Polyhedral shapes of CeO_2 nanoparticles. Journal Of Physical Chemistry B, 2003. **107**(49): p. 13563-13566.

10. Kuchibhatla, S., A.S. Karakoti, and S. Seal, Hierarchical assembly of inorganic nanostructure building blocks to octahedral superstructures - a true template-free self-assembly. Nanotechnology, 2007. **18**(7).

11. Alvarez, S., Polyhedra in (inorganic) chemistry. Dalton Transactions, 2005(13): p. 2209-2233.

12. Sayle, D.C., et al., "Simulating synthesis": Ceria nanosphere self-assembly into nanorods and framework architectures. Journal of the American Chemical Society, 2007. **129**(25): p. 7924-7935.

13. Billinge, S.J.L. and I. Levin, The problem with determining atomic structure at the nanoscale. Science, 2007. **316**(5824): p. 561-565.

14. Kirkland, E.J., Improved high resolution image processing of bright field electron micrographs : I. Theory. Ultramicroscopy, 1984. **15**(3): p. 151-172.

15. Yokota, Y., et al., Construction of an on-line system for FFT processing and analysis of atomic resolution microscopic images and its applications. Ultramicroscopy, 1981. **6**(4): p. 313-321.

16. Whitesides, G.M. and B. Grzybowski, Self-assembly at all scales. Science, 2002. **295**(5564): p. 2418-2421.

17. Manoharan, V.N., M.T. Elsesser, and D.J. Pine, Dense packing and symmetry in small clusters of microspheres. Science, 2003. **301**(5632): p. 483-487.

18. Lee Penn, R., K. Tanaka, and J. Erbs, Size dependent kinetics of oriented aggregation. Journal of Crystal Growth, 2007. **309**(1): p. 97-102.

2.3 Self-assembly of Cerium Oxide Nanostructures in Ice Moulds

2.3.1 Introduction

Nature epitomizes 'self-assembly' –living cells arranged in a myriad of complex forms and structures, acting as one particularly complex example. The challenge of synthesizing hierarchically ordered and complex structures with molecular level recognition is another example of a natural process that cannot yet be duplicated in the laboratory. Fundamental research in understanding such self-assembly of molecules has led to new strategies for synthesizing functional nanomaterials [1, 2]. Several nanomaterial structures, facilitated via self-assembly, have already been demonstrated by various researchers [3-13]. Similarities between self-assembly of nanoparticles and simple forms of life may lead to additional efforts to unravel and mimic Nature [1]. Among the multitudes of morphologies and configurations, one dimensional nanostructures (ODNS) have received significant attention from researchers, owing to their potential use in new generation electronics, photocatalysis, sensors, and biomedical applications [7].

Here, we demonstrate the self-assembly and time dependant evolution of CNPs into ultra-long polycrystalline ceria nanorods (length *ca.* 3 – 3.5 micron, diameter ca. 30 nm) using a simple water-based synthesis, freezing, and subsequent aging in ice. The mechanism we propose is effectively a natural form of templated self-assembly. Overtime in the frozen condition, particles gradually evolve into polycrystalline nanorods. Our understanding of the process involves structure templating associated with voids known to form in ice [14-16] and localized oriented attachment of CNPs. Oriented attachment and anisotropic growth of nanoparticles in solution [17, 18] are vital to the self-assembly of

polycrystalline nanoparticles in solution. Advances in MD-based simulations have enabled interesting and exciting observations in self-assembly [3, 19-21]. We used MD calculations to understand the observed aggregation process. We have recently reported the synthesis of polycrystalline ceria octahedral superstructures by self-assembly through oriented agglomeration in both water and poly(ethylene glycol) [22]. These contrast with the spherical (high index planes stabilized), single crystal CNPs synthesized by Feng et al. [23] in a high temperature gas phase reaction. Clearly, agglomeration kinetics and behavior of CNPs change with ambient conditions. Motivated by this, we have studied their aging characteristics under different conditions, including altering the solution environment and temperature. We have observed the evolution of ceria nanorods supported by the ice templates under freezing conditions. In addition to the formation of nanorods we also observe the formation of polyhedral superstructures, which appear during the freezing process.

2.3.2 Results and Discussion

In the present work, a seeding solution of CNPs was synthesized using a simple water based method by oxidizing the Ce(III) precursor salt to Ce(IV) . Several 3-5 nm crystallites nucleate and start to agglomerate within a short time frame (Figure 1a). The solution containing ceria crystallites was subjected to sub-zero temperatures (-18° C) and aged for different time scales. Crystalline CNPs agglomerate in an oriented fashion within 1 day of aging and result in rod type structures together with large faceted agglomerates (octahedral superstructures) (Figure1b, SI-1). Both the superstructures and the nanorods were constituted of truncated octahedral building blocks of CNPs [19]. The

observation of octahedral superstructure within one day of aging in ice directly contrasts the time dependent evolution of nanoparticles into polycrystalline superstructures [22]. Subsequent aging for one week facilitated long polycrystalline nanorods (Figure 16 c,d , SI-2). Retention of the initial 3-5 nm particle size, with predominant {111} surfaces, is observed even in the highly dense and polycrystalline ceria nanorods about 40 nm in diameter (SI-2). Further aging of the nanoparticles in ice (2 weeks) resulted in the formation of ultra-long ceria nanorods (Figure 16e, 16f, SI-3a,).
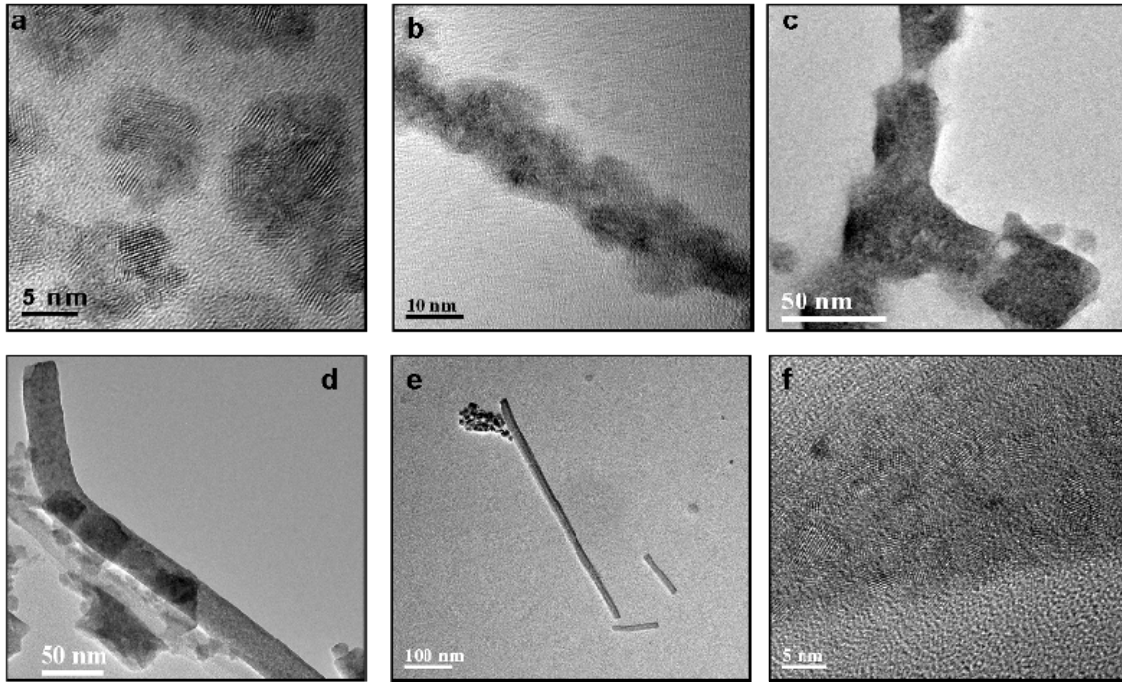
Figure 16: TEM images taken from frozen ceria solution (after melting) a) Immediately after the formation of CNPs (10-15 nm agglomerate contains of 3-5 nm ceria nanocrystals), and after freezing and subsequent aging for b) 1 day - the zigzag alignment nanoparticles into a one dimensional self assembled structure is apparent c) 1 week – initial ceria nanocrystals agglomerated in ice structure anisotropically to form long ceria nanorods d) 1 week-aged samples showing complete ceria nanorods e) 2 weeks – a long ceria nanorod (aspect ratio 1:20) formed after aging in ice f) 2 weeks - a high magnification image of the ceria nanorod of Figure 1e showing polycrystalline nature of ceria nanorods with 3-5 nm nanocrystallites. These 3-5 nm nanocrystallites are retained and serve as the building blocks for the formation of nanorods.

We propose simultaneous occurrence of two different processes during the freezing of ice, leading to the formation of nanorods along with observed octahedral superstructures. While the formation of octahedral superstructures is inherent to the process of freezing, the formation of nanorods occurs due to ice templating effect. Ishiguro et al [24] proved through both experimental and modeling studies that the "ice structure cannot accommodate foreign molecules other than water", this results in the well known "solute

rejection" phenomenon. This process is very well acknowledged by the metallurgical engineering literature for alloy solidification and zone refining kind of phenomena, where the progress of solidification front results in the rejection of impurity particles into the liquid phase. In the case of dilute ceria suspensions, as the freezing front proceeds from top to bottom, the CNPs will be expelled into the water phase. This leads to a significant increase in concentration of nanoparticles in the unfrozen sol, followed by aggregation and kinetically driven octahedral morphology evolution. The higher concentration of solute ceria particles and the increasing pressure exerted by the ice front on the water phase results in the chemico-physical process mentioned above. It is well known that the ice front will be porous with some capillaries present at the ice – water interface. The nanoparticle suspension will be absorbed into these channels due to pressure differences. Significantly higher concentration of nanoparticles results in their entrapment in these channels as the solidification continues. It was shown previously that high concentration of unfrozen brine sols were left out within channels formed during the freezing of a brine solution [25].
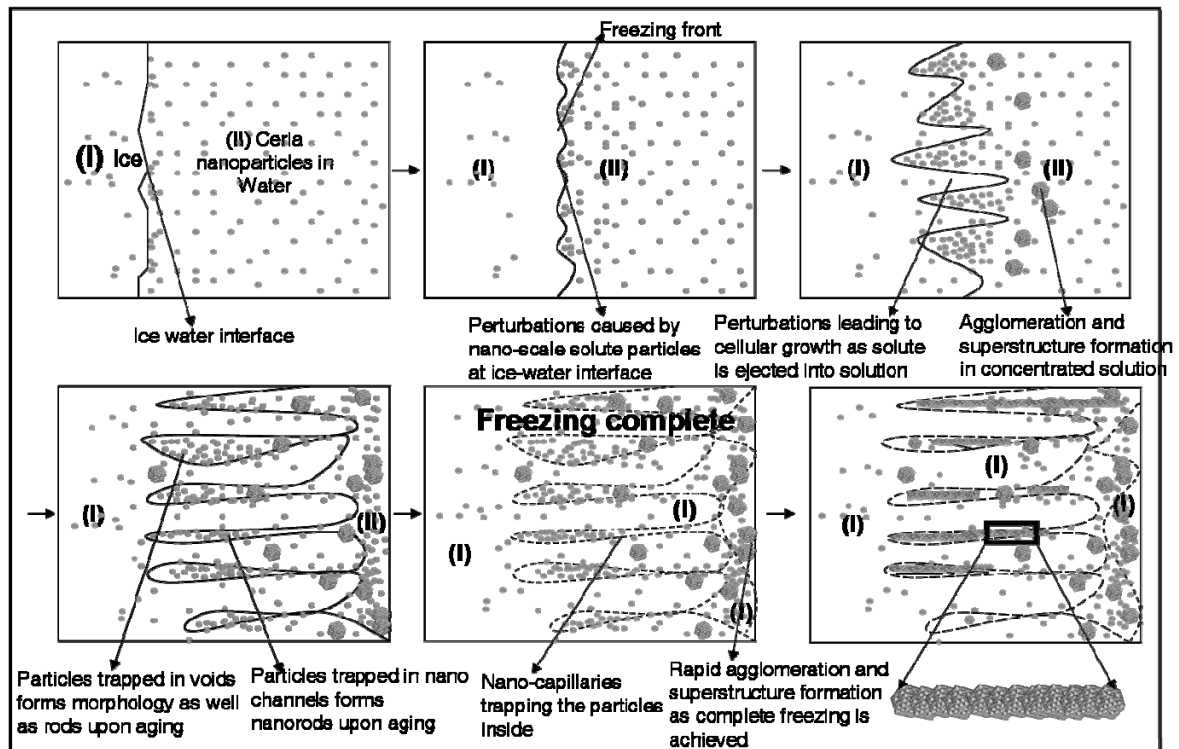
Figure 17: A systematic motion of the freezing front producing nano-voids and nano-capillaries during solidification of ice from water. The perturbations caused by the solute particle (CNPs in the present case) are assumed to be same as during the solidification of a binary alloy. However, the nanoparticles cause nano-level perturbations during the ice growth forming nano-channels in which solute particles can be trapped. Such a phenomenon is also observed during freezing of polar ice in which brine channels are formed (the brine channels are microscopic in dimension due to high concentration of salt and large size of secondary particles (25)). The rapid agglomeration of the solute which is not trapped and ejected in the remaining solution forms octahedral superstructure.

The formation of nanorods is assisted by the physical templating of ice. At -18 $^{\circ}$C under atmospheric pressure, ice conforms to the "Ice I" structural polymorph[26] and microstructural features, including nano and micro channels, evolve to accommodate the stress and expansion during solidification [27]. These channels, with nanometer diameters and a few microns in length, serve as nano-capillaries (hard templates) and the water, supersaturated with CNPs, is forced into the capillary, driven by capillary forces

emanating from the freezing front [28, 29]. The initially oriented particles are locked in the capillary under the ice pressure and undergo uni-dimensional oriented agglomeration to form ceria nanorods. It was observed that a very dilute solution and nanometer size of the particles are central to the formation of channels or capillaries. The perturbation, caused by nanoparticles at the ice and supercooled-liquid interface causes channel formation as depicted in Figure 17 (and SI-4). CNPs trapped in such nanochannels transform into nanorods with predominant {111} terminated surfaces. Specifically, particles trapped in long, nanochannels form the nanorods while those trapped in voids or wide capillaries or in the last portion of the frozen water will form octahedral superstructures. A schematic, depicting such morphological evolution, is presented in Figure 18a and b.
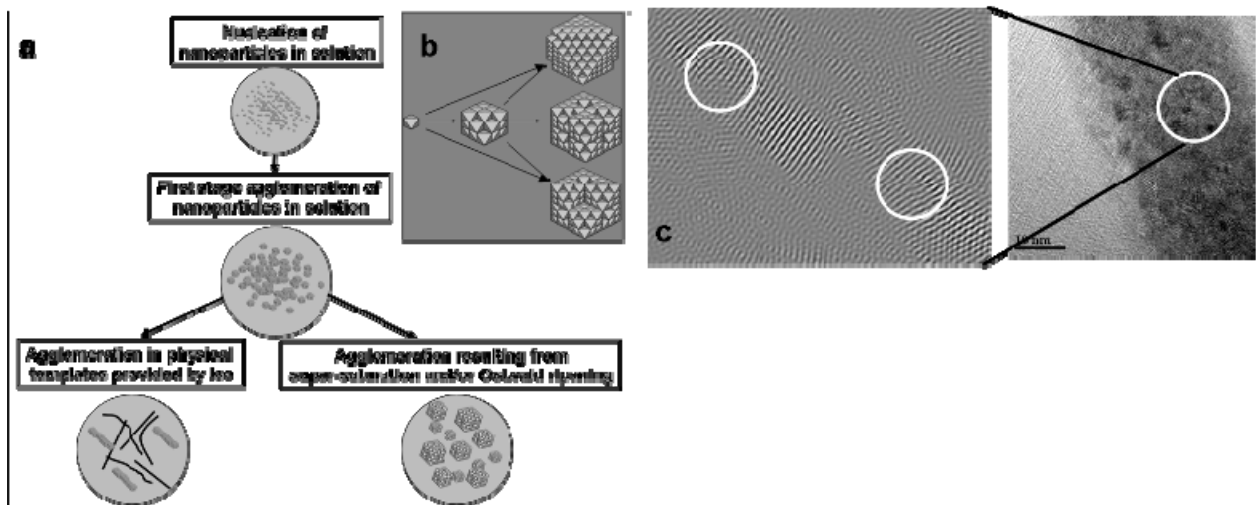
Figure 18: Schematic of the evolution of nanorods and octahedral morphology during freezing and subsequent aging of the CNPs. Initial seeds of CNPs having a truncated octahedral geometry grow in an oriented agglomeration to form truncated octahedrons during the initial stages. Upon further aging the particles trapped in ice capillaries form nanorods, while those remaining in solution during the forward motion of the freezing front agglomerate as octahedrons; b) building blocks of octahedral superstructure and

nanorods; it can be seen that the initial building block can attach via face to face or edge to edge type of attachment of different nanocrystals; c) Image generated by selected masking and inverse FFT of a high magnification image of ceria nanorods showing dislocations (circles) formed during orientation and self-assembly.

Once trapped inside the channels and surrounded by ice, the mobility of CNPs is restricted to essentially one dimension. However, the very high surface energy of the nanoparticles drives the intra – agglomerate rotation to achieve partial oriented attachment at two, three particle interfaces. Such orientation proceeds by incorporation of defects such as dislocations along the interfaces of nanoparticles as shown in Figure 18c. The white circles indicate the interfacial dislocations formed during the oriented agglomeration. Both the formation of octahedral morphologies and nanorods involve rotation and orientation of the nanoparticles to facilitate low energy configurations via coherent/semi-coherent interfaces. This can be visualized as an imperfect attachment as described in an earlier observation with titania nanoparticles [17, 18]. Higher activation energies and Brownian motion etc. are required for a full crystal rotation or recrystallization to facilitate complete coherence and formation of single crystals. However, in a time limited aggregation under freezing conditions, complete rotation is not achieved and screw/edge dislocations form at the interface between three or more orienting particles (SI-5). As three or more particles align, elastic deformation results in partial coherence together with the evolution of screw dislocations [18]. The formation of screw dislocations is also predicted by our theoretical investigation and is discussed later and shown in SI-6. Upon aging, the mis-orientation and associated dislocations are finally annihilated resulting in energetically stable interfaces.

A comparison of oriented attachment was made using the particle encounter complex (K_{os})[30] model, following equation 1.

$$K_{os} = \frac{4000 \prod N_{av} h^3}{3} \exp(-V_T(h)/kT),$$ (1)

Where N_{av} is Avogadro's number, V_T is the total interaction energy between two spherical particles, h is the separation distance between the particles, k is the Boltzmann constant, and T is the temperature. The K_{os} value for CNPs indicates a tendency to agglomerate at ambient temperatures even in a low concentration solution SI-7. It is expected that with the onset of ice nucleation and crystallization, the pH increases to a high (acidic) indeterminate value [31]. Yang et al. [11] suggested that oriented agglomeration at high particle concentration was possible only at high acidity or high alkalinity. These conditions are satisfied when the CNPs reach a stage of supersaturation while migrating into the aqueous region during freezing process which also increases the acidity in the remaining unfrozen solution. As the freezing front traverses through the system, the supersaturation in the liquid region forces the nanoparticles to agglomerate quickly into octahedral superstructures, driven primarily by the kinetics of the system rather than the thermodynamics. It is evident from our analysis that the formation of such superstructures is complete as soon as the freezing is complete. Conversely, several days of aging is required to facilitate superstructures at room temperature. Nanoparticles trapped in ice channels agglomerate in a similar fashion via localized oriented assembly to form nanorods.

66

The observation of polycrystalline nanorods under freezing conditions enlightens another side of oriented agglomeration, in which anisotropic self-assembly does not progress through a stage of amorphisation and complete reorientation to form single crystalline structures. The very low thermal energy during freezing and aging at -18 $^{\circ}$C is responsible for maintaining it's polycrystalline nature while the one dimensional confinement caused by channels in ice results in attachment of different polycrystalline particles. The role of ice as a physical template along with the importance of freezing rate was further investigated by subjecting the initial ceria seed solution to direct quenching in liquid nitrogen. During quenching under liquid-nitrogen environment, the total solution was frozen in 50 seconds. This extreme freezing rate does not allow the phenomena of freeze fractionation (solute rejection etc). It is also important to note that there is a fundamental difference in the freezing process when the vials are left in a "freezer" at -18 $^{\circ}$C and when they are gradually immersed into the liquid nitrogen. While the freezing front proceeds from top to bottom and the capillary phenomena occur in the former case, the same are not feasible in the latter. Hence, the nanoparticles are trapped (frost) as is at random positions and thus we have not observed significant differences between as synthesized particles and those frozen in liquid N_2 (i.e. octahedral superstructures were also not observed, SI-8). On the other hand, aging of CNPs solution at 2-3 $^{\circ}$C for 2 weeks resulted in formation of faceted agglomerated nanoparticles [SI-8]. The absence of nanorods from the unfrozen solution suggests that templating effect of ice is required for synthesis of nanorods.

Whitesides et al [1] have proposed the 'ground rules' for the self-assembly of basic building blocks as the ease to attain equilibrium between aggregated and non-aggregated states or to adjust their position relative to one another once in an aggregate. While the latter seems to happen in the formation of nanorods under the influence of capillary pressure, morphological evolution within the time frame of freezing reflects the tendency of {111} terminated CNPs, to assemble even under fast kinetic conditions. This kind of process has very important and broad implications in establishing the self -assembly mechanism in CNPs as the morphology appears within a very short time frame. This also suggests that the total time to achieve morphologically stable equilibrium conditions is very short in the case of CNPs, or the morphology can be achieved despite quenching the equilibrium conditions. This phenomenon could be unique to the fluorite structure of CNPs. The most interesting part of the present nanorod formation is the evolution of longer nanorods (up to 3.5 micron long) with time (aging under ice) which proves the dynamic nature of self-assembly in static ice templates. It can be observed directly from SI-9 that the zigzag attachment of CNPs through {111} planes occur within 1 day of aging at -18 ^{o}C. A strong evidence of oriented attachment is observed from the FFT pattern as shown in SI-9, which indicates preferential attachment of planes instead of random aggregation of nanoparticles.

Mao et al [32] have systematically studied the synthesis of variously aggregated quantum dots at low and high temperatures. It was reported that the anisotropy at low temperature arises due to the templating effect of the thiol groups and may produce spherically

68

aggregated structures at even lower temperatures. However the study was limited to 24 hrs of freezing and templating effect of ice was not considered. Synthesis of fibrous and layered sheets of composites exploiting the 'physics of ice formation' was demonstrated recently [27].
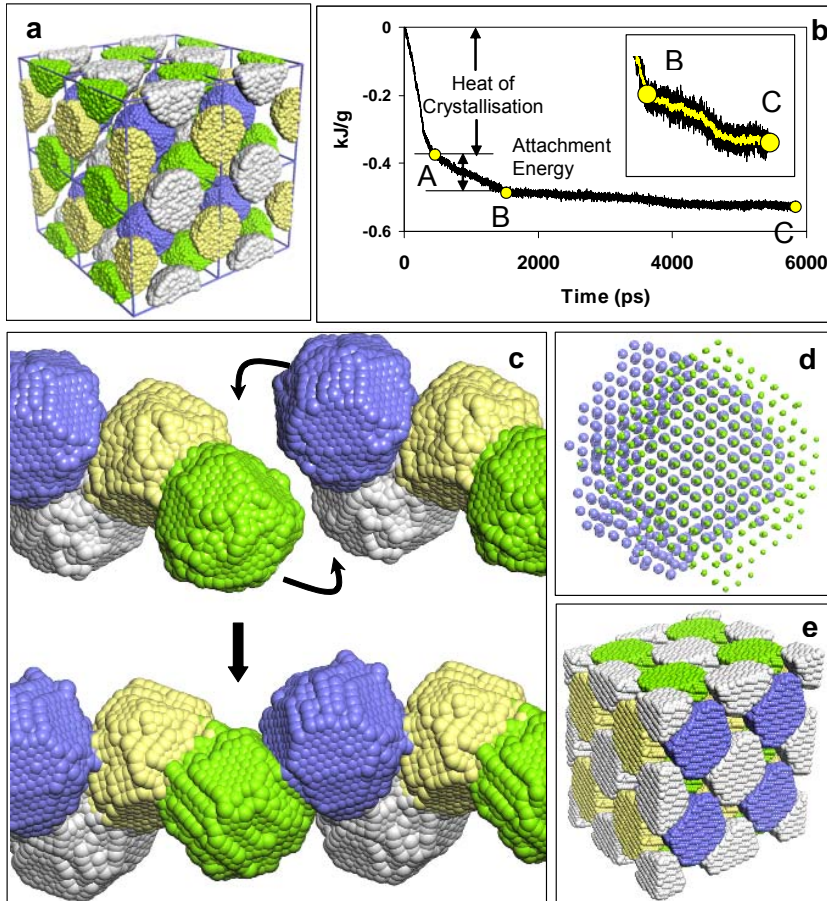
Figure 19: Results from MD simulation of self-assembly of nanorods and octahedral superstructure: Atom positions comprising the CeO_2 nanostructures. (a) Starting configuration comprising CeO_2 nanoparticles placed equally spaced into a simulation box a 2×2×2 supercell is shown; (b) configurational energy, calculated as a function of time; (c) structure of a chain/nanorod comprising CeO_2 nanocrystals. Top: after 300 ps of MD simulation. The arrows indicate the trajectory followed by the blue and green nanoparticles as they attach themselves to one another; bottom: after 1500 ps showing the attached configuration; (d) view showing the epitaxy between the nanoparticles attached at {111} surfaces; (e) close packed structure comprising CeO_2 nanocrystals (which

corresponds to Figure 18b). Cerium is colored to help visualize the individual CeO_2 nanocrystal secondary building units.

As evident from most of the existing literature and from the work quoted above, often the researchers have confined to complicated surfactant mediated assembly and high temperature routes for producing the 1-D nanostructures. We found interesting differences and similarities between Mao et al.'s work and our study. They have confined the studies to just 24 hrs and reported some intermediate meta-stable structures at sub-zero temperatures. In the present work, we have continued the aging treatment up to several days and proposed a possible mechanism of nanostructure assembly in the ice molds. Based on the present work, we believe that the long term aging study on the nanoparticles is central to our success in obtaining the 16-d, 18-d assemblies. If applied to other systems, the long term aging studies might reveal various exciting features.

In the present study, we have successfully exploited the physico-chemical processes happening during and after the freezing of CNP sols to mold one-dimensional nanorods (30 nm diameter) and three-dimensional superstructures. This is a first step in using ice moulds to direct the self-assembly of nanoparticles into different shapes, sizes and assemblages. Aforementioned observations are also validated with the help of MD simulations as discussed below.

In the present study, we have used molecular dynamics (MD) to simulate nanoparticle self-assembly. Specifically, we explored agglomeration constrained in one and three

dimensions, which led to models of chains/nanorods and octahedral superstructures, respectively. The simulation code and potential models have been described previously in reference 3. To facilitate one-dimensional agglomeration, amorphous/molten CeO_2 nanoparticles, each comprising 6144 atoms and about 5 nm in diameter, were positioned equally spaced, within a cubic simulation cell box 13nm in size, Figure 19(a). Each simulation cell comprised four nanoparticles. Constant volume MD simulation was applied to the system for 6800 ps at 3200 K. The high temperature accelerates the dynamical simulation such that the crystallization and aggregation are complete within the (small) timescale of the simulation. The simulations revealed attractive forces acting between neighboring amorphous/molten nanoparticles. Accordingly, under the MD simulation, the nanoparticles started to move closer to one another and started to crystallize. Specifically, nucleating seeds spontaneously evolved within the nanoparticles facilitating their crystallization. The resulting nanocrystal morphologies comprised {111} octahedra with the sharp corners truncated by {100} in accord with the experiment. Once crystalline, the nanoparticles continued to be attractive towards one another.

The configurational energy of the system (Figure 19b) was calculated as a function of time. The first 300 ps of time is associated with a steep gradient and reflects, in part, the crystallization of the nanoparticles. The energy difference between the start of the simulation, where all the nanoparticles are amorphous, and fully crystalline nanoparticles, is loosely associated with the heat of crystallization. After 300 ps, the nanoparticles have already aggregated together forming part of a chain, Figure 19(c). During the next 1200

ps, Figure 19(b), point A to point B, two nanoparticles (green and blue, Figure 19(c)) attach themselves to one another via {111} surfaces; a plan view of the epitaxy between the two nanoparticles is shown in Figure 19(d). The attachment energy can be determined as the energy difference between point A and point B, Figure 19(b). A movie showing the attachment is available as supporting information SI-10. As the MD proceeds, the energy continues to reduce reflecting annealing conditions. This may include, for example, surface relaxation, rotation of the nanoparticles to facilitate a better fit, annealing out of dislocations etc. An illustration is shown in supporting information SI-6 in which a screw dislocation anneals out and facilitates coherent matching between the atomic planes of two attached CeO_2 nanoparticles. We also modeled a three dimensional aggregation of {111}-terminated CNPs, which form a close packed octahedral structure as shown in Figure 19e (SI-11a).

Our simulations, where we simulate the self-assembly *directly*, predict that when the system is constrained in one-dimension (modeling the reduced dimensionality of the ice cavities), the CNPs attach via {111} faces resulting in a 'zigzag' structure of the nanorod, Figure 19(c); rather than, for example, a parallel chain via attachment of {110}. Clearly, random 'zigzag' attachment would not facilitate a linear chain. However, the constraining influence of the ice mold forces nanorod evolution. By simulating self-assembly dynamically, similar to experiment, the models derived are metastable and do not represent thermodynamically the lowest energy structures. Accordingly, after attachment, the nanoparticles (attempt to) rotate to improve the epitaxy and area of coherence. We

72

also observe from the simulations that once attached, the translational and rotational degrees of freedom for the individual nanocrystals are reduced and therefore optimum attachment (thermodynamic) is difficult to attain. We note that the atomistic model of the nanorod/chain, Figure 19(c), can be used to help describe and understand the observed structure, Figure 16b, which is the 1-day old sample. During prolonged aging, the ice becomes harder and denser and will impose high localized pressure upon the chain within the ice-mold. Accordingly, we performed MD simulations on the chain under 0.1 - 0.5 GPa pressure. The animations of the simulation revealed that the nanocrystals reorient and pack tighter together. In contrast, when we do not constrain the nanocrystals to one-dimension (unconstrained) the resulting (kinetically driven) models are three-dimensional, figure 19(e). A more detailed description of the three dimensional geometry of the superstructures is provided in SI -10(a) and was found to retain their nanocrystal identity upon rearrangement giving rise to polycrystalline superstructures.

2.3.3 Conclusions

In this chapter, we have successfully presented the use of simple and natural phenomena such as formation of ice from water to architecturally sculpt 1-D ceria nanostructures. The green chemical synthesis route adopted and the MD simulations used to confirm the morphology evolution of the ceria nanostructures demonstrates a unique combination of experiment and simulation of nanoparticle behavior. The long term aging studies on nanoparticles in various conditions possibly lead to mind-probing findings in the synthesis and self-assembly of nanostructures. While much has been learned from various resources of Nature, harnessing the use of ice as tool to self assemble nanomaterials

73

should be explored further. By altering freezing rates, initial particle concentration, and aging temperature, it should be possible to use these processes and changes in ice structures to sculpt desirable nanostructures comprising nanoparticle building blocks. Clearly, water/ice environments are pivotal to the natural world and its evolution. Understanding and controlling the behavior of CNPs in such environments, as we have done here, is a first step to facilitate future advances spanning, for example, nanofluidics to nano-bio applications [33].

2.3.4 Experimental Details

Stoichiometric amounts of cerium nitrate (III) hexahydrate (Sigma-Aldrich) were dissolved in deionized water (18.2 MΩ) and 20% PEG (600 MW. from Sigma-Aldrich) + DI water mixtures. This solution was then oxidized using hydrogen peroxide (30% w/w Sigma Aldrich) to form the CNPs. Vials containing 15 ml of the solution were stored at 2-3 ^{o}C and another set was frozen in a laboratory chemical freezer. For fast freezing another set of vials containing solution were immersed directly in liquid nitrogen at a rate of 10 mm/sec. The solution freezes instantaneously upon immersion in the solution. Thus the rate of propagation of solid front can be taken as 10 mm/sec.

REFERENCES

1. Whitesides, G.M. and B. Grzybowski, Self-assembly at all scales. Science, 2002. **295**(5564): p. 2418-2421.

2. Service, R.F., How Far Can We Push Chemical Self-Assembly? Science, 2005. **309**(5731): p. 95-.

3. Sayle, D.C., et al., "Simulating synthesis": Ceria nanosphere self-assembly into nanorods and framework architectures. Journal Of The American Chemical Society, 2007. **129**(25): p. 7924-7935.

4. Yang, P.D., et al., Hierarchically ordered oxides. Science, 1998. **282**(5397): p. 2244-2246.

5. Striolo, A., Controlled assembly of spherical nanoparticles: Nanowires and spherulites. Small, 2007. **3**(4): p. 628-635.

6. Edwards, E.W., D.Y. Wang, and H. Mohwald, Hierarchical organization of colloidal particles: From colloidal crystallization to supraparticle chemistry. Macromolecular Chemistry And Physics, 2007. **208**(5): p. 439-445.

7. Kuchibhatla, S., et al., One dimensional nanostructured materials. Progress In Materials Science, 2007. **52**(5): p. 699-913.

8. Karakoti, A.S., et al., Direct Synthesis of Nanoceria in Aqueous Polyhydroxyl Solutions. Journal of Physical Chemistry C, 2007. **111**(46): p.17232-17240

9. Duan, H.W., et al., Directing self-assembly of nanoparticles at water/oil interfaces. Angewandte Chemie-International Edition, 2004. **43**(42): p. 5639-5642.

10. Zhang, H.Z., et al., Water-driven structure transformation in nanoparticles at room temperature. Nature, 2003. **424**(6952): p. 1025-1029.

11. Yang, M., et al., Preparation of ZnO nanowires in a neutral aqueous system: Concentration effect on the orientation attachment process. European Journal Of Inorganic Chemistry, 2006, **19**: p. 3818-3822.

12. Kuiry, S.C., et al., Spontaneous self-assembly of cerium oxide nanoparticles to nanorods through supraaggregate formation. Journal of Physical Chemistry B, 2005. **109**(15): p. 6936-6939.

13. Kuo, L.Y. and P. Shen, Shape dependent coalescence and preferred orientation of CeO2 nanocrystallites. Materials Science and Engineering A-Structural Materials Properties Microstructure And Processing, 2000. **277**(1-2): p. 258-265.

14.   Bjerrum, N., Structure and Properties of Ice. Science, 1952. **115**: p. 385-390.

15. Worster, M.G. and J.S. Wettlaufer, Natural convection, solute trapping, and channel formation during solidification of saltwater. Journal of Physical Chemistry B, 1997. **101**(32): p. 6132-6136.

16.   Soper, A.K., Water and ice. Science, 2002, **297**(5585): p. 1288-1289.

17. Penn, R.L., et al., Epitaxial assembly in aged colloids. Journal of Physical Chemistry B, 2001. **105**(11): p. 2177-2182.

18. Penn, R.L. and J.F. Banfield, Imperfect oriented attachment: Dislocation generation in defect-free nanocrystals. Science, 1998. **281**(5379): p. 969-971.

19.Sayle, T.X.T., S.C. Parker, and D.C. Sayle, Shape of CeO_2 nanoparticles using simulated amorphisation and recrystallization. Chemical Communications, 2004(21): p. 2438-2439.

20.Martin, P., et al., Atomistic modeling of multilayered ceria nanotubes. Nano Letters, 2007. **7**(3): p. 543-546.

21.Sayle, D.C., et al., Simulating self-assembly of ZnS nanoparticles into mesoporous materials. Journal of The American Chemical Society, 2006. **128**(47): p. 15283-15291.

22.Kuchibhatla, S., A.S. Karakoti, and S. Seal, Hierarchical assembly of inorganic nanostructure building blocks to octahedral superstructures - a true template-free self-assembly. Nanotechnology, 2007. **18**(7).

23.Feng, X.D., et al., Converting ceria polyhedral nanoparticles into single-crystal nanospheres. Science, 2006. **312**(5779): p. 1504-1508.

24.Ishiguro, H. and B. Rubinsky, Mechanical Interactions Between Ice Crystals And Red-Blood-Cells During Directional Solidification. Cryobiology, 1994. **31**(5): p. 483-500.

25.Panday, S. and M.Y. Corapcioglu, Solute Rejection in Freezing Soils. Water Resources Research, 1991. **27**(1): p. 99-208.

26. http://www.uwgb.edu/dutchs/PETROLGY/Ice%20Structure.HTM.

27.Deville, S., et al., Freezing as a path to build complex composites. Science, 2006. **311**(5760): p. 515-518.

28.Scheie, P.O., The Upward Force On Liquid In A Capillary-Tube. American Journal Of Physics, 1989. **57**(3): p. 279-280.

29. Bougamont, M., S. Tulaczyk, and I. Joughin, Response of subglacial sediments to basal freeze-on 2. Application in numerical modeling of the recent stoppage of Ice Stream C, West Antarctica Journal of Geophysical Research, 2003. **108**(B4): p. 2222.

30. Penn, R.L., Kinetics of oriented aggregation. Journal of Physical Chemistry B, 2004. **108**(34): p. 12707-12712.

31. Franks, F., Freeze-drying of bioproducts: putting principles into practice. European Journal Of Pharmaceutics And Biopharmaceutics, 1998. **45**(3): p. 221-229.

32. Mao, C.B., J.F. Qi, and A.M. Belcher, Building quantum dots into solids with well-defined shapes. Advanced Functional Materials, 2003. **13**(8): p. 648-656.

33. Chen, J.P., et al., Rare earth nanoparticles prevent retinal degeneration induced by intracellular peroxides. Nature Nanotechnology, 2006. **1**(2): p. 142-150.

2.3.5 Supporting Information
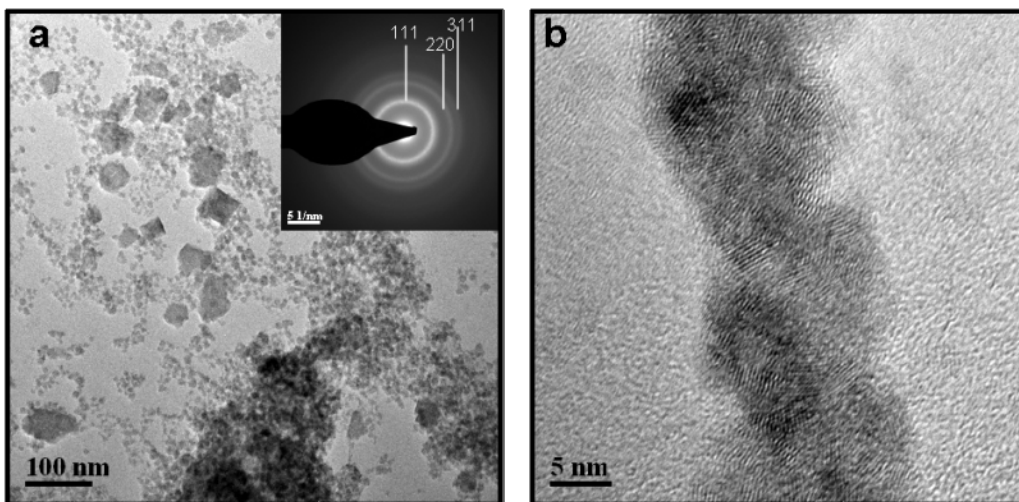
SI 1: TEM images from one day aged frozen solution of ceria a) Image shows CNPs with small and large agglomerates (inset electron diffraction pattern confirming the fluorite structure of ceria; also one can see truncated morphology of agglomerating nanoparticles which is usually observed upon controlled ageing) b) Particles orienting together and agglomerating in anisotropic way to give oriented agglomeration.
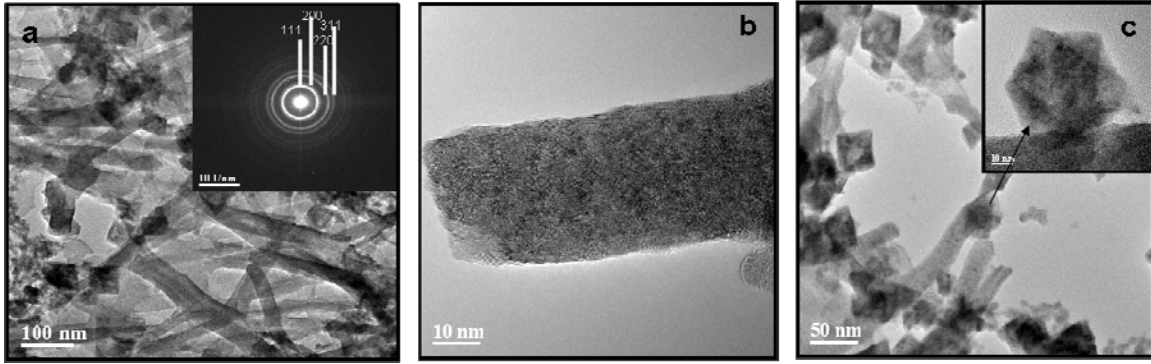
SI 2: TEM images of one week-aged frozen solution of ceria. a) bunch of ceria nanorods with some octahedral structures (SAED in the inset confirms the fluorite structure of the rods and particles) b) the dense packing of individual 3-5 nm CNPs making up the nanorods c) TEM image showing the superstructure assembly of ceria octahedra along with nanorod (inset shows the star shape morphology of the superoctahedral ceria)
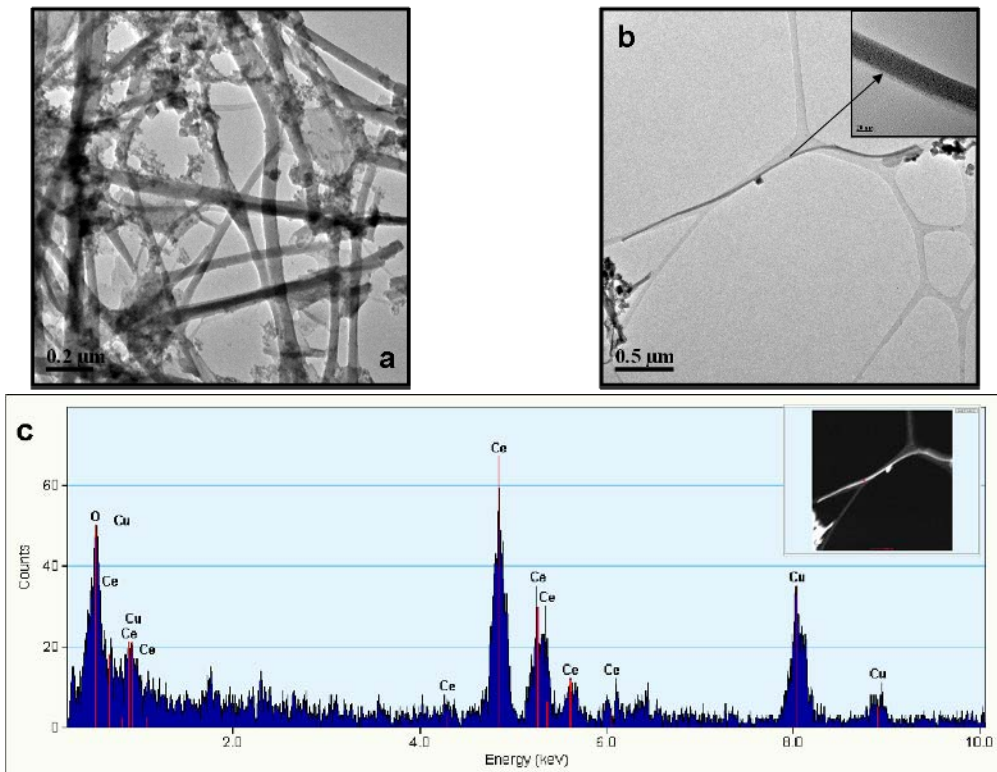
SI 3: TEM image of ceria nanorods taken from three weeks aged frozen solution of ceria. a) confirms high density of long ceria nanorods and octahedral arrangement of agglomerated nanoparticles after 2 weeks of aging b) 3.5 micron long nanorod of ceria (inset shows the diameter as 40 nm) c) EDX spectrum collected on a spot at the nanorod showing the signals from cerium and oxygen.
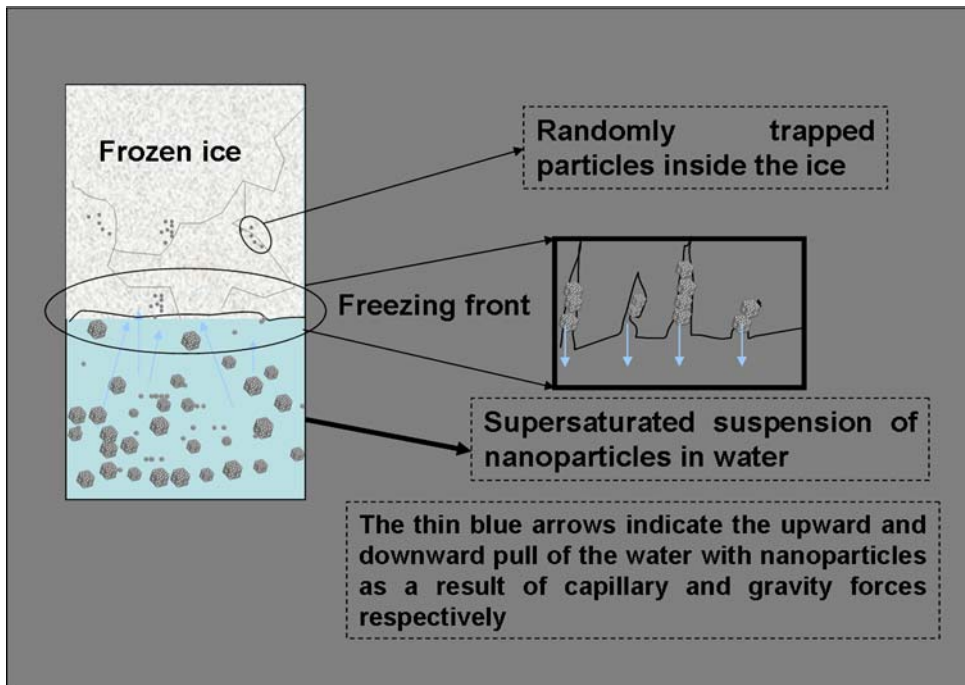
SI-4 Schematic of the process of freezing and entrapment of particles in the ice channels as the liquid moves out of the capillary during the progress of the ice front. The schematic tries to simulate a real situation during the freezing as the ice front progresses from top to bottom. The particles are sucked into the channels along with water into the nano channels and are trapped inside the channels as the water freezes and/or drives out of the channels.
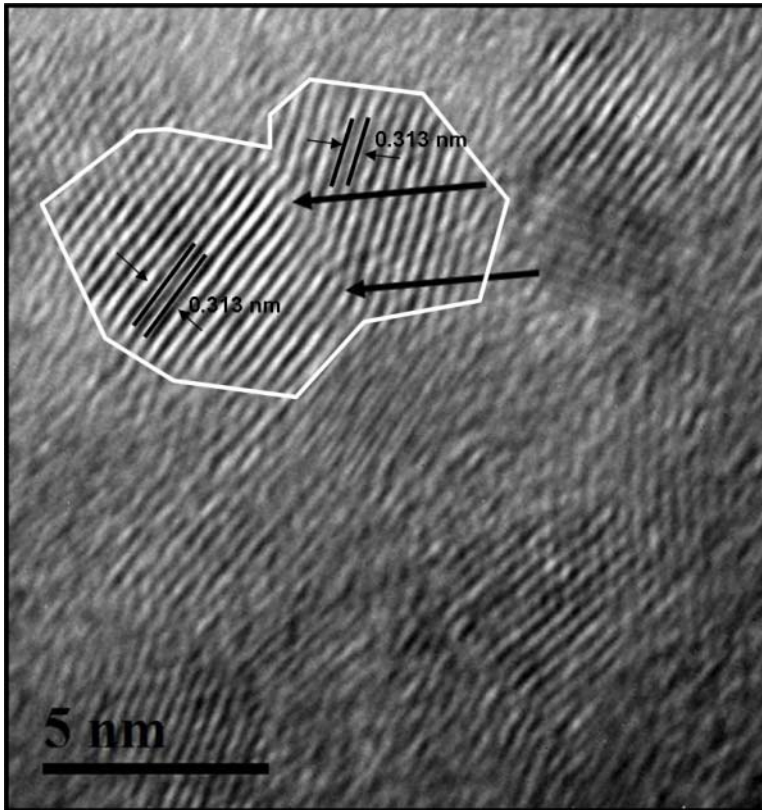
SI 5: HRTEM image of orientation attachment of CNPs. Arrows indicate the presence of dislocations at interface during the orientation of two {111} surface terminated CNPs. A semi-coherent interface is formed with dislocations which get annihilated over a period of time with aging (SI 6).
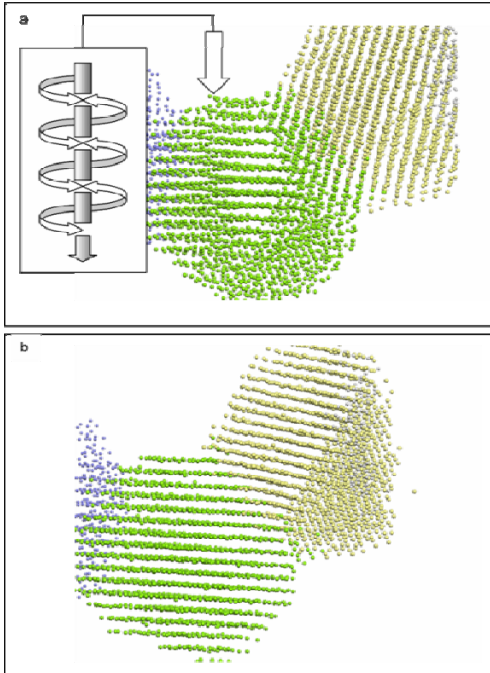
SI 6: Atomistic structure of a screw dislocation. (a) Snapshot of part of the simulation cell taken after 990 ps of MD simulation showing two CNPs (green and yellow); a third (blue) is partially visible. Within the green nanoparticle, a screw dislocation has evolved. The arrow indicates the position of the core region, which resides at the center of the nanoparticle and traverses its entire diameter. (b) After 6800 ps, the screw dislocation can be seen to have annealed out.

SI-7: K_{os} was calculated using the supporting equations for the total interaction energy VT

$$V_T(h) = \pi R\left(\frac{-H_{121}}{12\pi h} + \frac{64c_{io}^* kT\Gamma_0^2 e^{-\kappa h}}{\kappa^2}\right)$$

For a non symmetrical electrolyte the κ was calculated using

$$\frac{1}{\kappa} = \sqrt{\frac{\varepsilon_r \varepsilon_o kT}{2000e^2 N_{Av} I}}$$

Where ε_r is the unitless dielectric constant of the medium, ε_o is the vacuum permittivity, κ is the reciprocal of Debye length, T is the temperature, I is the ionic strength and N_{Av} is the Avogadro's number.

While the Ѓo is given by

$$\Gamma_o = \frac{\exp(ze\phi_o/2kT) - 1}{\exp(ze\phi_o/2kT) + 1}$$

It must be noted that the estimation of K_{os} assumes a spherical shape of the nanoparticles a homogenous distribution of surface charge over the particle surface. For CNPs in a 30 mM solution using a surface potential value of 30 mV, a room temperature value of 298 K, particle size of 5 nm, and obtaining other values from reference (31) the stability constant was found on the order of 10^{-3}. It must be noted that value of K_{os} obtained is for CNPs in solution at room temperature and not for rapidly changing conditions during the freezing of ice.
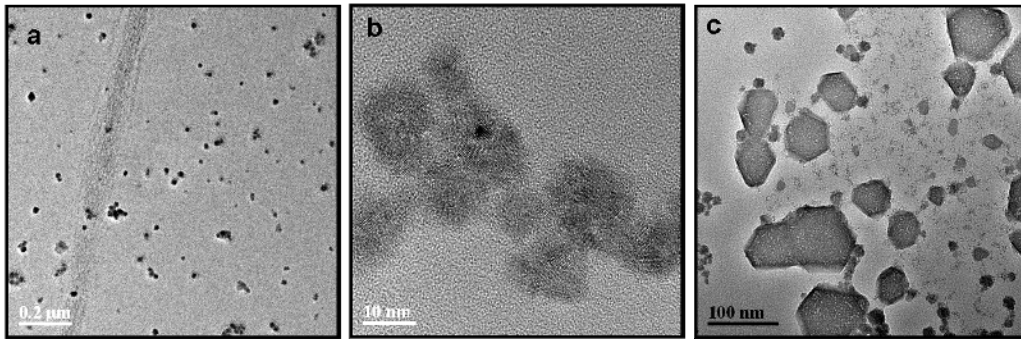
SI 8: CNPs formed in ice (fast freezing) after 2 weeks of aging a) well dispersed nanoparticles which does not show any anisotropic behavior b) high magnification images of CNPs showing the individual 3-5 nm CNPs c) truncated octahedron in refrigerated (2-3 ^{o}C) nanoceria after 3 weeks of aging.
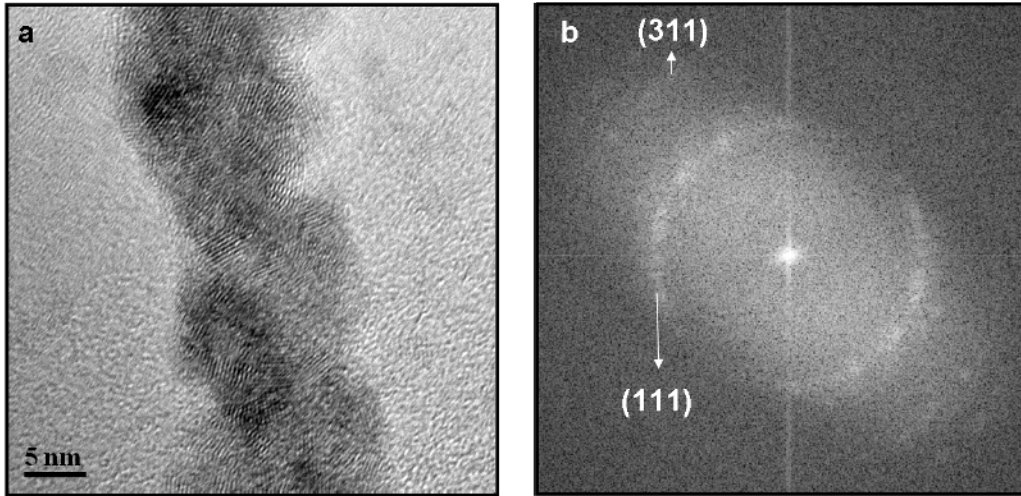
SI 9: High magnification TEM image from one day aged solution of CNPs in ice a) shows the zigzag oriented attachment of nanoparticles b) the FFT pattern of Figure (a) shows preferred orientation (texture) of {111} planes in during the evolution of nanorods from CNPs.

SI 11a: when we do not constrain the nanocrystals to one-dimension (unconstrained) the resulting (kinetically driven) models are three-dimensional, Figure 4(e). However, in contrast to the 1D chain, the CeO_2 nanocrystals comprising the 3D superlattice are tightly bound to twelve nearest neighbors. Accordingly, the degrees of freedom are very much reduced and the activation energy associated with any movement of one nanocrystal (to improve, for example, epitaxy or coherence) is so high as to prevent rearrangement. Thus the initial agglomeration (kinetically driven) gets locked into the structure and any extended periods of simulated annealing have little influence upon structural rearrangement. The simulation thus provides model atom positions for the schematics shown in Figure 3b. We note that the CeO_2 nanocrystals in the close-packed structure are not space filling, rather the nanocrystals occupy 73% of the space (calculated using solvent surface of 1.4 Å; Ce^{4+}=0.92 Å, O^{2-}= 1.32 Å). We also performed simulations at 20 GPa pressure and found that the nanocrystals do not agglomerate into the bulk parent material; rather the nanocrystals retain their individual identity, while becoming more space filling.

CHAPTER 3:
INFLUENCE OF AGING AND ENVIRONMENT ON NANOPARTICLE
CHEMISTRY

Despite the significant attention and numerous publications devoted to nano-sized materials, the physics and chemistry driving their properties are occasionally explored. Understanding and controlling the properties of nanoscale materials remains a significant challenge to the scientific community across the globe [1, 2]. Cerium oxide (CeO_2, ceria) is among the frequently studied oxides because of current and potential uses as a catalyst [3, 4], in solid oxide fuel cell technology [5, 6], and for UV-blocking applications [7]. Chemical mechanical planarization and solar cells [8] are among the newer applications where the nanoceria particles may have an impact. Our group has recently shown the ability of CNPs (CNPs) to protect retinal cells (in vivo) from reactive oxygen species (ROS) and to protect human breast-line cells from radiation damage during cancer treatment by mimicking superoxide dismutase (SOD) activity [9, 10].

A key property of CNPs in either the traditional applications or in the nano-bio regime is their ability to effectively switch between the +3 and +4 oxidation states. Especially for NPs, the oxidation state observed is influenced by the synthesis and processing conditions, storage time (aging), and environment. These factors combine to influence physical (and chemical) properties of CNPs, including lattice parameter and optical absorption [7, 11]. Another noteworthy aspect in CNPs is the blue shift in optical absorption with decreasing particle size. The exciton confinement (quantum size effect) that leads to blue shifts in optical transmission spectra is widely observed in semiconductor and some oxide NPs. Although ceria is one of the extensively studied oxides for quantum confinement effects, current literature on the quantum confinement effects in ceria has been inconsistent [12-14] and has stimulated a lively debate [15, 16]. Many researchers

have observed a blue shift in the optical absorption edge with decrease in particle size and often used the effective mass approximation theory {EMA theory: When the dimensions of a material reach those of its Bohr exciton radius, the energy of the lowest excited state increases, i.e. blue shift occurs in the optical absorption with decrease in size. The combination of quantum confinement and effective mass approximation theory can be used to derive a R^{-2} dependence of the band gap energy for a spherical particle and the relation can be written as: $\Delta E_g = E_g(R) - E_g = \dfrac{h^2}{8R^2}\left(\dfrac{1}{m_e} + \dfrac{1}{m_h}\right)$ } to interpret the particle size from the shift in the optical absorption edge (SI -1). While some groups have attributed this to quantum confinement, others have ascribed it to the presence of the Ce^{3+} oxidation state in the NPs [11, 17]. Zhang et al [18], reported that adsorbed hydroxyl radicals on the surface of the CNPs are capable of creating a surface-energy band and thereby causing absorption at longer wavelengths, compensating the confinement effect, for particle sizes below 4 nm. The general tendency for an increased amount of Ce^{3+} with decreasing particle size below 10 nm has also been widely reported[18]. In either case, researchers usually assume that the particles remain static with time and ignore any interaction with the environment, an assumption that, we believe, does not always apply.

Although synthesis, processing, storage conditions, and local environment of NPs are known to play a significant role in determining their properties, this important information about particles and their history is often not reported [19]. Lieber's group [20] has demonstrated large anisotropy in polarization and photoconductivity as a result of dielectric contrast between nanowires and the surrounding environment rather than the quantum-confinement effect. Structural changes in ZnO NPs in the presence of water and alcohol were observed by Zhang et al. [21]. In other reported literature as well, we have observed indications of environmentally induced changes in NPs apparently of similar or identical size [22].

The subtle aspects in the seemingly simple synthesis, aging time and effect of local environment on the chemistry of CNPs are reported in this chapter. While the first section (3.1) deals with the chemical changes and oxidation switching in CNPs aged under water based environment in the absence of any additives or surfactants; later part (3.2) deals with effects of monomer and polymer additives on this behavior. Based on the available literature and the experimental observations, an effort has been made to propose a possible mechanism that drives the oxidation state switching in CNPs.

3.1 Oxidation State Switching in Nanoceria and Its Implication to Confinement Effects

3.1.1 Introduction

Here we examine the time dependent chemical state switching of CNPs while suspended in aqueous solutions as a function of local environment and aging time. An overview of this phenomenon is shown in Figure 20. It is important to recognize that the effects are reversible. The ceria particles respond (sometimes slowly) to the oxygen activity of the solution. Because these chemical state changes influence both physical and chemical properties of the particles; they may impact NP behavior important for specific applications, such as catalysis or biomedical materials. Our experience and previous results [23] also indicate that the interaction of CNPs with the polymers and organic molecules is dynamic and depends on the solvent and processing conditions. In particular, solvent properties have been observed to influence both the particle size and the chemistry as a result of surface interactions [24]. Although it was hypothesized that the chemical state of the NPs is reversible, systematic analysis and a detailed mechanistic

91

understanding of this phenomenon as a function of aging and environment are not available [23, 24]. Here we analyze the ability of CNPs to switch their oxidation state in various aqueous media, propose a mechanism, and suggest how these changes may influence reported observations of quantum confinement. We also, simultaneously, provide experimental and analytical support for a previous hypothesis about the ability of CNPs to protect retinal cells through ROS quenching [9].
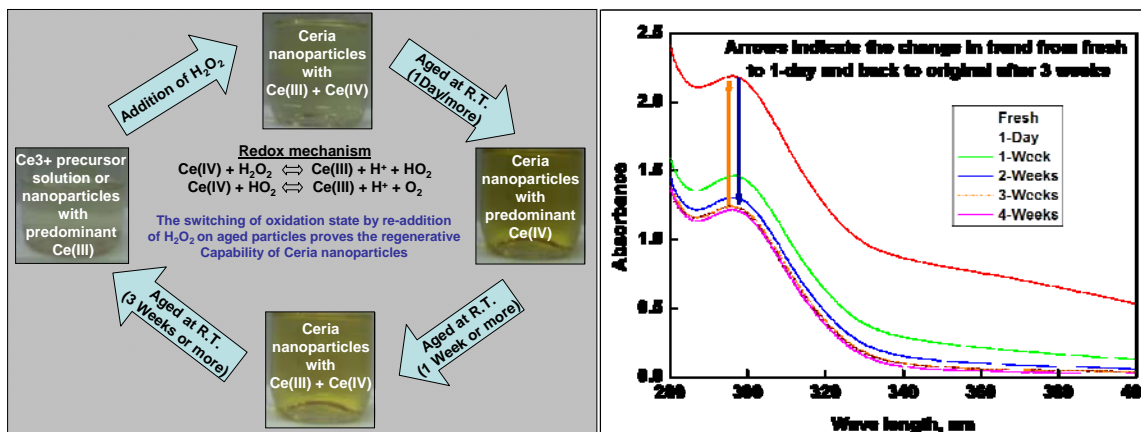
Figure 20: a) Schematic representation of the regenerative capability and oxidation state switching of CNPs in an aqueous environment. The pictures of bottles containing the NP suspension in DI water indicate the color changes after different aging periods. The mechanism of oxidation-state change in the presence of hydrogen peroxide and hydroperoxyl radicals is shown; (b) UV-Vis absorption spectra of ceria NP suspension indicating the shift in the absorption as a function of time. It is evident from the plots that the absorption spectra for freshly synthesized CNPs and those after 3 weeks of aging are almost identical.

3.1.2 Experimental Work- Synthesis and characterization of CNPs

Unless specifically noted, the CNPs used in this work were synthesized by a room-temperature wet chemical route without any surfactants or additives. $Ce(NO_3)_3 \cdot 6H_2O$, was dissolved in DI water (18.2 MΩ), and a calculated amount of 30% H_2O_2 was added drop wise to yield a final 30 mM CNP suspension. The colorless solution slowly turns to a characteristic yellow color indicating the oxidation of Ce^{3+} to Ce^{4+}. A Varian Cary-1

UV-Visible (UV-Vis) spectrophotometer was used to characterize the CNPs suspended in solution. Characteristic Ce^{4+} and Ce^{3+} spectra were collected using control solutions made from Ce^{4+}-ammonium nitrate and Ce^{3+}-nitrate in DI water, respectively. In the as prepared condition, the transmission spectra were obtained at two-minute intervals during the first sixty minutes (Figure SI-2). Later, the spectra were collected every day for 1 week and then after 2, 3 and 4 weeks of aging (Figure 20b). The absorbance values were calculated from the transmission data using the Beer-Lambert law and were used to estimate the band-edge. Transmission electron microscopy (TEM) and X-ray photo electron spectroscopy (XPS) were carried out on various samples and representative data are quoted in relevant contexts.

The concentration of Ce^{4+} initially increases imparting the characteristic yellow color with a maximum in intensity after one day of aging (Figure 20). The intensity of yellow color starts fading after 1 week or more aging indicating a decrease in the amount of Ce^{4+} in the solution. After 3 weeks of aging, the solution appears pale yellow in color indicating the further reduction of Ce^{4+} and regeneration of Ce^{3+}. At this stage, it can be unequivocally stated that the environment is not oxidizing and that the CNPs are stable with a Ce^{3+} oxidation state. A simple filtration experiment (detailed procedure: SI-3) has been carried out to confirm that the color of the solution is a result of the variations in the chemistry of the NPs. It is clear from the images and the analysis presented in the supporting information that all the changes are indeed occurring on the NPs. The CNPs were also synthesized in various aqueous media such as poly (ethylene glycol) (PEG),

93

ethylene glycol (EG), dextran, and glucose using similar conditions as mentioned above to understand the role of additives.

To understand the actual time-dependent behavior of CNPs, we: 1) analyzed the optical absorption data using the conventional data analysis techniques existing in literature; 2) examined the chemical changes occurring in the CNPs with time and the environment; and 3) interpreted the results of (1) and (2) in terms of the quantum-confinement effect in CNPs.

3.1.3 Conventional Data Analysis (to determine band gap from UV-Vis data)

The absorbance can be calculated from transmission data using the Beer-Lambert law:

Absorbance (A) = log (100/%T) = ε C l   1

Where ε is the molar absorptivity, [L·mol^{-1}cm^{-1}], C is the chromophore concentration in solution, [mol·L^{-1}], and l is the path length [cm], T is the transmittance.

Band-gap values can be calculated by plotting $(\alpha E)^2$ Vs E for direct and $\alpha^{0.5}$ Vs E for indirect transitions [7] and extrapolating these plots to zero absorbance. Here, E is the energy.

E= hc/λ (1248.62/ λ); where λ is the wavelength [nm]; α is the optical absorption coefficient ($\alpha = (2.303 \times 10^3 A \cdot \rho) / l \cdot c$, ρ is the solid-phase density (7.13 g/cc for CeO_2)).
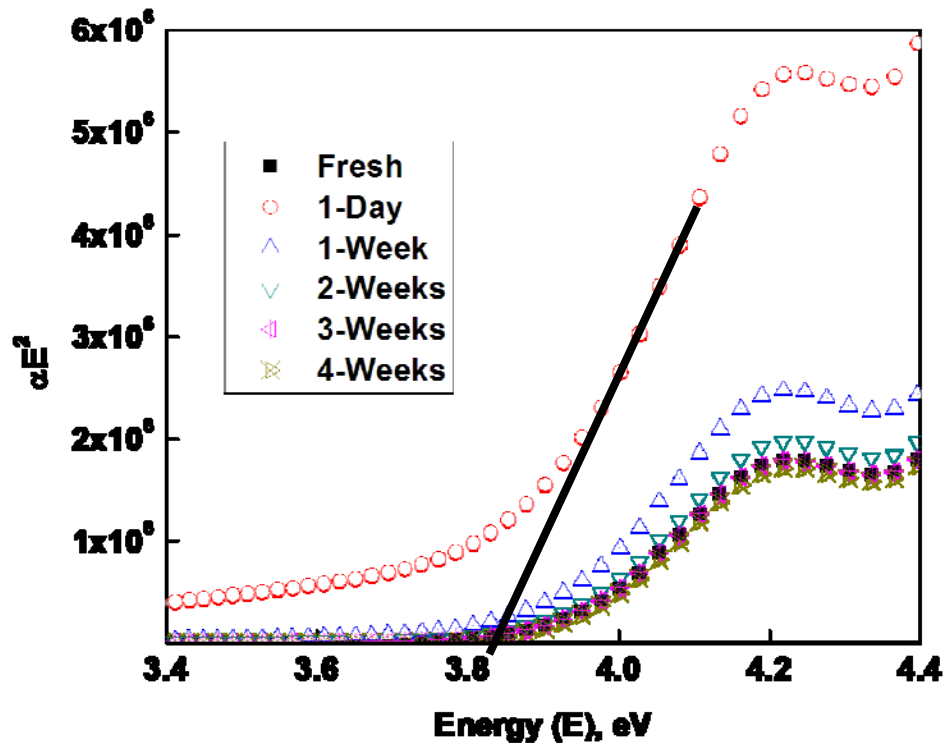
Figure 21: $(\alpha E)^2$ Vs E plots for CNP suspension in DI water after various aging periods. An estimate of the band gap can be obtained with $\alpha E = const (E-E_g)^n$ {E is the energy and E_g is the band gap n = 0.5 for a direct allowed transition}. The band gap value can be obtained from the energy intercept of the plot between αE^2 and E, as shown by the black line for the data corresponding to 1-day aged sample.

Because it was shown earlier that the transitions in CNPs are direct in Nature, [7] we confined our analysis to $(\alpha E)^2$ Vs E plots only. These are shown for CNPs that were aged in as synthesized conditions at room temperature for various time periods (Figure 21). The method of extrapolating the plots to obtain the band edge value is also shown for a representative data set from freshly synthesized NPs. The band gap values obtained from this method are plotted in Figure 22.
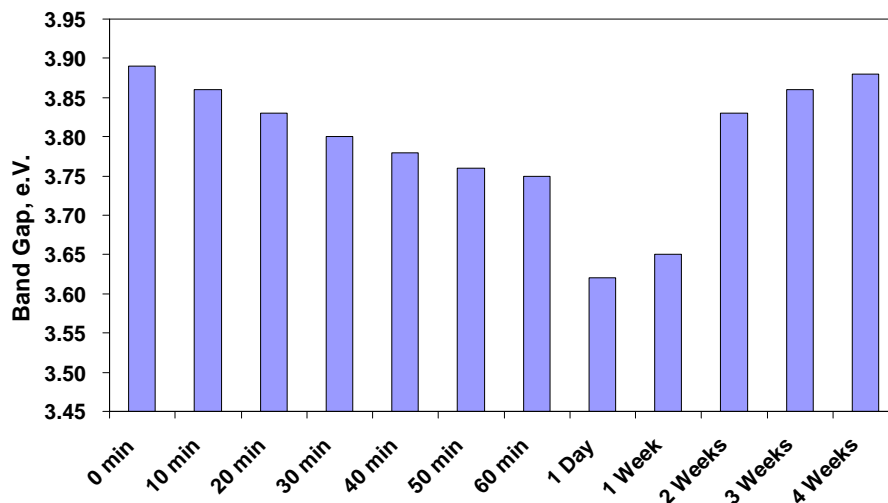
Figure 22: Band gap variation in water based CNPs as a function of time. Data was collected at 2-minute intervals immediately after the oxidizer is added. Selective data points corresponding to 0 – 60 minutes are presented. The data clearly shows that the band gap values dropped from ~3.9 eV to 3.75 eV within first 60 min. The lowest band gap value for a 1-day aged sample is indicative of the contribution from Ce^{4+}. Increase in the band gap from 1 week of aging is indicative of the change in the oxidation state to Ce^{3+}. It should be noted that the individual particle size did not increase beyond 3 – 5 nm, after the first 60 minutes.

3.1.4 Band-Gap Analysis and Correlation with Microscopic and Visual Observations

The TEM images collected initially after synthesis (~15–30 minutes) have shown 15- to 20- nm agglomerates of 3- to 5-nm particles, which is in the range of the Bohr exciton radius (∼7 nm for CNPs). Particle sizes in this range and smaller are of major interest when considering the quantum confinement effect [15]. The optical absorption edge in ceria is expected to be a result of overlapping O_{2p} and Ce_{4f} charge-transfer bands and the spin-orbit splitting of Ce_{4f} [25]. Time dependent UV-Vis spectra show absorption in the visible region with a clear red shift in the first sixty minutes after synthesis (Figure SI-2). It should be carefully noted, that the confinement effects result in a "blue-shift with decreasing particle size"; this can be viewed as "a red shift with increasing particle size."

96

In the experiments reported, after the initial nucleation, the particle size gradually increases with time and red-shift was observed. This red-shift and the increasing particle size could be interpreted as a result of confinement effects [26]. However, it should be noted that there are at least two significant changes happening in the system after the oxidizer is added, 1) ceria NP nucleation and growth; and 2) simultaneous change in oxidation state from +3 to +4. We believe that the observed red shift might also be a result of the change in oxidation state, supported by the mechanisms discussed in this manuscript. Based upon the measurements from the dissolved salts, the absorption edges for Ce^{3+} and Ce^{4+} are 3.76 eV and 3.2 eV, respectively. This indicates that the change in the oxidation state from Ce^{3+} to Ce^{4+} also leads to apparent changes in the electronic structure.

When we continued the analysis of the NP suspension aged for one day at room temperature, there was a significant red shift in the absorption edge from ~3.9 eV to 3.6 eV (Figure. 22). There was no significant difference in either the color of the solution or the change in edge energy for up to one week of aging (data not shown). Aging of the ceria suspension beyond 1 week resulted in a gradual reversal of the oxidation state to 3+. The absorption spectrum for the sample aged for 3-weeks almost overlaps with that of the fresh sample (Figure. 20b). At this point, the solution is mostly colorless and there is no significant precipitation. The band edge values and the color of the solution indicate the dominance of Ce^{3+} species. This indicates that the CNPs have switched their oxidation state from +3 to +4 and eventually back to +3 again. During this entire oxidation /

97

reduction process we did not see any significant changes in NP size, despite the variation in the agglomeration for different solutions as we discuss later. We are able to observe this interesting behavior of CNPs only because of the long term studies. Some of the reported studies on CNPs were confined to first few minutes or hours after synthesis. In order to efficiently use the NPs in various applications, it is important to understand their long and short term stability and the associated chemical changes.

3.1.5 Chemistry behind the Dynamic Nature of CNPs

As mentioned before, two simultaneous processes occur when the CNPs are synthesized, namely, the oxidation of Ce^{3+} to Ce^{4+} and the nucleation and/growth of NPs. Hence, it is important to account for the chemical changes in the ceria system during and after the synthesis stages to properly understand the variation in the band edge values of ceria. The chemical reactions that lead to the formation of CNPs [27] as the precursor is initially oxidized are the following:

$$Ce^{3+} + OH^- + \tfrac{1}{2}\, H_2O_2 \rightarrow Ce(OH)_2^{2+} \qquad\qquad (2a)$$

$$Ce(OH)_2^{2+} + 2\, OH^- \rightarrow Ce(OH)_4 \rightarrow CeO_2 \cdot 2H_2O \qquad\qquad (2b)$$
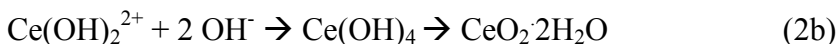
It is well known that peroxide dissociates relatively quickly, hence the actual species participating in the regeneration of Ce^{3+} from Ce^{4+} should be determined. In order to explain this, we note long established literature on oxidation and reduction kinetics of Ce^{4+}/Ce^{3+} in the presence of hydrogen peroxide [28-33]. Several authors have critically analyzed the catalytic oxidation of Ce^{3+} to Ce^{4+} in the presence of hydrogen peroxide [28-33]. The key aspect of the hydrogen peroxide dissociation is the formation of the hydroperoxy or perhydroxyl radical. Formation of perhydroxyl species during the

reaction of Ce^{4+} with hydrogen peroxide has been confirmed by electron spin resonance spectroscopy [34].The hydroperoxy radical is known to disproportionate in the oxidation and reduction of solutions with cations of multiple valency states.

$$H_2O_2 \rightarrow HO_2 + H^+ + e^- \qquad\qquad 3(a)$$

$$HO_2 + HO_2 \rightarrow H_2O_2 + O_2 \qquad\qquad 3(b)$$

Our experiments are consistent with earlier observations indicating that CNPs can be stable in either a Ce^{+3} or Ce^{4+} oxidation state in aqueous media under suitable conditions. Hence, the Ce^{3+} is formed from the Ce^{4+} oxidation state in the presence of the hydroperoxy species, following the chemical reaction (4).

$$Ce^{4+} + HO_2 \rightarrow Ce^{3+} + H^+ + O_2 \qquad\qquad (4)$$

The hydrogen peroxide converts the Ce^{3+} to Ce^{4+} immediately after it is added to the Ce^{3+} solution. The Ce^{4+} ions will quickly bond with the available hydroxyl radicals and nucleate the hydrated ceria particles to form a stable suspension at a pH of ~3.5. After this stage, the solution will become depleted of the Ce^{3+} ions and will be rich in Ce^{4+}(in the particles) and HO_2 radicals. This will drive reaction 4 and leads to the reduction of Ce^{4+} to Ce^{3+}. Hence, there must be competing reactions occurring simultaneously as long as the relative concentrations of Ce^{4+}, Ce^{3+} and HO_2 radical provide the driving force. Once the solution is depleted of the oxidizing species, cerium will revert back to its stable oxidation state in aqueous medium i.e., Ce^{3+} oxidation state will become stable. So, we propose that the regenerative capability of CNPs is determined by their immediate environment. This implies that the Ce^{4+} ions can be reduced and regenerated as the environment changes. Such a mechanism has been suggested in the oxidation of reactive

oxygen species (ROS) to protect retinal cells [9]. The formation of Ce^{4+} by reaction with H_2O_2 is much faster than the reduction by hydroperoxyl species. The reduction reaction involves solid NPs whereas the initial oxidation reaction involves ions in solution to form solid NPs. Once the NPs have formed, the process of reduction is reversible and oxidation of the NPs could be induced by the addition of oxidizing species like H_2O_2. This is demonstrated in Figure 4, where addition of H_2O_2 to a NP suspension that had been aged for three weeks (and contained predominantly Ce^{3+} NPs) regenerates the Ce^{4+} oxidation state. The process of re-oxidation, however, is slower than the initial oxidation reaction as it involves solid NPs rather than ions.
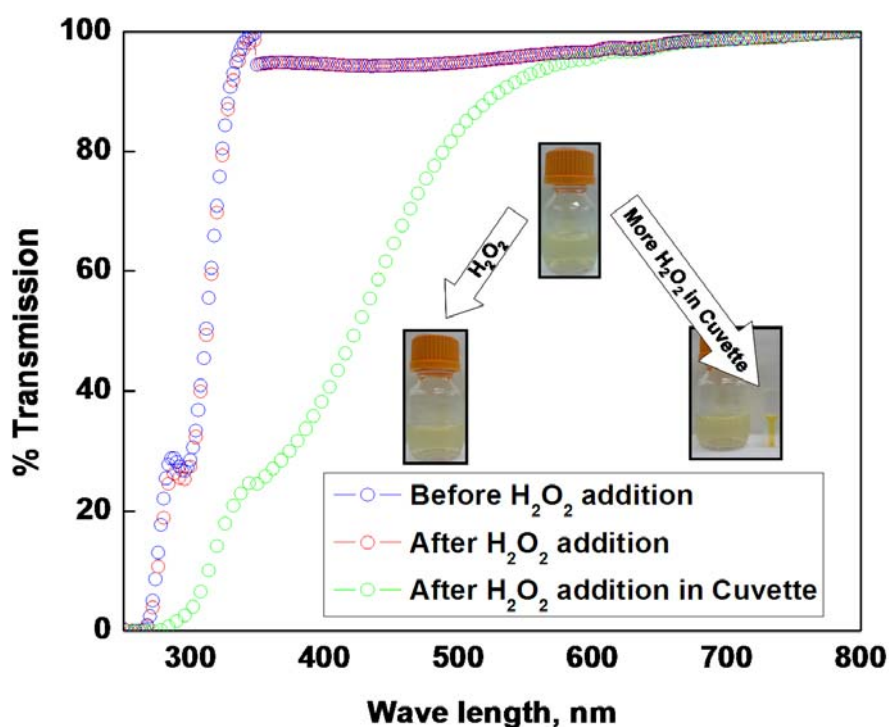
Figure 23: UV-Vis transmission spectra indicating the effect of H_2O_2 addition on the ceria NPs aged for 3 weeks at room temperature in DI water. (change in environment) Change in the color of the solution is an indication of change in the oxidation state. The inset pictures represent the corresponding color changes with the addition of H_2O_2.

100

Irrespective of the nature of the NPs – i.e. individual particles, small and large agglomerates – we have observed reversible oxidation state changes in various aqueous media. The effect of different solvents on the oxidation state of as synthesized CNPs is clearly shown in Figure 24. Each additive has its own effect and significantly influences the chemical nature of the NP suspension as evidenced by the differences in the optical absorption data. The effect of dextran and glucose in acidic and basic environments is critically discussed in a previous publication [23]. In our studies, we have not seen any significant difference in the variation of absorption edge as a function of agglomeration. Studies carried out with NPs synthesized in various aqueous media such as ethylene glycol, poly(ethylene glycol), dextran and glucose at different concentrations also support this observation. The most important point to be noted is that irrespective of the media, the individual CNPs remained 3-7 nm in size, below the Bohr radius (~7 nm), Figure SI-3. [14, 23] However, the kinetics of oxidation state formation and switching vary among the different solutions (see Figure SI-4). This result confirms that the solution environment plays a significant role in influencing the oxidation state (or the rate of oxidation state transition) and thereby the band edge as a function of time. We have shown that the individual NPs of ceria remain 3-5 nm even after aging for 4-6 weeks and observed they remain the same even after ~400 days of aging (not shown here) [14]. Thus, after the initial nucleation stage the size of the NPs does not change. With aforementioned experimental results and analysis, it is clear that the CNPs have dynamic oxidation states, which can be tuned by choosing suitable environments and aging conditions.

101
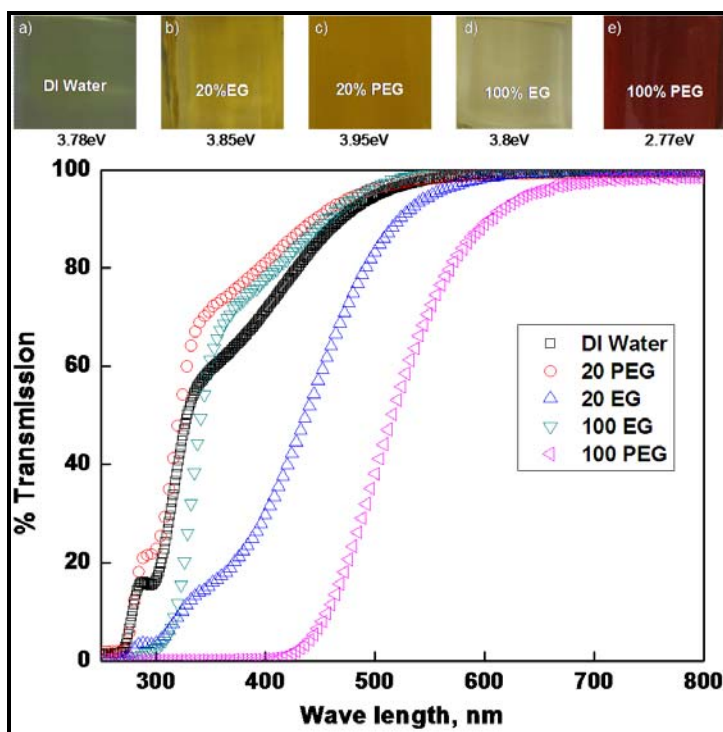
Figure 24 : Representative color of 30 mM ceria NP solutions (immediately after synthesis) in (a) DI water (b) 20% ethylene glycol (c) 20% poly(ethylene glycol) (d) 100% ethylene glycol (e) 100% poly(ethylene glycol) solutions. Darker yellow/orange brown color indicates higher amounts of Ce^{4+} as a function of variation in the environment and the light yellow color indicates predominant Ce^{3+}. The number (XX) shown at the bottom of each image is the band edge value obtained from the transmission data. All the systems in as synthesized conditions have shown a particle size ~3-5nm and agglomerate sizes of 10-20nm (TEM images are available in SI)

3.1.5 Implications of Chemical State Changes to the Band Gap Analysis

A number of researchers have shown that the lattice parameter expansion in the ceria NP system with decrease in particle size is a result of an increase in the fraction of cerium species in the Ce^{3+} oxidation state and the associated oxygen-vacancy formation. However, the same fact has not always been considered in analyzing the optical absorption data of CNPs. Henceforth, data presented in this chapter and the dynamic nature of the CNPs' chemistry should be carefully considered while analyzing the

confinement effects in CNPs. As usually applied, the effective mass approximation (EMA) theory presents only the radial dependence of the band gap in the quantum dots and does not consider a change in the chemical state of the semiconductor NPs. Hence, the validity of the EMA theory to interpret quantum confinement is questionable for species having variable chemistry, such as cerium oxide NPs. The role of local environment in influencing the "chemistry" of CNPs also indicates that the interpretation of confinement effects may not always be appropriate without accounting for their influence.

3.1.6 Conclusions

We have presented, with experiments and data analysis, the dynamic nature of CNPs and the changes of their oxidation state as a function of aging (time) and environmental conditions. During the stage of particle nucleation and growth, both the particle size and chemical state change with time. After the particles reach 3 nm to 5 nm, particle size remains constant and the oxidation state depends primarily and reversibly on the environment (and time). Often, the synthesis, analysis and relevant operational (in various applications) conditions are not the same. In such cases, aging time and environmentally induced changes in particles may play a significant role in the results reported and hence lead to discrepancies in various studies. By simultaneously studying the NPs both in the presence and absence of organic additives over a period of time (long term studies) there is an increased scope for properly interpreting the complex nature of NPs. It is also proposed that the band edge in CNPs can be chemistry driven and may not always be due to pure quantum confinement effects driven by particle size changes.

Having appreciated the facts, measurements of the effects of other parameters including temperature and storage conditions are also important. Similar studies in other systems might reveal more exciting features of NPs.

REFERENCES

1. Billinge, S.J.L. and I. Levin, The problem with determining atomic structure at the nanoscale. Science, 2007. **316**(5824): p. 561-565.

2. Campbell, C.T., S.C. Parker, and D.E. Starr, The effect of size-dependent nanoparticle energetics on catalyst sintering. Science, 2002. **298**(5594): p. 811-814.

3. Campbell, C.T. and C.H.F. Peden, Chemistry - Oxygen vacancies and catalysis on ceria surfaces. Science, 2005. **309**(5735): p. 713-714.

4. Fu, Q., H. Saltsburg, and M. Flytzani-Stephanopoulos, Active Nonmetallic Au and Pt Species on Ceria-Based Water-Gas Shift Catalysts. Science, 2003. **301**(5635): p. 935-938.

5. Stambouli, A.B. and E. Traversa, Solid oxide fuel cells (SOFCs): a review of an environmentally clean and efficient source of energy. Renewable & Sustainable Energy Reviews, 2002. **6**(5): p. 433-455.

6. Shao, Z.P. and S.M. Haile, A high-performance cathode for the next generation of solid-oxide fuel cells. Nature, 2004. **431**(7005): p. 170-173.

7. Tsunekawa, S., T. Fukuda, and A. Kasuya, Blue shift in ultraviolet absorption spectra of monodisperse CeO_{2-x} nanoparticles. Journal of Applied Physics, 2000. **87**(3): p. 1318-1321.

8. Corma, A., et al., Hierarchically mesostructured doped CeO_2 with potential for solar-cell use. Nature Materials, 2004. **3**(6): p. 394-397.

9. Chen, J., et al., Rare earth nanoparticles prevent retinal degeneration induced by intracellular peroxides. Nat Nano, 2006. **1**(2): p. 142-150.

10.Tarnuzzer, R.W., et al., Vacancy engineered ceria nanostructures for protection from radiation-induced cellular damage. Nano Letters, 2005. **5**(12): p. 2573-2577.

11.Deshpande, S., et al., Size dependency variation in lattice parameter and valency states in nanocrystalline cerium oxide. Applied Physics Letters, 2005. **87**(13).

12.Andersson, D.A., et al., Optimization of ionic conductivity in doped ceria. Proceedings of the National Academy of Sciences of the United States of America, 2006. **103**(10): p. 3518-3521.

13.Han, W.Q., L. Wu, and Y. Zhu, Formation and Oxidation State of CeO_{2-x} Nanotubes. J. Am. Chem. Soc., 2005. **127**(37): p. 12814-12815.

14.Kuchibhatla, S., A.S. Karakoti, and S. Seal, Hierarchical assembly of inorganic nanostructure building blocks to octahedral superstructures - a true template-free self-assembly. Nanotechnology, 2007. **18**(7): p. 075303(4pp).

15.Hernandez-Alonso, M.D., et al., Confinement effects in quasi-stoichiometric CeO_2 nanoparticles. Physical Chemistry Chemical Physics, 2004. **6**(13): p. 3524-3529.

16.Masui, T., et al., Characterization of Cerium(IV) Oxide Ultrafine Particles Prepared Using Reversed Micelles. Chem. Mater., 1997. **9**(10): p. 2197-2204.

17.Wu, L.J., et al., Oxidation state and lattice expansion of CeO_{2-x} nanoparticles as a function of particle size. Physical Review B, 2004. **69**(12).

18.Zhang, Y.W., et al., Facile alcohothermal synthesis, size-dependent ultraviolet absorption, and enhanced CO conversion activity of ceria nanocrystals. Journal of Physical Chemistry B, 2003. **107**(37): p. 10159-10167.

19. Candace, S., Particle Size Matters: Studies fail to include basics for asserting toxicity, in Small Times Magazine. 2006, March 17.

20. Wang, J.F., et al., Highly polarized photoluminescence and photodetection from single indium phosphide nanowires. Science, 2001. **293**(5534): p. 1455-1457.

21. Zhang, H.Z., et al., Water-driven structure transformation in nanoparticles at room temperature. Nature, 2003. **424**(6952): p. 1025-1029.

22. Baer, D.R., et al., Characterization Challenges for Nanomaterials. Surface and Interface Analysis, 2008, **40**: p. 529-537

23. Karakoti, A.S., et al., Direct Synthesis of Nanoceria in Aqueous Polyhydroxyl Solutions. J. Phys. Chem. C, 2007. **111**(46): p. 17232-17240.

24. Yin, L.X., et al., Sonochemical synthesis of cerium oxide nanoparticles - Effect of additives and quantum size effect. Journal of Colloid and Interface Science, 2002. **246**(1): p. 78-84.

25. Fangxin, L., et al., Optical properties of nanocrystalline ceria. Applied Optics, 1997. **36**(13): p. 2796 - 2798.

26. Feng, Z., et al., Cerium oxide nanoparticles: Size-selective formation and structure analysis. Applied Physics Letters, 2002. **80**(1): p. 127-129.

27. Hayes, S.A., et al., The phase stability of cerium species in aqueous systems - I. E-pH diagram for the Ce-HClO$_4$-H$_2$O system. Journal of the Electrochemical Society, 2002. **149**(12): p. C623-C630.

28.Charles R. Pottenger, D.C.J., Mechanism of cerium (IV) oxidation of glucose and cellulose. Journal of Polymer Science Part A-1: Polymer Chemistry, 1970. **8**(2): p. 301-318.

29.Czapski, G., B.H.J. Bielski, and N. Sutin, The Kinetics of The Oxidation of Hydrogen Peroxide by Cerium(Iv). J. Phys. Chem., 1963. **67**(1): p. 201-203.

30.Medalia, A. and B. Byrne, Spectrophotometric Determination of of Cerium (IV). Anal. Chem., 1951. **23**(3): p. 453-456.

31.Sigler, P.B. and B.J. Masters, The Hydrogen Peroxide-induced Ce*(III)-Ce(IV) Exchange System. J. Am. Chem. Soc., 1957. **79**(24): p. 6353-6357.

32.Gryder, J.W. and R.W. Dodson, The Kinetics of the Exchange Reaction between the Two Oxidation States of Cerium in Acid Solution. J. Am. Chem. Soc., 1951. **73**(6): p. 2890-2895.

33.Saito, E. and B.H.J. Bielski, The Electron Paramagnetic Resonance Spectrum of The HO_2 Radical in Aqueous Solution. J. Am. Chem. Soc., 1961. **83**(21): p. 4467-4468.

34.Bielski, B.H.J. and E. Saito, Activation Energy for Disproportionation of Ho2 Radical in Acid Solutions. Journal of Physical Chemistry, 1962. **66**(11): p. 2266-&.

3.1.6 Supporting Information

Table 2: (SI-1) -Summary of ceria synthesis and analysis by various researchers

Precursor/Method of Synthesis/Oxidizer	Particle Size, nm	Band Gap, (eV)	Comments	ref
Ce(III)/Micro emulsion/TMAOH Heptane and dodecane solvents	5 – 10	2.92	a) support QC but no size dependence was reported b) attribute the effects observed to Ce3+ and some unknown physicochemical aspects	1
Ce(III) / Composite hydroxide mediated approach/ powders suspended in ethanol	varies with time and temperature 3 – 7	blue shift with decrease in size	a) do not make any comment about confinement effects	2
Ce(III)/ Sonochemical/ TAAOH/Azocarbonamide	3 – 5	3.68 – 3.0	a) support QC b) variation in	3

			particle size is attributed to the alkyl chain length in TAAOH	
Ce(III)/ homogeneous precipitation/ Alcohol + water/ NaOH	varies with the amount of alcohol 4 – 9	no /comments	a) attribute the variation in the particle size to dielectric properties of the solvent b) no comments on QC	4
Ce(III)/ hydrothermal/ size fractionation/ Alcohol + surfactant	varies with surfactant 2 – 3	3.18 – 2.83	a) support QC b) propose the possible contribution of Ce3+ c) increase in Ce3+ with decrease in particle size	5

Ce(III)/ Successive microemulsion	2 – 3	4.2 – 3.6	a) deny the QC b) possible contribution of Ce3+ c) propose that the charge transfer is direct	6
Ce(III)/NH₄OH/particles dispersed in alcohol	2.6 and 4.1	3.44 and 3.38	a) band gap variation is negligible b) deny the QC c) propose the charge transfer to be both direct and indirect	7
Ce(III) nitrate/ hexamethyl tetramine	3 – 12	blue shift with decrease in particle size	a) support QC b) no consideration of chemistry c) lattice expansion due to Ce3+ but do not	8

			consider the same in case of UV-Vis analysis	

It is quite evident from the above table, that there are clear differences in the way the shift in optical absorption of ceria NPs is being interpreted by different researchers.
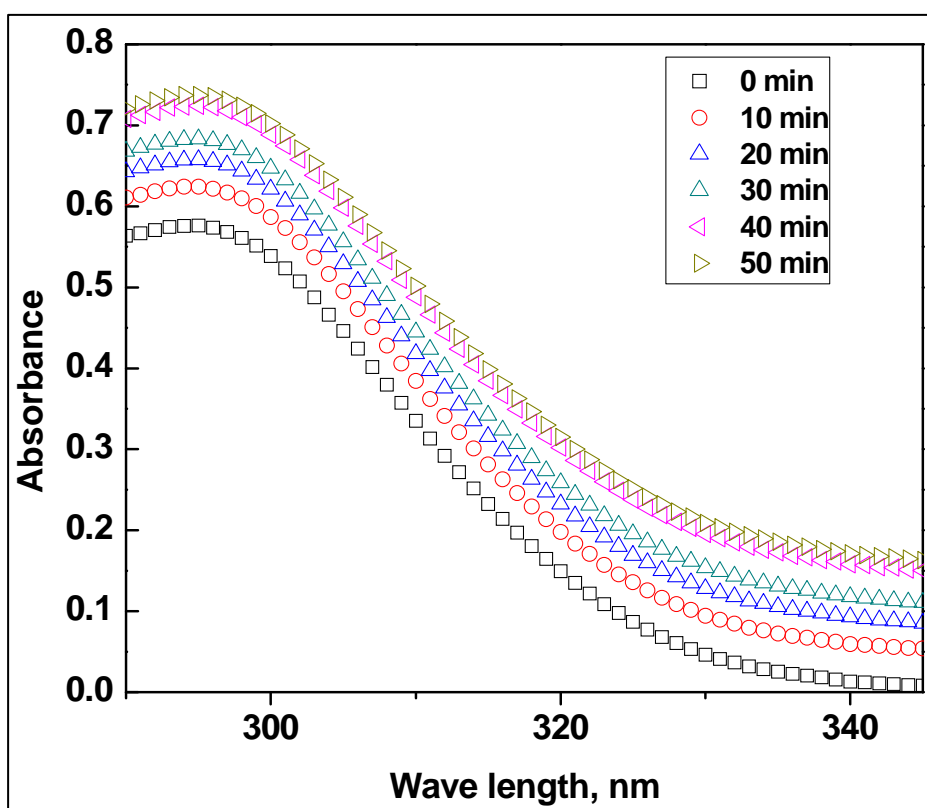
Figure SI-1: The absorbance values of CNPs synthesized in DI water as a function of time. Data was collected at every two minutes during first 60 minutes, from which data at every 10 minutes is presented here.
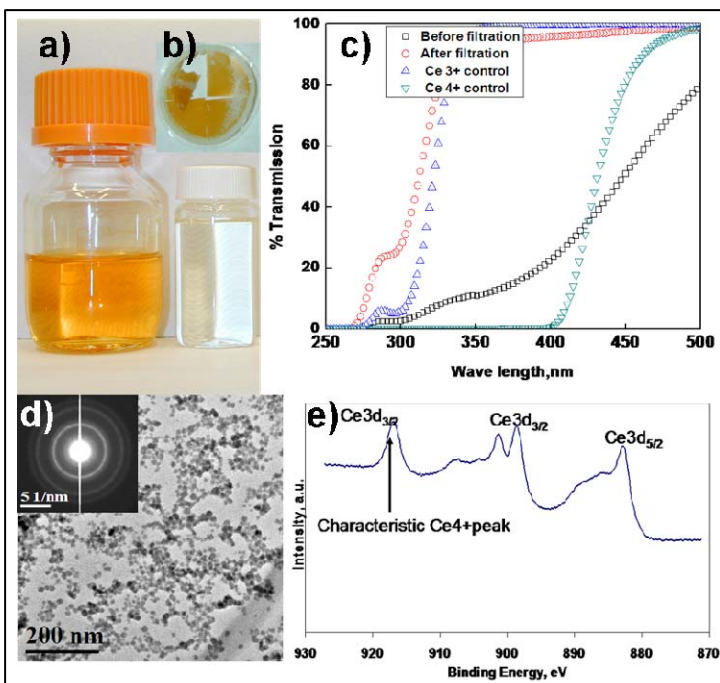
Figure SI-2: Pictorial representation of the filtration experiment a) with the pre and post filtration solutions b) the filter paper with nanoparticles c) the corresponding transmission spectra along with the control Ce^{3+} and Ce^{4+} spectra d) representative TEM image (inset) SAED pattern confirming the fluorite structure of ceria and e) Ce_{3d} X-ray photoelectron spectrum of the nanoparticles on the filter paper

Explanation for Figure SI-2:

The solution with nanoparticles was filtered (20-nm alumina filter from Millipore(TM)) after 1 day of aging. Both the spectral and visual confirmations are provided in Fig. SI-2. The solution before and after filtration show clear difference and the filter paper shows the presence of yellow colored CNPs. The post filtration solution was found colorless demonstrating the role of nanoparticles in its color. The optical absorption spectrum confirms the absence of Ce^{4+} in the solution. Apparently, the suspension contains a maximum amount of 4+ oxidation state after 1-day (Fig-1). The solution shown in the

picture, Figure SI-2, has 5 times more hydrogen peroxide than the optimal amount and is purely used to show the pronounce effect of the particle oxidation state induced color changes. The HRTEM image in Fig. SI-2 was obtained by dipping a carbon coated copper grid in the CNP suspension, before filtration. It is clear from the image that the agglomerates are ~20 nm constituted by 3-5 nm individual particles. The XPS data (Fig SI-2-e) also confirm the 4+ oxidation state of the nanoparticles on the filter.
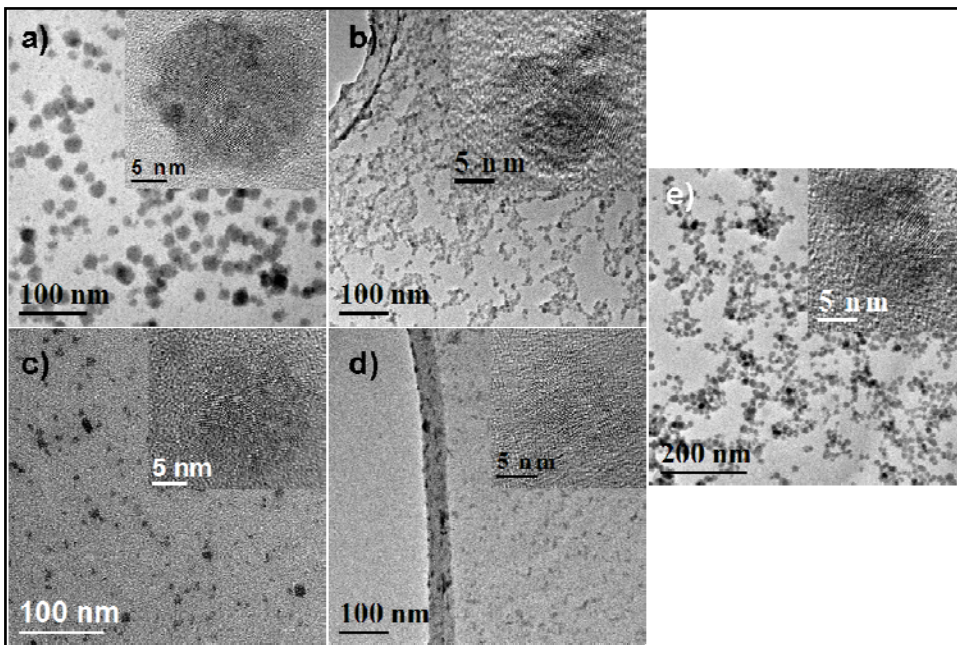
Figure SI-3. HRTEM images of CNPs synthesized in a) 20 PEG b) 20 EG c) 100EG d) 100PEG e) DI water are shown. It is clear from the in set images that irrespective of the synthesis medium individual nanoparticles are 3 – 5 nm with agglomerate size ranging from 10-20 nm.
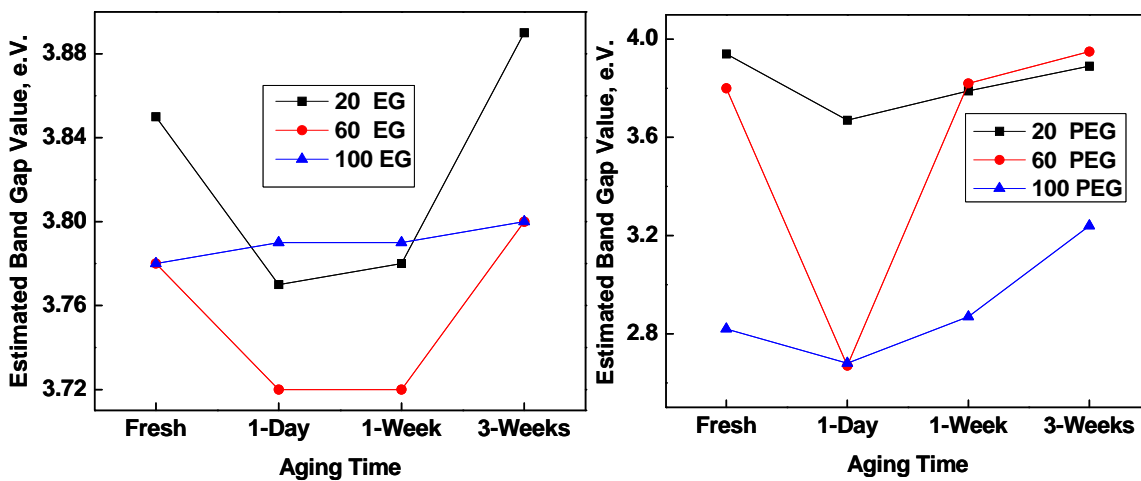
Figure SI-4: Graphs present two completely different trends in the band gap variation as a function of time in both EG (left) and PEG (right) systems. The numbers 20, 60, 100 are the percentage of EG and PEG with remaining DI water. It is evident that both CNPs synthesized and aged in EG and PEG result in quite distinct band gap values, a direct indication of the amount of Ce4+ in the nanoparticles. More detailed studies to understand the nanoparticles' surface chemistry as a function of additives is underway.

REFERENCES FOR SUPPORTING INFORMATION

1. Hernandez-Alonso, M. D. et al. Confinement effects in quasi-stoichiometric CeO_2 nanoparticles. Physical Chemistry Chemical Physics 6, 3524-3529 (2004).

2. Hu, C. G., Zhang, Z. W., Liu, H., Gao, P. X. & Wang, Z. L. Direct synthesis and structure characterization of ultrafine CeO_2 nanoparticles. Nanotechnology 17, 5983-5987 (2006).

3. Yin, L. X., Wang, Y. Q., Pang, G. S., Koltypin, Y. & Gedanken, A. Sonochemical synthesis of cerium oxide nanoparticles - Effect of additives and quantum size effect. Journal of Colloid and Interface Science 246, 78-84 (2002).

4. Chen, H. I. & Chang, H. Y. Homogeneous precipitation of cerium dioxide nanoparticles in alcohol/water mixed solvents. Colloids and Surfaces A-Physicochemical And Engineering Aspects 242, 61-69 (2004).

5. Tsunekawa, S. et al. Ultraviolet absorption spectra of CeO_2 nano-particles. Materials Science Forum 315-317, 439-445 (1999).

6. Tsunekawa, S., Fukuda, T. & Kasuya, A. Blue shift in ultraviolet absorption spectra of monodisperse CeO_{2-x} nanoparticles. Journal of Applied Physics 87, 1318-1321 (2000).

7. Masui, T. et al. Characterization of Cerium (IV) Oxide Ultrafine Particles Prepared Using Reversed Micelles. Chem. Mater. 9, 2197-2204 (1997).

8. Feng, Z. et al. Cerium oxide nanoparticles: Size-selective formation and structure analysis. Applied Physics Letters 80, 127-129 (2002).

3.2 Tuning the Band Gap of Nano-Ceria Using Mono and Poly-Ols

3.2.1 Introduction

Cerium oxide, (Ceria), is a widely studied rare-earth oxide with potential uses in WGS catalysis, solid oxide fuel cells, solar cells, UV-protection, and solar cells. Of late, a significant amount of focus is devoted to the bio-medical applications and toxicity of nanoceria [1-4]. With its mixed oxidation states of +3 and +4, nanoceria particles below 10 nm are often nonstoichiometric and hence are written as CeO_{2-x} rather than CeO_2. In almost every application of interest, the key property of ceria is its oxygen-buffering capability, stemming from its ability to effectively switch between +4 and +3 oxidation state. It was shown earlier by various researchers that the lattice parameter of ceria will increase with decrease in particle size. This anomalous behavior has been attributed to the higher amount of oxygen vacancies as a result of increasing Ce^{3+} concentration with decrease in particle size [5, 6]. We have earlier seen the time and environment dependent oxidation states in CNPs suspended in aqueous media [7]. When the CNPs were aged for longer time periods at room temperature in as synthesized condition, we observed the hierarchical assembly of individual CNPs into a fractal, superoctahedral morphology [8]. Motivated by these results, when we synthesized CNPs in various monomer and polymer solvent concentrations, we learned that the size, chemistry and the band gap of CNPs could be tuned by varying the synthesis medium.

3.2.2 Experiments and Analysis

Here we report the synthesis of CNPs in aqueous solvents based on ethylene glycol and polyethylene glycol over a range of compositions, in particular 0, 20, 40, 60, 80 and

100% with DI-water. A Detailed synthesis method is already explained in the previous chapters. The as synthesized and aged CNPs were analyzed using UV-Vis and HRTEM. While UV-Vis data from nanoparticle suspension was used to calculate the band gap as a function of time, HRTEM was used to analyze the size, shape and structure of the CNPs. The UV-Vis transmission spectra for the nanoparticle suspensions were collected in as synthesized condition, aged at room temperature for an interval of 1-day up to 1 week and after 2 weeks of aging. The HRTEM images were obtained by gently dipping holey carbon grids in the nanoparticle suspensions.

A significant shift in the absorption spectra was observed both as a function of time and the amount of glycol in the solution. A few representative spectra and the pictures representing the color of the solutions are presented in Figure 25. The color of the solution is a result of charge transfer. The CNPs suspensions with increasing concentration of Ce^{4+} will change the color from light yellow to orange red color. From Figure 25 (d) and (e), it is evident that with the increasing concentration of PEG the amount of Ce^{4+} in solution will be higher. However, significant differences were not found in case of the EG-based suspensions. When these suspensions were aged for more than one week, significant differences could be observed in the color of various suspensions (Figure 25e). This indicates that the variation in the oxidation state of cerium is dependent on the surrounding environment.
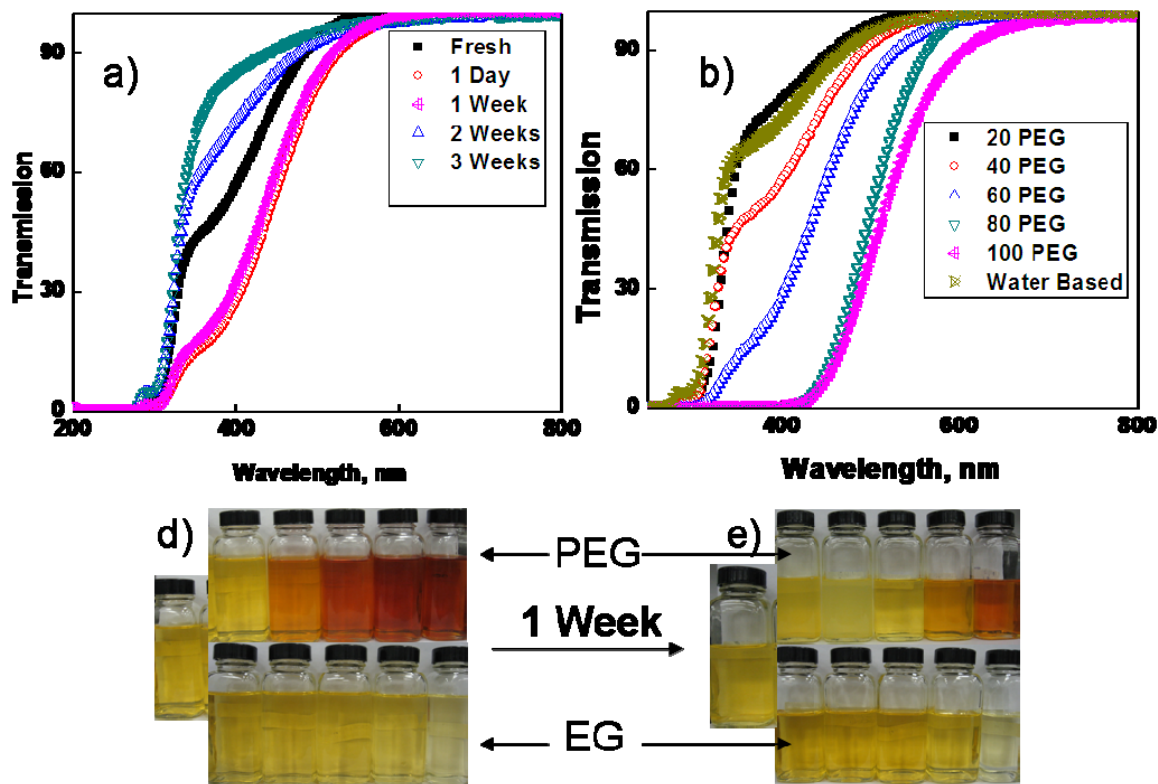
Figure 25: a) UV-Vis transmission spectra of CNPs synthesized in 20EG + 80 DIW solution from as synthesized condition to 3 weeks of aging b) the UV-Vis transmission data of as synthesized CNPs in different concentrations of PEG alone. Data corresponding to water based CNPs is also included; d) and e) are representative images of the bottles containing CNPs in as synthesized condition and after 1 week of aging in various solvents. The bottles at extreme left in both the picture represent the water based CNPs. The variation in the absorption behavior of CNPs as a function of both aging and environment is illustrated with these images.

Tsunekawa et al [9] have categorically shown that the electronic transitions in ceria are direct in nature. The band gap calculation from the optical absorption data is explained in Chapter 3.1. The variation in the band gap values for selected compositions of the solvents at different aging times is presented in Figure 26.

HRTEM analysis has revealed that the nanoparticles are of ~ 3 – 5nm in size, with their agglomerate size dependent on the solvent composition. A few representative images of the freshly synthesized CNPs are presented in Figure 27. While the 20 and 40 % PEG solutions were observed to form the superoctahedral agglomerates through hierarchical assembly, the sols beyond 60% PEG were found to retain the individual nanoparticles without significant agglomeration even after 2 weeks of aging. No significant changes were observed in EG based sols and hence most of the discussion in this chapter is confined to the data for nanoparticles suspensions in PEG.
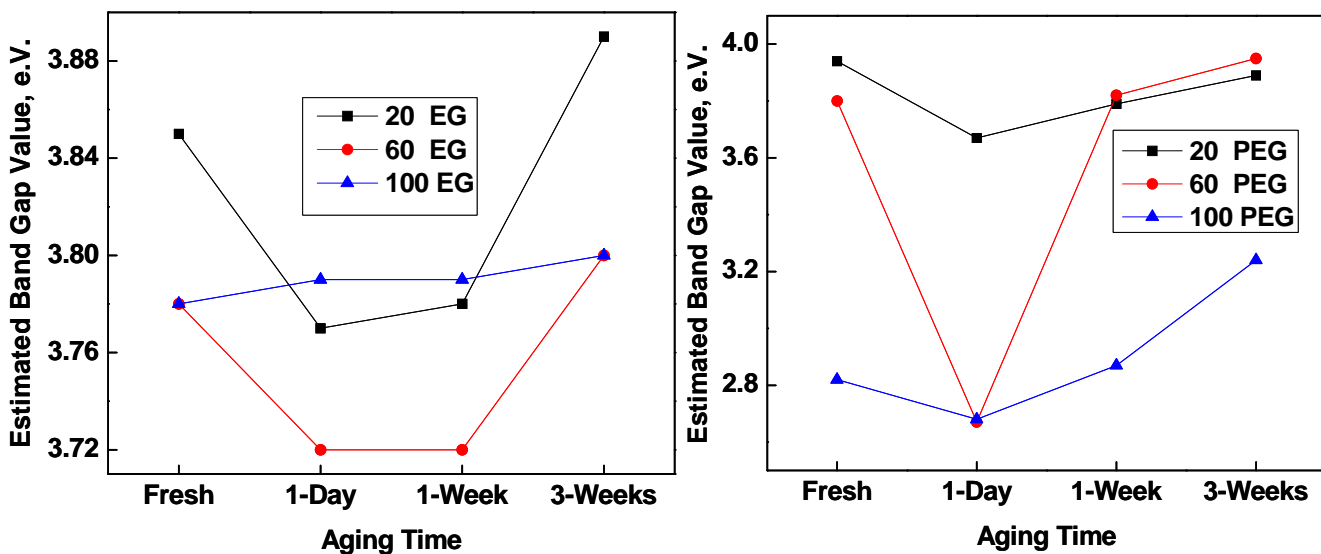
Figure 26. Graphs present two completely different trends in the band gap variation as a function of time in both EG (left) and PEG (right) systems. The numbers 20, 60, 100 are the percentage of EG and PEG with remaining DI water. It is evident that both CNPs synthesized and aged in EG and PEG result in quite distinct band-gap values, a direct indication of the amount of Ce^{4+} in the nanoparticles.

The contribution of the mono and poly-ols in tuning the chemistry and the size are a result of their variable interaction with the nanoparticles. While some of the previous researchers have attributed the band gap changes to possible confinement effects in nanoceria, we have systematically shown that the apparent changes in ceria band gap are mostly driven by the changes in the nanoparticles' chemistry than the size. The band gap values calculated for all the systems in this work at different aging periods have been carefully analyzed and were found to agree with the color of the solution or in other words the oxidation state of the CNPs. The higher the amount of Ce^{4+}, the lower will be the band gap. The correlation between the spectra obtained from the nanoceria samples in different solvents and their oxidation state was achieved by comparing the spectra from nanoparticles suspension with the characteristic Ce^{4+} and Ce^{3+} spectra obtained by

122

dissolving the respective salts in DI water. It is shown in the previous section that the color changes in CNP suspensions are indeed a result of a change in the oxidation state of the nanoparticles through a simple filtration experiments.

The regenerative oxidation and reduction of Ce^{3+} and Ce^{4+} stem from the interaction of Ce with the surrounding environment, as per the following equations [10]:

$$Ce^{3+} + OH^- + \frac{1}{2} H_2O_2 \rightarrow Ce(OH)_2^{2+} \tag{1}$$

$$Ce(OH)_2^{2+} + 2\ OH^- \rightarrow Ce(OH)_4 \rightarrow CeO_2\cdot2H_2O \tag{2}$$

$$Ce^{4+} + HO_2 \rightarrow Ce^{3+} + H^+ + O_2 \tag{3}$$
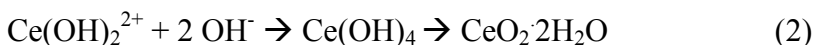
It is clear from the above equations and some of the previous studies that the Ce^{4+} is capable of oxidizing species in its vicinity and form Ce^{3+}. In addition to the $HO_2^.$ radicals generated from the oxidizer, H_2O_2, Ce^{4+} has the capability to oxidize various species including water to form Ce^{3+}. The Ce^{3+} species can be oxidized to Ce^{4+} not only by adding an oxidizer but by any other oxidizing species in its vicinity. This is the reason behind significantly higher amount of Ce^{4+} in 100% PEG solution (Figure 1). In PEG the oxygen from the ether groups acts as a base and oxidizes the Ce^{3+} [11]. However, when there is a significant amount of water in its vicinity, the PEG-oxygen will have a higher tendency to form hydrogen bonds with the water molecules. This means that the amount of Ce^{4+} purely depends on the amount of externally added oxidizer until a critical concentration beyond which both the oxidizer and the oxygen from ether groups will control the chemistry, although the EG is also expected to show an interaction similar to a base because of terminal OH groups. Significant differences in the oxidation state of Ce as a function of amount of solvent was not found in freshly synthesized condition.

However, differences were observed in the reduction of Ce^{4+} to Ce^{3+}. In great contrast to the 100PEG, 100EG system has not shown significant amount of Ce^{4+} and was also found to lose its light yellow color quickly around 1 week of aging. This could be a result of stronger interaction between EG and cerium. Uekawa et al. [11] have shown with IR spectra that the strength of coordination between EG and cerium is higher compared to PEG and this fact may influence the hydrolysis, a primary step for the formation of cerium oxide. A consistent observation in all the systems is that the initial oxidation of Ce^{3+} to Ce^{4+} was much faster than the reduction of Ce^{4+} back to Ce^{3+}. This agrees with previous titration experiments which show that the reduction of Ce^{4+} while oxidizing water is a slower reaction compared to the oxidation of Ce^{3+} by oxygen [10]. Focus of this chapter is to show the band gap variation as a function of time and solvent composition. Detailed studies pertaining to the overlayer thickness and other surface chemistry related aspects to explore the atomistic interaction between the organic molecules and ceria have potential future scope.
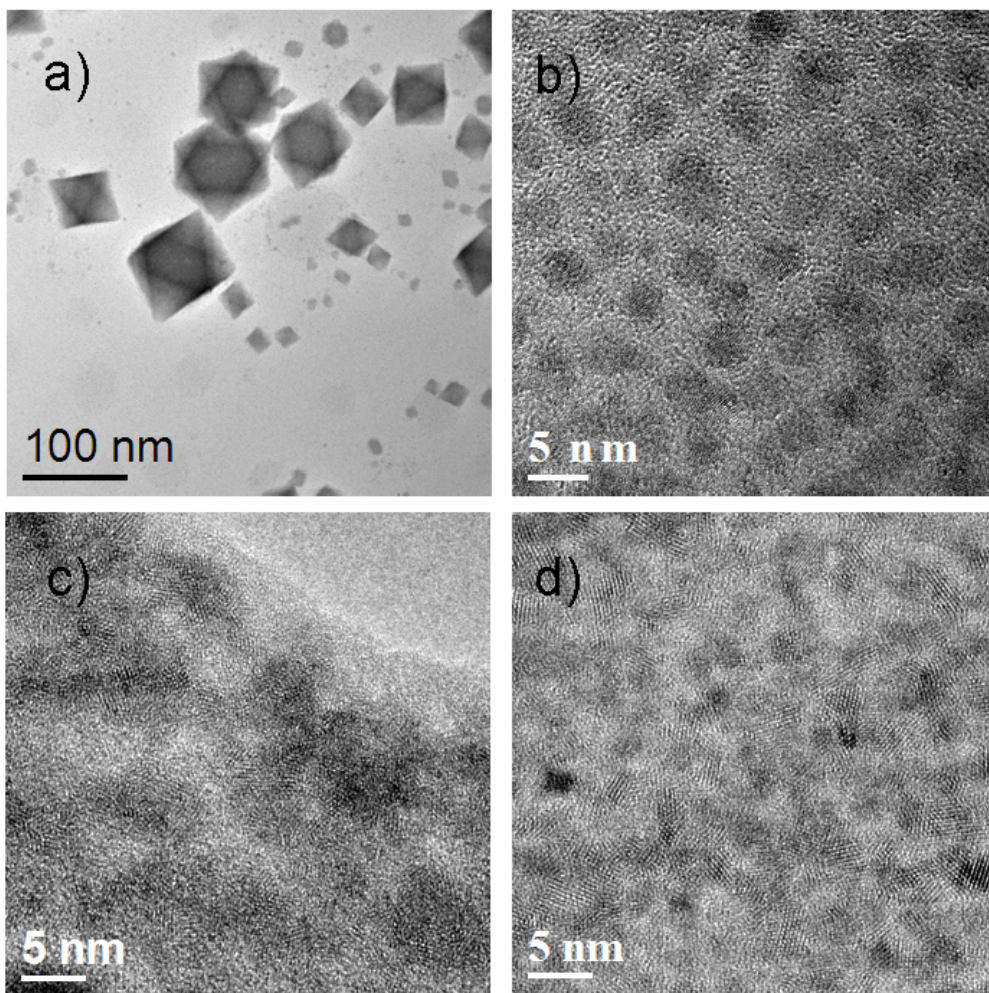
Figure 27: HRTEM images of CNPs synthesized and aged for 2 weeks in a) 40 PEG b) 60 PEG c) 40EG d) 60 EG. The scale bar in a) had to be higher to show the octahedral morphology and the particles being very small in other cases very high magnification images are present. We did not see any morphology in compositions these systems even after 2 weeks of aging, confirming the ability of the additives to constrain agglomeration.

The HRTEM analysis showed that the agglomeration tendency decreases with increasing PEG content. Selected HRTEM images are presented in Figure 27. In the case of 60PEG and above, individual nanoparticles of 3-5 nm were observed even after 2 weeks of aging. Some small agglomerates were found occasionally, which could have formed within the

water pockets available in high PEG solutions. Formation of superoctahedra through self-assembly was not observed. The primary explanation for this interesting trend could be derived from 2 main features of the glycol based solvents. With the increase in glycol content from 0 to 100 (PEG) the dielectric constant of the solvent decreases from 79 to 13 and the viscosity increases from 0.89 cps to 36.45 cps at 25 ^{o}C (see Table -1, pg: 121). Particle size has a proportional dependence to the dielectric constant; the viscosity has an inverse relationship to the agglomeration tendency. Although a detailed explanation of the colloidal stability and agglomeration kinetics are not the focus of this study, it is important to note that the low dielectric constant and high viscosity will be ideal to achieve smaller particle size with less agglomeration probability. The probability of agglomeration is proportional to the total number of collisions which in turn is dependent on viscosity. Particle radius (R) = A + B/ε; where A and B are constants for a given system that account for various characteristics including the interfacial tension, charge state, and potential energy difference at a given particle size. Hence, the higher amount of glycols in water will support the smaller particle size while simultaneously reducing the agglomeration tendency. In addition to the steric hindrance aspect, higher amounts of glycol surrounding the nanoparticles will act as a physical barrier for the van der Waals forces to overcome. When two particles come closer, the inter-particle region acts as a fine capillary and the adsorbed species will be pushed out of the interface forming agglomerates. However, the capillary forces may not be effective beyond a critical inter-particle distance where the solvent volume is very high to be removed, hence preserve the

individual particles intact. A schematic of this feature is provided in the SI along with the dielectric constant and viscosity at room temperature for selected solvents.

3.2.3 Conclusions

It is evident from the above results that the size and band gap of CNPs could be tuned with appropriate solvents and aging conditions. This environment dependent band gap variation may have significant impact on the use of ceria in sensors, radiation blocking and bio-medical applications.

REFERENCES

1. Murray, E.P., T. Tsai, and S.A. Barnett, A direct-methane fuel cell with a ceria-based anode. Nature, 1999. **400**(6745): p. 649-651.

2. Chen, J., et al., Rare earth nanoparticles prevent retinal degeneration induced by intracellular peroxides. Nat Nano, 2006. **1**(2): p. 142-150.

3. Corma, A., et al., Hierarchically mesostructured doped CeO_2 with potential for solar-cell use. Nature Materials, 2004. **3**(6): p. 394-397.

4. Campbell, C.T. and C.H.F. Peden, Chemistry - Oxygen vacancies and catalysis on ceria surfaces. Science, 2005. **309**(5735): p. 713-714.

5. Deshpande, S., et al., Size dependency variation in lattice parameter and valency states in nanocrystalline cerium oxide. Applied Physics Letters, 2005. **87**(13).

6. Tsunekawa, S., et al., Ultraviolet absorption spectra of CeO_2 nano-particles. Materials Science Forum, 1999. **315-317**: p. 439-445.

7. Karakoti, A.S., et al., Direct Synthesis of Nanoceria in Aqueous Polyhydroxyl Solutions. J. Phys. Chem. C, 2007. **111**(46): p. 17232-17240.

8. Kuchibhatla, S., A.S. Karakoti, and S. Seal, Hierarchical assembly of inorganic nanostructure building blocks to octahedral superstructures - a true template-free self-assembly. Nanotechnology, 2007. **18**(7): p. 075303(4pp).

9. Tsunekawa, S., T. Fukuda, and A. Kasuya, Blue shift in ultraviolet absorption spectra of monodisperse CeO_{2-x} nanoparticles. Journal of Applied Physics, 2000. **87**(3): p. 1318-1321.

10. Hayes, S.A., et al., The phase stability of cerium species in aqueous systems - I. E-pH diagram for the Ce-HClO$_4$-H$_2$O system. Journal of The Electrochemical Society, 2002. **149**(12): p. C623-C630.

11. Uekawa, N., et al., Characterization of CeO$_2$ fine particles prepared by the homogeneous precipitation method with a mixed solution of ethylene glycol and polyethylene glycol. Journal Of Materials Research, 2004. **19**(4): p. 1087-1092.

3.2.4 Supporting information
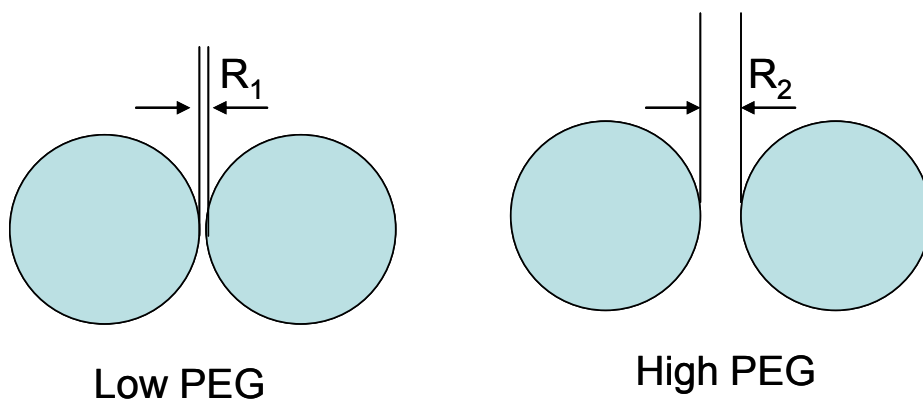
Figure: SI-1 As the R1 < R2 the capillary pressure will be lower in case of R2, making it difficult for the adsorbed species to b removed and there by the individual particles can be kept intact.

CHAPTER 4:
EFFECT OF GROWTH CONDITIONS ON THE STRUCTURE OF NANOSCALE CERIA BASED THIN FILMS

4.1 Growth Rate Induced Epitaxial Orientation of Cerium Oxide Thin Films on Sapphire (0001)

Cerium oxide (ceria, CeO_2), is a widely studied functional material with applications spanning from traditional three way catalysis [1] to the state-of-the-art microelectronic applications [2, 3]. Recently, doped ceria has gained a significant attention from the solid oxide fuel cells (SOFCs) [4, 5] as a potential electrolyte material. Various researchers have reported the growth of pure and doped cerium oxide films on Si, sapphire (Al_2O_3), yttria stabilized zirconia (YSZ) and other oxide substrates [6, 7]. However, a precise understanding of the influence of growth rate on the orientation and quality of the films on a given substrate is unavailable in the open literature. We believe, it is of high importance to realize the effects of growth rate, especially when the films of potential interest are in the nanoscale. The thermodynamic and kinetic aspects in the nanoregime might be different from that of the bulk materials [8]. It was reported earlier that creation of vacancies on the low energy (111) surface is much more difficult than that on the (100) surface [9]. Hence, the ability to tune the orientation of the films to cater for the needs of various experiments is of fundamental interest.

Our group has recently shown the ability to grow single and multi-layered, pure and doped ceria films on sapphire substrates for understanding the dopant distribution and the underlying mechanisms behind higher ionic conductivity in these films [5, 6, 10-13]. In

131

this study we, for the first time, show that the epitaxial orientation of ceria films on sapphire (0001) substrates can be tuned as a function of growth rate. Various *ex situ* and *in situ* techniques have been used to understand the structural features of the films. MD simulations were used to understand the stability of ceria in various configurations on sapphire (0001), complementing the experimental studies.

The film growth was carried out in a custom-made dual chamber molecular beam epitaxy (MBE) system with an electron cyclotron resonance oxygen plasma source and a built-in reflection high energy electron diffraction (RHEED) capability for real time monitoring of the growth process. Pre-cleaned Al_2O_3 (0001) substrates (10 mm × 10 mm × 1 mm) were used to deposit the ceria films in 2 x 10^{-5} torr oxygen plasma (200 W) and the Ce (99.9% pure) evaporated using electron beam assisted evaporation at 4.5 kV. The growth rate, measured *in situ* by quartz crystal oscillator (QCO) based thickness monitor, was calibrated by analyzing the as grown films with the help of various *ex situ* techniques, such as x-ray reflectivity (XRR), Rutherford backscattering spectrometry (RBS), and x-ray photoelectron spectroscopy (XPS) depth profile analysis. High resolution x-ray diffraction (HRXRD), glancing incidence x-ray diffraction (GIXRD), and RBS measurements in random and channeling directions were used to analyze epitaxial orientation and quality of the as grown films. Atomic force microscopy (AFM) and RHEED measurements were used to understand the surface morphology and type of growth, respectively.

The perplexing observation of the epitaxial (100) film was critically analyzed using RBS in channeling direction, x-ray in-plane reflection and MD simulations. The HRXRD and the RHEED patterns for the films deposited at a low and high growth rates are presented in Figure 28. When the films were grown at low deposition rates (< 8 Å/min), we observed spots in the RHEED pattern, indicating the transmission diffraction. Appearance of the spot pattern from the very initial stage till the end of deposition implies a 3-d island growth of the ceria films. The RHEED patterns for the films grown at a high deposition rate (up to 30 Å/min) show streaks; indicating an epitaxial, layered growth [14]. Although a detailed analysis of the RHEED patterns is not the focus of this article, a primary conclusion based on the observations is that the growth of ceria (200) on sapphire (0001) substrates falls under the Volmer-Weber growth mode [15, 16].
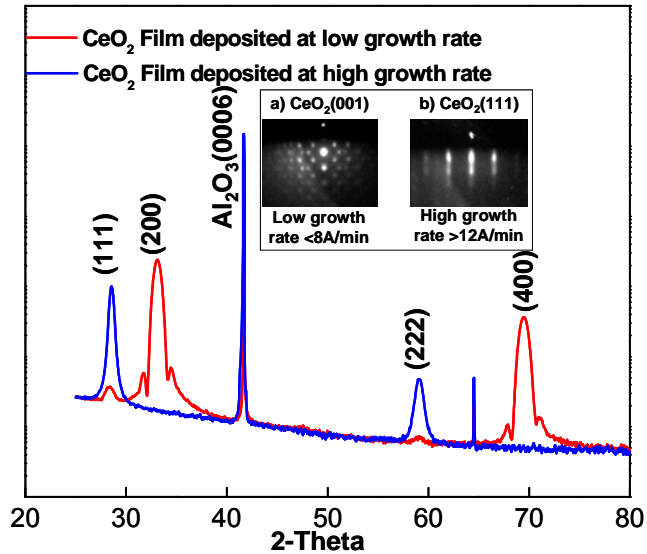
Figure 28: (i) The HRXRD patterns for ceria films deposited at 650°C at different growth rates, the inset a, b are the RHEED patterns for CeO_2 (100) and (111), respectively.

The quality of both (111) and (100) films was examined by comparing the RBS measurements in channeling and random directions and simulations based on SIMNRA software. The representative data are shown in Figure 29. The χ_{min} value, calculated from the ratio of backscattering intensity at the region just below the surface peak in the random and channeling directions, obtained for Ce from (100), (111) films was ~ 19% and 45%, respectively. These χ_{min} values are higher than expected for a defect-free crystal. However, it can be stated that the ceria (100) film is of a much better epitaxial quality compared to the ceria (111) film. The channeling data for ceria (100) shown in Figure 29(a) suggests that bulk of the film is "epitaxial", with some roughness at the surface, as evident from the AFM [17].

134
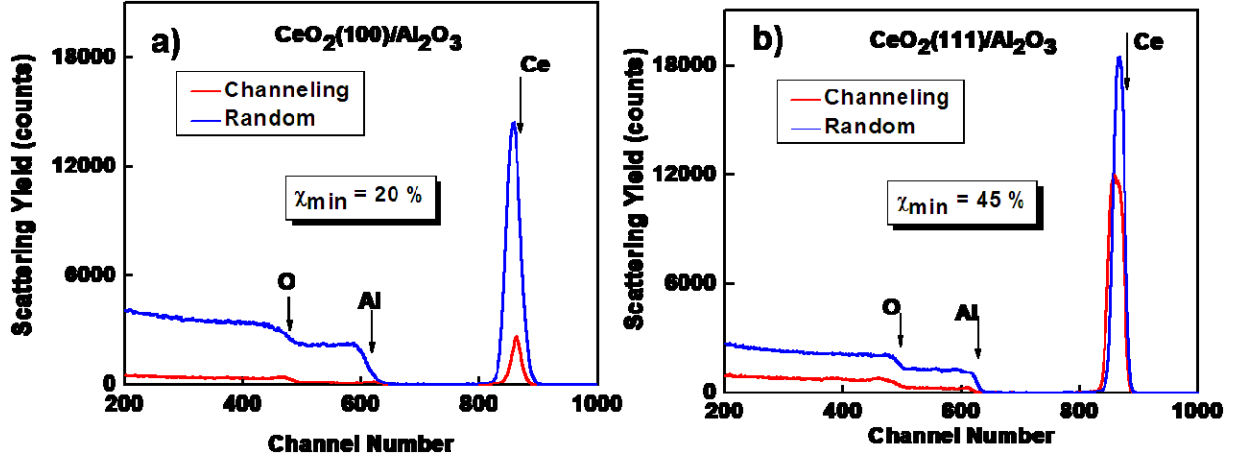
Figure 29: RBS spectra in random and channeling direction for films deposited at
a) low growth rate – (100) oriented film b) high growth rate – (111) film

In order to further explore the reasons behind differences in the epitaxial quality of these films, x-ray in-plane reflection measurements were carried out. The data is presented in the form of pole figures in Figure 30. The epitaxial single domain ceria (111) film should have three poles corresponding to (110) at 35.26° (tilt), whereas four poles are expected for a single domain epitaxial ceria (100) film at 45° (tilt). While ceria (111) film showed three (110) poles at 35.26°, the film with (100) orientation showed 12 poles at 45°. This implies that the (100) film has three in-plane domains at 30° to each other. GIXRD measurements further confirmed the absence of any polycrystalline material in these films (data not shown). We have also acquired the X-ray rocking curves for ceria films after observing the interesting trends from XRD and RBS for the ceria (111) films. The full width at half maximum for the ceria (111) film was observed to be as high as $\sim3.6^{\circ}$.

Based on the RBS and XRD analysis, the reason for the differences in the epitaxial quality of the ceria films could be explained. The slightly higher than ideal χ_{min} value for the ceria (100) film could be a result of the three in-plane domains and minor (111) orientation. Multiple in-plane orientations might have contributed to additional de-channeling of the beam, leading to the relatively high χ_{min} value. In the case of ceria (111) film, to retain the single in-plane domain, the ceria lattice must have been significantly strained to achieve the lattice match with the sapphire substrate. However, this strain might not have been high enough, that the crystal structure completely brakes down. This strain is quite evident from the omega scan results, indicating of a significantly distorted interface region. The displaced atomic positions in the ceria (111) lattice result in significantly higher back scattering yield, resulting in a very high χ_{min} value.

In order to understand the interface structure and the structural stability aspects of ceria on sapphire in different orientations, we have relied upon MD simulations. The epitaxial 3-d growth of (100) ceria films is strongly supported by our molecular dynamic (MD) simulations, performed using the DL_Poly code [17, 18]. Within the current computational capabilities, it is very difficult to model the actual growth of the films. However, the relative stabilities of various orientations can be studied and the retention of crystallinity under various conditions can be explored. For the simulation analysis, the periodic conditions are imposed along three directions, but a vacuum normal to the surface is included to represent the free surface. The ions are distributed in two regions: region one consists of the CeO_2 thin film and the first six repeat units of the α-Al_2O_3

(0001) matrix within which ions are allowed to move, whereas region two comprises a fixed support with four repeat units of Al_2O_3 that ensure the correct crystalline matrix. The model systems of CeO_2 supported on a sapphire substrate, as a first step, are employed to explore the orientation relationship of nanostructured epitaxial ceria films. Model system with the normal of the CeO_2 film along the [001] direction was generated, consisting of four repeat units that were placed directly on the top of ten repeat units of the Al_2O_3 (0001) matrix.
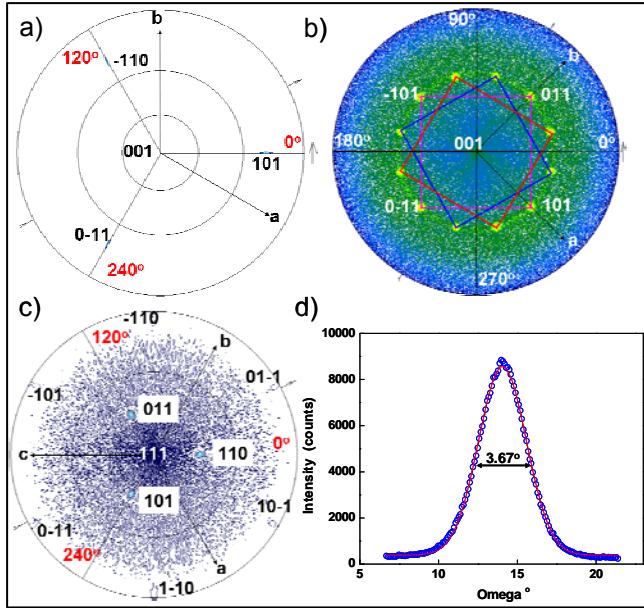
Figure 30: (110) Pole figures data corresponding to the in-plane orientation of a) Al_2O_3 (0001) b) CeO_2 (200) c) CeO_2 (111) and d) rocking curve scan for the ceria (111) film. While the CeO_2 (200) film indicates three in-plane domains, the CeO_2 (111) and Al_2O_3 (0001) have single in-plane domain.

It has been observed that an amorphous transition of the CeO_2 film eliminates all memory of the starting configuration, and evolves structurally in response solely to the lattice misfit and underlying Al_2O_3. To further demonstrate observed phenomena, we have generated a larger sub-cell of Al_2O_3 matrix with the $8 \times 5 \times 10$ atomic units, giving the total number of ions in the CeO_2 (001)/Al_2O_3 (0001) system to be 25200. For the CeO_2 (001)/Al_2O_3 (0001) model, the $5 \times 5 \times 4$ unit cells of the CeO_2 thin film, consisting of 400 Ce and 800 O atoms, was placed directly on a 5×3 Al_2O_3 support, giving a total number of 10,200 ions within the simulation cell. The lattice misfit associated with the CeO_2 thin film is -12.2% and -8.8% along the [100] and [010] directions, respectively.

$a = [110]/[11\bar{2}0]$ $b = [010]/[1\bar{1}00]$
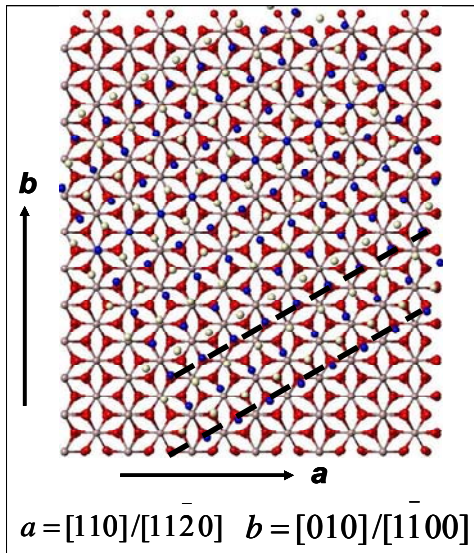
Figure 31: A proposed model of the CeO$_2$ film on the Al$_2$O$_3$ substrate, where the film is rotated 60 degree against the substrate. The atomic configurations show that the CeO$_2$ film lies almost coherent with the underlying the Al$_2$O$_3$ substrate. The red spheres represent the oxygen atoms in the substrate and the blue spheres indicate the oxygen atoms in the films.

Relaxed atomic structure of the CeO$_2$ (001)/ Al$_2$O$_3$ (0001) model is shown in Figure SI-2, where the oxygen atoms are omitted for clarification, and the cerium and aluminum atoms are represented by the large spheres with yellow and pink colors, respectively. The atomic configurations from the top view and side view are demonstrated in SI-Figures 2a and 2b, respectively. Inspection of the final relaxed structure for this model system reveals that the considerable strain within CeO$_2$ film results in its amorphous state without any long-range order preserved. The surface of the CeO$_2$ film is highly disordered, whereas the interface preserves a certain degree of order, accommodating the misfit between the CeO$_2$ film and the Al$_2$O$_3$ support.

However, when the cell size of the CeO_2 film was kept the same as the previous model and the film is placed on the Al_2O_3 (0001) support without any lattice misfit, Figure SI-3, we observed that the film remains crystalline.. Because the dimensions of the film along the [100] and [010] directions are much smaller than those of the substrate, there exist two additional free surfaces with the normal along these directions to accommodate the interfacial strain.

While the film with strain completely lost its crystallinity at equilibration, the unstrained film retained the (100) orientation. This indicates that the ceria (100) films can be stable through island growth and cannot withstand the mismatch while growing as 2-d layers. Although some disordered atomic arrangement appeared near the free surface, as expected due to the surface stresses, the atomic configuration inside the CeO_2 film was found to be highly-ordered. The first atomic layer (composing only Ce atoms) of the CeO_2 film at the interface demonstrates that some Ce atoms are relaxed to lie along the $[01\overline{1}0]$ direction, with each Ce atom on the top of Al atom or O atom.

Following the simulation and pole figure analyses, the possible configuration resulting in the 3- in plane domains can be visualized as shown in Figure 30. The model was generated by placing the CeO_2 (100) film on the top of the substrate and rotating 60° against the Al_2O_3 substrate, such that the original [100] direction of the film re-orients along the $[01\overline{1}0]$ direction of the substrate. As evidenced by the simulations and previous reports [7], excellent oxygen sublattice match is marked in Figure 28. Furthermore, the

corundum crystal structure ($R\overline{3}c$) of α-Al$_2$O$_3$ with three-fold symmetry supports the growth of the CeO$_2$ film along the (1$\overline{1}$00) directions, resulting in the 3 in-plane domains observed experimentally.

The nucleation of (100) clusters can also be viewed as a kinetically driven process. The number of atoms required to grow a (111) nucleus is larger as compared to that the (100) cluster as a result of the packing differences in both the planes [19]. Hence, when the growth rate is higher, it will be very easy to form thermodynamically and energetically stable (111) nuclei. However, the same might not be possible when there is insufficient impingement of adatoms on the substrate (low deposition rate); hence, the atoms are forced to take next energetically favorable configuration, i.e. (100).

MD simulations for the ceria (111) film on sapphire (0001) surface indicate that despite a significant interfacial strain, the ceria (111) films stayed epitaxial when simulated under initially strained conditions (similar to 2-d layered growth). Representative simulation results are shown in Figure SI-4. The simulation results, XRD and RBS data together should be carefully analyzed in order understand the complex nature of the ceria (111) film growth on sapphire (0001). HRXRD showed (Figure 28) that the ceria films grown at high growth rate are (111) epitaxial films. However, RBS in channeling direction being very sensitive to even the slight deviations from the lattice positions can result in a high channeling yield. This deviation in the atomic positions is also supported by a relatively broad peak from the rocking curve (width > 3.68° at half the maximum height),

Figure 30d. This deviation from the ideal lattice positions might result in de-channeling and there by increase the channeling yield.

4.1.1. Conclusions
 We have demonstrated with our experimental results that the epitaxial orientation of the ceria films can be tuned by varying the growth rate on sapphire (0001) substrate. In order to retain the crystallinity and epitaxial nature, the ceria (100) prefers to grow as 3-d clusters due to higher strain relaxation compared to the 2-d layers. The 3 in-plane domains in the films was attributed to the 3-fold symmetry of the Al_2O_3 (0001) surface. Although the ceria (111) films grow as epitaxial films, significant strain at the atomic level results in higher back scattering yield. MD Simulation results have been used to complement the experimental observations. For the first time we have shown the ability to grow ceria films of different orientations on a single substrate.

REFERENCES

1. Fu, Q., H. Saltsburg, and M. Flytzani-Stephanopoulos, Active Nonmetallic Au and Pt Species on Ceria-Based Water-Gas Shift Catalysts. Science, 2003. **301**(5635): p. 935-938.

2. Ami, T., et al., Room-temperature epitaxial growth of CeO_2(001) thin films on Si(001) substrates by electron beam evaporation. Applied Physics Letters, 2001. **78**(10): p. 1361-1363.

3. Kang, J.F., et al., Crystal-orientation controlled epitaxial CeO_2 dielectric thin films on Si(100) substrates using pulsed laser deposition. Microelectronic Engineering, 2001. **56**(1-2): p. 191-194.

4. Andersson, D.A., et al., Optimization of ionic conductivity in doped ceria. Proceedings of the National Academy of Sciences of the United States of America, 2006. **103**(10): p. 3518-3521.

5. Azad, S., et al., Nanoscale effects on ion conductance of layer-by-layer structures of gadolinia-doped ceria and zirconia. Applied Physics Letters, 2005. **86**(13).

6. Wang, C.M., S. Thevuthasan, and C.H.F. Peden, Interface structure of an epitaxial cubic ceria film on cubic zirconia. Journal of the American Ceramic Society, 2003. **86**(2): p. 363-365.

7. Kim, Y.J., et al., Growth and structure of epitaxial CeO_2 by oxygen-plasma-assisted molecular beam epitaxy. Journal of Vacuum Science & Technology a-Vacuum Surfaces and Films, 1999. **17**(3): p. 926-935.

8. Rowlinson, J.S., The Molecular Theory of Small Systems. Chemical Society Reviews, 1983. **12**(3): p. 251-265.

9. Conesa, J.C., Computer Modeling of Surfaces and Defects on Cerium Dioxide. Surface Science, 1995. **339**(3): p. 337-352.

10.Bera, D., et al., Growth and characterization of highly oriented gadolinia-doped ceria (111) thin films on zirconia (111)/sapphire (0001) substrates. Thin Solid Films. **In Press, Corrected Proof**.

11.Wang, C.M., et al., Distribution of oxygen vacancies and gadolinium dopants in ZrO_2-CeO_2 multi-layer films grown on alpha-Al_2O_3. Solid State Ionics, 2006. **177**(15-16): p. 1299-1306.

12.Yu, Z.Q., et al., Conductivity of oriented samaria-doped ceria thin films grown by oxygen-plasma-assisted molecular beam epitaxy. Electrochemical and Solid State Letters, 2008. **11**(5): p. B76-B78.

13.Yu, Z.Q., et al., Growth and structure of epitaxial $Ce_{0.8}Sm_{0.2}O_{1.9}$ by oxygen-plasma-assisted molecular beam epitaxy. Journal of Crystal Growth. **In Press, Corrected Proof**.

14.Chambers, S.A., Epitaxial growth and properties of thin film oxides. Surface Science Reports, 2000. **39**(5-6): p. 105-180.

15.Ohring, M., The Materials Science of Thin Films. 2002, San Diego: Academic Press.

16.Zinkeallmang, M., L.C. Feldman, and M.H. Grabow, Clustering on Surfaces. Surface Science Reports, 1992. **16**(8): p. 377-463.

17.   Supporting-information.

18.Smith, W. and T.R. Forester, The DL_POLY Molecular Simulation Package.

19. The planar density in a typical FCC structure is almost 4 times higher for (111) compared to (100) planes.

4.1.2 Supporting Information
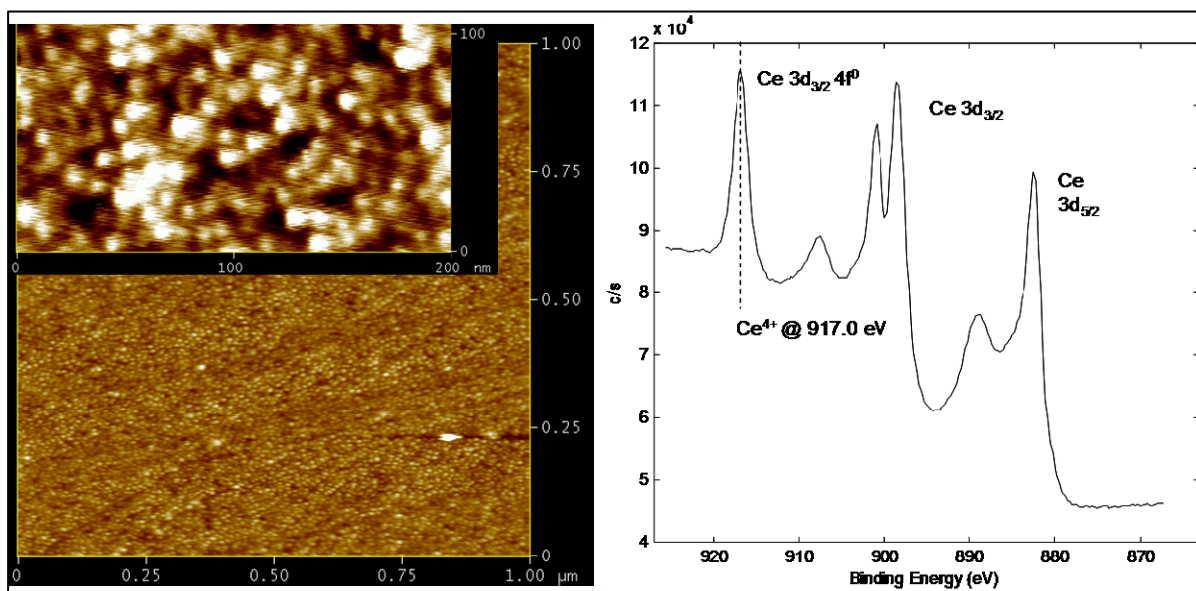

Figure SI-1: Left) Low and high (in set) magnification AFM images confirming the clustered nature of the film surface. The film roughness was of the order of few angstroms; Right) High resolution XPS data clearly indicates pure "4+" oxidation state of cerium, with characteristic Ce4+ peak identified. The Ce3d spectrum is complicated with a number of peaks with spin orbit splitting.

Figure SI-2: Relaxed atomic structures of the CeO_2 (001)/Al_2O_3 (0001) system; (a) top view and (b) side view, the oxygen atoms are eliminated for clarification. The yellow spheres represent Ce atoms, and the pink spheres indicate Al atoms.

Figure SI-3: Relaxed atomic structures of the CeO$_2$ film in a large cell without applied strain; (a) side view and (b) top view in which the Ce atoms at the first layer near the interface are plotted. Atom presentation is the same as that in Figure. SI-1.
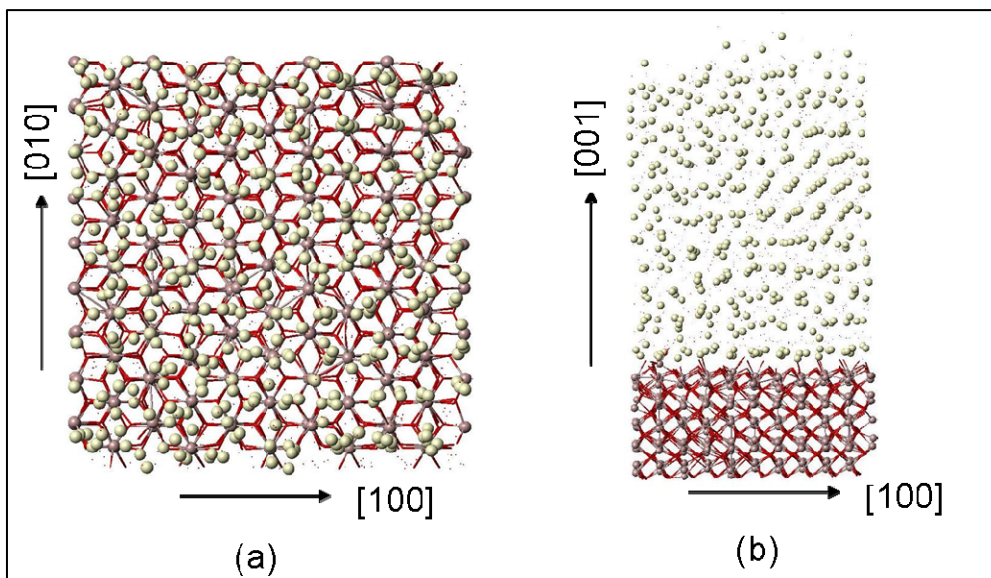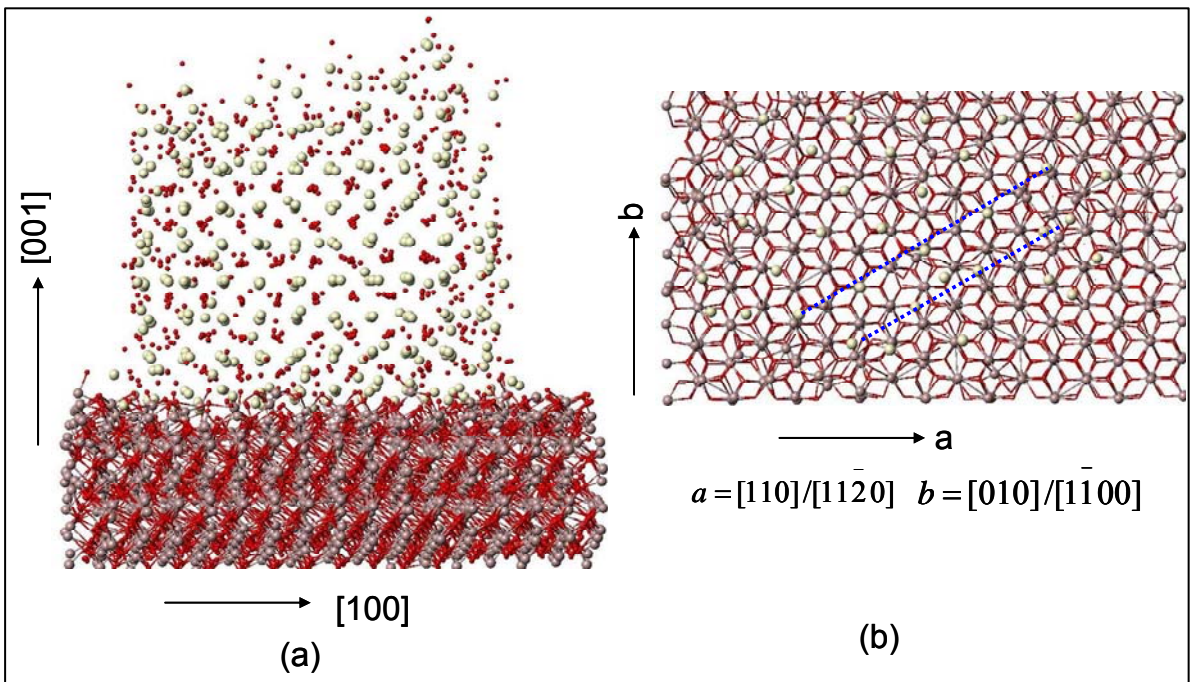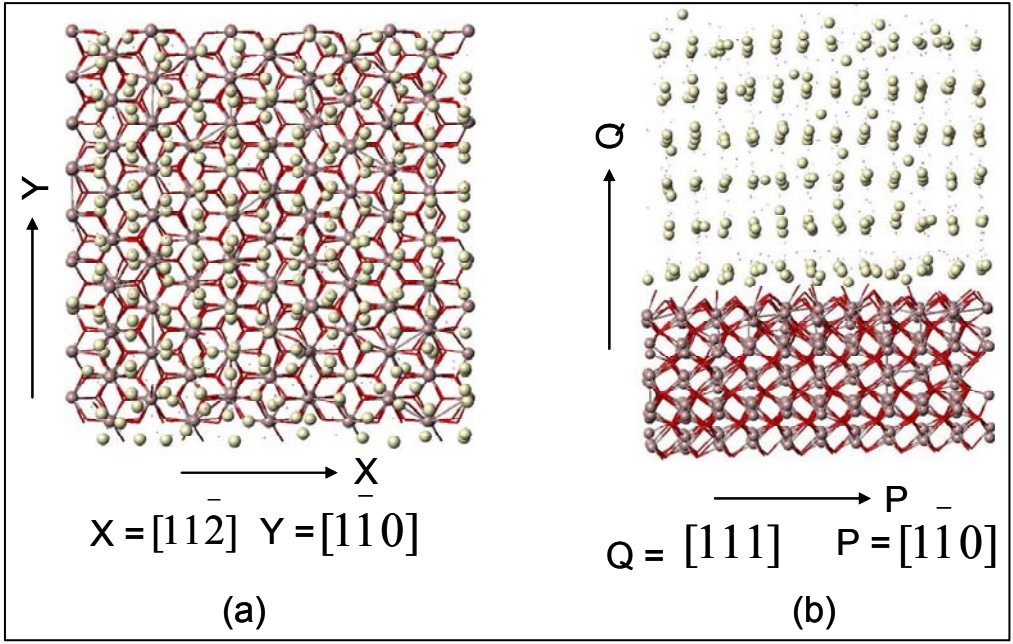
Figure SI-4: Relaxed atomic structures of the CeO_2 (111)/Al_2O_3 (0001) system; (a) top view and (b) side view, where the oxygen atoms are eliminated for clarification.

CHAPTER 5:
SUMMARY, CHALLENGES AND FUTURE SCOPE

It is evident from this dissertation that the nanoceria has a unique, intriguing characteristic of time and local environment dependent change in oxidation state. As opposed to the conventional methodology of synthesizing, precipitating, drying and characterizing the properties of nanoparticles, this dissertation reported the studies on the nanoparticles in as synthesized environment and conditions that are of more practical importance. Another significant contribution of this dissertation is the emphasis and the need for long term aging studies of the nanoparticles. The mind probing features of CNPs in terms of both structure and chemistry have been realized exclusively as a consequence of the long term aging studies.

Following is a summary of what we have learnt from this *"wonder nanomaterial"* during the course of this doctoral program.

1. CNPs can be synthesized at room temperature in bio-compatible media such as PEG while imparting long term stability.

2. Upon aging nanoceria at room temperature in as synthesized condition, a symmetry driven hierarchical assembly results in polycrystalline superoctahedral morphology through oriented agglomeration of individual nanoparticle building blocks. This morphology evolution and the agglomeration kinetics can be tuned by the use of appropriate additives such as glycols.

150

3. CNPs when aged in frozen condition, after room temperature synthesis, result in formation of high aspect ratio nanorods through oriented aggregation of individual nanoparticles in the porous channels of ice.

4. A systematic UV-Vis spectral analysis has revealed that the nanoparticle band gap can be tuned and is primarily driven by the oxidation state changes in ceria but not because of the quantum confinement effect resulting from their nano size.

5. The oxidation state of ceria (+3 or +4) can be reversibly tuned as a function of time and local environment.

6. The epitaxial orientation of nanoceria films can be tuned by varying the deposition rate through molecular beam epitaxy. While growth rates below 8 Å/min result in ceria (100) epitaxial films, higher growth rates up to 30 Å/min lead to the formation of epitaxial (111) films of ceria.

5.1 Challenges and Future Scope

It has been quite a challenging experience for the author and the collaborators involved in this work. Systematic laboratory work and repeated brain storming sessions were needed to reach a stage where some preliminary, logical explanation could be provided for the observed structural and chemical properties of ceria. While the significance of this work has been emphasized in the previous section, there are at least a few observations that are still elusive. In addition to some unique observations about the CNPs, the experience from this research also provides some specific directives based on which future studies on CNPs and other nanoparticle systems should be undertaken.

Following are some aspects/questions that remained unanswered at the time of this dissertation submission:

- What is the relation between oxidation state and morphology of CNPs?

- What is the role of ambient light on the chemistry and structure of CNPs and in general various nanomaterials?

  o Superoctahedral structures were not observed when the nanoparticles are aged in the absence of "LIGHT"

- Why are 20% EG and 40% PEG magic numbers?

  o Author observed special trend in oxidation state switching and agglomeration behavior in nanoceria

- What is the role of Zeta potential in controlling various characteristics?

  o Because of various technical problems, bubble formation and the instability of PEG under measurement conditions, zeta potential values could not be obtained. Ability to find these values as a function of aging time and local environment may help propose a comprehensive mechanism behind agglomeration and surface chemical behavior of CNPs

- What is the affect of thickness on the oxidation state of CNPs'?

  o When the CNPs are deposited on a substrate –

    ▪ Thicker regions are rich in Ce^{4+} oxidation state

    ▪ Thinner regions are rich in Ce^{3+} oxidation state

- What is the role of laboratory environment – humidity, temperature control, lighting used on the behavior of CNPs?

- o Some times the suspensions which are stable in UCF (Orlando, Florida) –
  were not stable in PNNL (Richland, Washington)
- What is the effect of treatments such as stirring / ultrasonication during synthesis
- What is the effect of amount of oxidizer on the morphology of CNPs?
  - o Preliminary experimentation has not shown any significant affect of
    oxidizer concentration on the agglomeration characteristics of CNPs
- What is the role of small impurities present in the "Analytical Standard"
  chemicals used in the laboratory?
  - o Cerium nitrate precursor used in this study is 99% pure and may contain
    trace La impurity

Most of the above mentioned observations may not have any significance while talking about traditional materials or synthesis techniques. However, they are of paramount importance while dealing with nanoscale materials. Significantly higher surface reactivity of the nanoparticles, while providing opportunities to harvest and realize progress in various fields, may also cause some damage with possible toxic effects. Hence, comprehensive laboratory scale studies are highly desired which include every possible parameter that can have a possible impact on the behavior of nanomaterials.

Based on authors experience as a graduate student, it may be quite appropriate to say "Nature often is too complicated to explore within the duration of a "Ph.D.", however dedicated efforts may unravel some unique features that the Nature has in its store.

APPENDIX - 1

Chapter 2.1: Satyanarayana VNT Kuchibhatla, A.S. Karakoti, and S. Seal, Hierarchical assembly of inorganic nanostructure building blocks to octahedral superstructures - a true template-free self-assembly, **Nanotechnology, 2007. 18(7): p. 075303(4pp).**

Chapter 2.2: S. Kuchibhatla, A. S. Karakoti, H. Heinrich, D.C.Sayle, S.Seal, "Symmetry-Driven Spontaneous Self-Assembly of Nanoscale Ceria Building Blocks to Fractal Super-octahedra" **(To be submitted)**

Citation 2.3: A.S. Karakoti, Satyanarayana VNT Kuchibhatla, D.R. Baer, S. Thevuthasan, Dean C. Sayle, S. Seal; Self-assembly Mechanism of Nanostructures in Ice Moulds, **Small, [Under review]**

Chapter 3.1: Satyanarayana VNT Kuchibhatla, A. S. Karakoti, S. Samudrala, S. Seal, , M.H. Engelhard, J. E. Amonette, D.R.Baer, S. Thevuthasan, Influence of aging and environment on nanoparticle chemistry – implication to confinement effects in nanoceria, **Nature Nanotechnology [Under review]**

Chapter 3.2: Satyanarayana VNT Kuchibhatla, A. S. Karakoti, S. Seal, Tuning the band gap of nano-ceria using mono and poly-ols, **(To be submitted).**

Chapter 4.1: Satyanarayana VNT Kuchibhatla, F. Gao, P. Nachimuthu, W. Jiang, V.Shutthanandan, M.H. Engelhard, S.Seal, S. Thevuthasan; Growth rate induced epitaxial orientation of cerium oxide thin films on sapphire (0001), **Physical Review Letters, [To be submitted]**